

Sexual dimorphism in the physiological function of ATP-sensitive potassium channels

by

Trenton David Colburn

B.S., Kansas State University, 2016

B.S., Kansas State University, 2016

M.S., Kansas State University, 2016

AN ABSTRACT OF A DISSERTATION

submitted in partial fulfillment of the requirements for the degree

DOCTOR OF PHILOSOPHY

Department of Kinesiology
College of Health and Human Sciences

KANSAS STATE UNIVERSITY
Manhattan, Kansas

2020

Abstract

ATP-sensitive K⁺ (K_{ATP}) channels are metabolic sensors present in vascular (endothelial), muscle (smooth, cardiac and skeletal), nervous and pancreatic tissues which open in response to a decreasing ATP:ADP ratio (i.e., during exercise and/or hypoxia) and close following pharmacological blockade (i.e., sulphonylureas such as glibenclamide (GLI)). Comprised of four pore-forming inward rectifying K⁺ subunits surrounded by four sulphonylurea receptors, vascular K_{ATP} channels support increased muscle blood flow (\dot{Q}_m) and microvascular oxygen delivery ($\dot{Q}O_2mv$)-to-utilization ($\dot{V}O_2mv$) matching (PO_2mv) in exercising/contracting skeletal muscle by hyperpolarizing smooth muscle cells via K⁺ efflux and subsequently reducing the influx of calcium ions. There is also evidence that K_{ATP} channels limit myocardial damage following ischemia in a sex-dependent manner, via greater ventricular K_{ATP} channel content in females. GLI is a commonly prescribed diabetes medication that inhibits pancreatic K_{ATP} channels and increases insulin release. Unfortunately, one off-target consequence of GLI is inhibition of vascular K_{ATP} channel-mediated vasodilation which may impair exercise tolerance. Therefore, the overall aim of this dissertation was to determine whether vascular K_{ATP} channel function supports exercise tolerance, and whether sex differences in K_{ATP} channel function exist in determining fast-twitch oxidative muscle $\dot{Q}O_2$ and $\dot{V}O_2$; since this muscle type is recruited at the threshold between heavy- and severe-intensity exercise in humans leading to $\dot{V}O_{2max}$ and exhaustion.

In order to assess $\dot{Q}O_2$ and $\dot{V}O_2$ in subsequent K_{ATP} channel studies, our first investigation (Chapter 2) compared the partial pressure of O₂ in the interstitial (PO_{2is}) and microvascular (PO_{2mv}) compartments during twitch contractions in muscles spanning the range of fiber types and oxidative capacity. We demonstrated that a significant resistance to transcapillary O₂ flux resides in all muscles such that PO_{2is} is significantly lower than PO_{2mv} (transcapillary PO₂ =

$\text{PO}_2\text{mv} - \text{PO}_2\text{is}$), and that this resistance was lowest in highly oxidative fast-twitch muscle. This novel finding provided the ability to estimate PO_2mv from PO_2is measurements in Chapters 3 and 4, and estimate convective ($\dot{Q}\text{O}_2$) and diffusive (DO_2) O_2 transport since the convergence of $\dot{Q}\text{O}_2$ and DO_2 establishes muscle O_2 utilization ($\dot{V}\text{O}_2$). In the second investigation (Chapter 3), we demonstrated that systemic GLI administration in female rats reduced $\dot{V}\text{O}_{2\text{max}}$ and submaximal exercise tolerance during treadmill running (critical speed (CS), metabolic threshold separating heavy-intensity exercise from severe-intensity exercise which leads to $\dot{V}\text{O}_{2\text{max}}$). Topical administration of GLI via superfusion onto fast-twitch oxidative muscle impaired \dot{Q}_m and PO_2is and subsequently lowered $\dot{V}\text{O}_2$ during twitch contractions via reduced $\dot{Q}\text{O}_2$ and DO_2 . The third investigation further utilized male and ovariectomized female (F+OVX) rats (Chapter 4) to assess sex differences in vascular K_{ATP} channel function (male vs female) and the effect of ovariectomy (female vs F+OVX; models for pre- and post-menopause). GLI superfusion lowered $\dot{V}\text{O}_2$ via impaired \dot{Q}_m and $\dot{Q}\text{O}_2$, and thus PO_2is , in male and female, but not F+OVX, rats. Furthermore, females demonstrated impaired DO_2 which, in combination with impaired $\dot{Q}\text{O}_2$, would help describe or account for the greater GLI-induced speeding of PO_2is fall during the rest-contraction transient compared to males.

Collectively, the results herein demonstrate that vascular K_{ATP} channels support submaximal exercise tolerance in health via improved convective and diffusive O_2 transport in fast-twitch oxidative muscle. GLI-induced K_{ATP} channel inhibition lowers the threshold separating heavy- and severe-intensity exercise (i.e., CS) and ultimately leads to compromised $\dot{V}\text{O}_{2\text{max}}$ and earlier onset of exhaustion. Furthermore, exercise intolerance and adverse cardiovascular events in diabetic patients may be further exacerbated by sulphonylurea medication, especially in premenopausal females.

Sexual dimorphism in the physiological function of ATP-sensitive potassium channels

by

Trenton David Colburn

B.S., Kansas State University, 2016

B.S., Kansas State University, 2016

M.S., Kansas State University, 2016

A DISSERTATION

submitted in partial fulfillment of the requirements for the degree

DOCTOR OF PHILOSOPHY

Department of Kinesiology
College of Health and Human Sciences

KANSAS STATE UNIVERSITY
Manhattan, Kansas

2020

Approved by:

Major Professor
Dr. Timothy I. Musch

Copyright

© Trenton Colburn 2020.

Abstract

ATP-sensitive K⁺ (K_{ATP}) channels are metabolic sensors present in vascular (endothelial), muscle (smooth, cardiac and skeletal), nervous and pancreatic tissues which open in response to a decreasing ATP:ADP ratio (i.e., during exercise and/or hypoxia) and close following pharmacological blockade (i.e., sulphonylureas such as glibenclamide (GLI)). Comprised of four pore-forming inward rectifying K⁺ subunits surrounded by four sulphonylurea receptors, vascular K_{ATP} channels support increased muscle blood flow (\dot{Q}_m) and microvascular oxygen delivery ($\dot{Q}O_2mv$)-to-utilization ($\dot{V}O_2mv$) matching (PO_2mv) in exercising/contracting skeletal muscle by hyperpolarizing smooth muscle cells via K⁺ efflux and subsequently reducing the influx of calcium ions. There is also evidence that K_{ATP} channels limit myocardial damage following ischemia in a sex-dependent manner, via greater ventricular K_{ATP} channel content in females. GLI is a commonly prescribed diabetes medication that inhibits pancreatic K_{ATP} channels and increases insulin release. Unfortunately, one off-target consequence of GLI is inhibition of vascular K_{ATP} channel-mediated vasodilation which may impair exercise tolerance. Therefore, the overall aim of this dissertation was to determine whether vascular K_{ATP} channel function supports exercise tolerance, and whether sex differences in K_{ATP} channel function exist in determining fast-twitch oxidative muscle $\dot{Q}O_2$ and $\dot{V}O_2$; since this muscle type is recruited at the threshold between heavy- and severe-intensity exercise in humans leading to $\dot{V}O_{2max}$ and exhaustion.

In order to assess $\dot{Q}O_2$ and $\dot{V}O_2$ in subsequent K_{ATP} channel studies, our first investigation (Chapter 2) compared the partial pressure of O₂ in the interstitial (PO_{2is}) and microvascular (PO_{2mv}) compartments during twitch contractions in muscles spanning the range of fiber types and oxidative capacity. We demonstrated that a significant resistance to transcapillary O₂ flux resides in all muscles such that PO_{2is} is significantly lower than PO_{2mv} (transcapillary PO₂ =

$\text{PO}_2\text{mv} - \text{PO}_2\text{is}$), and that this resistance was lowest in highly oxidative fast-twitch muscle. This novel finding provided the ability to estimate PO_2mv from PO_2is measurements in Chapters 3 and 4, and estimate convective ($\dot{Q}\text{O}_2$) and diffusive (DO_2) O_2 transport since the convergence of $\dot{Q}\text{O}_2$ and DO_2 establishes muscle O_2 utilization ($\dot{V}\text{O}_2$). In the second investigation (Chapter 3), we demonstrated that systemic GLI administration in female rats reduced $\dot{V}\text{O}_{2\text{max}}$ and submaximal exercise tolerance during treadmill running (critical speed (CS), metabolic threshold separating heavy-intensity exercise from severe-intensity exercise which leads to $\dot{V}\text{O}_{2\text{max}}$). Topical administration of GLI via superfusion onto fast-twitch oxidative muscle impaired \dot{Q}_m and PO_2is and subsequently lowered $\dot{V}\text{O}_2$ during twitch contractions via reduced $\dot{Q}\text{O}_2$ and DO_2 . The third investigation further utilized male and ovariectomized female (F+OVX) rats (Chapter 4) to assess sex differences in vascular K_{ATP} channel function (male vs female) and the effect of ovariectomy (female vs F+OVX; models for pre- and post-menopause). GLI superfusion lowered $\dot{V}\text{O}_2$ via impaired \dot{Q}_m and $\dot{Q}\text{O}_2$, and thus PO_2is , in male and female, but not F+OVX, rats. Furthermore, females demonstrated impaired DO_2 which, in combination with impaired $\dot{Q}\text{O}_2$, would help describe or account for the greater GLI-induced speeding of PO_2is fall during the rest-contraction transient compared to males.

Collectively, the results herein demonstrate that vascular K_{ATP} channels support submaximal exercise tolerance in health via improved convective and diffusive O_2 transport in fast-twitch oxidative muscle. GLI-induced K_{ATP} channel inhibition lowers the threshold separating heavy- and severe-intensity exercise (i.e., CS) and ultimately leads to compromised $\dot{V}\text{O}_{2\text{max}}$ and earlier onset of exhaustion. Furthermore, exercise intolerance and adverse cardiovascular events in diabetic patients may be further exacerbated by sulphonylurea medication, especially in premenopausal females.

Table of Contents

List of Figures	x
List of Tables	xi
Acknowledgements.....	xii
Preface.....	xiii
Chapter 1 - Introduction.....	1
References.....	6
Chapter 2 - Transcapillary PO ₂ gradients in contracting muscles across the fibre type and oxidative continuum	10
Summary	11
Introduction.....	12
Methods	15
Results.....	21
Discussion.....	24
References.....	36
Chapter 3 - Vascular ATP-sensitive K ⁺ channels support maximal aerobic capacity and critical speed via convective and diffusive O ₂ transport.....	50
Summary	51
Introduction.....	52
Methods	55
Results.....	66
Discussion.....	69
References.....	78
Chapter 4 - Sexual dimorphism in vascular ATP-sensitive K ⁺ channel function supporting interstitial PO ₂ via convective and/or diffusive O ₂ transport.....	93
Summary	94
Introduction.....	95
Methods	98
Results.....	106
Discussion.....	109

References.....	115
Chapter 5 - Conclusions.....	126
Appendix A - Curriculum Vitae	128

List of Figures

Figure 2.1. Interstitial PO ₂ from rest to contractions in muscles of differing fibre type and oxidative capacity	45
Figures 2.2A-D. Microvascular and interstitial PO ₂ and transcapillary PO ₂ from rest to contractions	46
Figure 2.3. Microvascular and interstitial PO _{2 nadir} following the onset of contractions.....	47
Figure 2.4. Transcapillary pressure gradient for O ₂ flux	48
Figure 2.5. The flow of O ₂ from red blood cell to myocyte	49
Figure 3.1. Effect of systemic K _{ATP} channel inhibition on maximal and submaximal exercise...	89
Figure 3.2. Speed-duration relationship following systemic K _{ATP} channel inhibition	90
Figure 3.3. Interstitial PO ₂ of fast-twitch oxidative muscle following local K _{ATP} channel inhibition	91
Figure 3.4. The effect of local K _{ATP} channel inhibition on the convective and diffusive determinants of oxygen transport.....	92
Figures 4.1A-C. Effect of local K _{ATP} channel inhibition on interstitial PO ₂ of fast-twitch oxidative muscle	123
Figure 4.2. Total PO _{2is} during twitch contractions.....	124
Figures 4.3A-C. Convective and diffusive determinants of oxygen transport following local K _{ATP} channel inhibition between sexes.....	125

List of Tables

Table 2.1. Arterial blood samples following microvascular and interstitial PO ₂ measurements .	42
Table 2.2. Microvascular and interstitial PO ₂ kinetics parameters following the onset of twitch contractions	43
Table 2.3. Microvascular oxygen transport from rest to contractions	44
Table 3.1. Doppler echocardiographic assessment of left ventricular function during control and systemic K _{ATP} channel inhibition.....	86
Table 3.2. Individual maximal oxygen uptake and speed-duration relationship parameters during control and systemic K _{ATP} channel inhibition.....	87
Table 3.3. Interstitial PO ₂ kinetics parameters during 180 s twitch contractions and 240 s recovery during control and local K _{ATP} channel inhibition	88
Table 4.1. Effect of local K _{ATP} channel inhibition on interstitial PO ₂ kinetics parameters during 180 s twitch contractions within fast-twitch oxidative muscle of male, female and ovariectomized female rats	121
Table 4.2. Effect of local K _{ATP} channel inhibition on O ₂ delivery and utilization characteristics during 180 s twitch contractions within fast-twitch oxidative muscle of male, female and ovariectomized female rats	122

Acknowledgements

I would like to thank my committee for their support and guidance throughout my journey at Kansas State University. To Dr. Timothy I. Musch and Dr. David C. Poole, thank you for your constant support, academically and in daily life. Specifically, I want to thank Dr. Timothy I. Musch for the constant excitement of being in the laboratory and encouraging myself and others to “walk through the open door” whenever life presents opportunities. To Dr. David C. Poole, I would like to thank for encouraging myself and others to think critically and dig deeper, stressing the motto of the Royal Society (“*Nullius in verba*” meaning “take nobody’s word for it”). I would also like to thank Dr. Bradley J. Behnke and Dr. Thomas J. Barstow for their willingness to have quick, yet very insightful, hallway conversations that spurred my thinking and approach to current projects. I also want to thank my fellow lab mates and colleagues over the years: Scott Ferguson, Clark Holdsworth, Jesse Craig, Daniel Hirai, Ramona Weber, Kiana Schulze, Sue Hageman, Ayaka Tabuchi, Dryden Baumfalk, Alex Opuku-Acheampong, Andrew Horn, Olivia Kunkel, Steven Copp, Alec Butenas, Korynne Rollins, Carl Ade, Jacob Caldwell, Steven Hammond, Shannon Parr, Vanessa Turpin, Josh Smith, Shane Hammer, Andrew Alexander, Kaylin Didier. The pursuit of lively conversations, pushing each other to be better scientists, and maintaining a collaborative approach to learning is what made this journey extremely enjoyable. Finally, I would like to thank my wife, Alayna, for being a pillar of encouragement and support as she also embarked on her own doctoral journey.

Preface

Chapters 2 and 3 of this dissertation represent original research articles that have been published following the peer-review process (citations below) and are reproduced herein with the permission of the publisher. Chapter 4 of this dissertation represents an original research article that is currently in the peer-review process.

Colburn TD, Hirai DM, Craig JC, Ferguson SK, Weber RE, Schulze KM, Behnke BJ, Musch TI & Poole DC (2020). Transcapillary PO₂ gradients in contracting muscles across the fibre type and oxidative continuum. *J Physiol* **598**, 3187-3202.

Colburn TD, Weber RE, Hageman KS, Caldwell JT, Schulze KM, Ade CJ, Behnke BJ, Poole DC & Musch TI (2020). Vascular ATP-sensitive K⁺ channels support maximal aerobic capacity and critical speed via convective and diffusive O₂ transport. *J Physiol* **598**, 4843-4858.

Chapter 1 - Introduction

ATP-sensitive K⁺ (K_{ATP}) channels were first described in ventricular myocytes in the early 1980s (Noma 1983; Trube and Hescheler 1984) following studies that demonstrated hypoxia and dinitrophenol (metabolic inhibition) led to the shortening of action potentials (Isenberg et al. 1983; Van der Heyden et al. 1983). Since then, K_{ATP} channels have been found throughout the body in pancreatic, neural, muscular (cardiac, skeletal, smooth), and endothelial tissue. *In vivo*, K_{ATP} channels are opened by a decrease in the ratio of intracellular ATP:ADP and constitute one of several transmembrane potassium channel classes regulating K⁺ ion efflux, and thus membrane potential and downstream cellular Ca²⁺ handling/influx (Flagg et al., 2010; Foster & Coetze 2016; Quayle, Nelson & Standen 1997). While tissues differ in their composition of pore-forming inwardly rectifying K⁺ subunits (Kir6.1 and/or Kir6.2) and surrounding sulphonylurea receptors (SUR1, SUR2A and/or SUR2B) which regulate channel opening and closing, vascular smooth muscle K_{ATP} channels are largely considered to be composed of four Kir6.1 subunits and four SUR2B receptors (Aziz et al. 2014; Miki et al. 2002; Yamada et al. 1997). In the clinical setting, oral sulphonylureas, K_{ATP} channel closers such as glibenclamide (GLI; inhibits SUR1, SUR2A and SUR2B) and tolbutamide, are widely prescribed to type 2 diabetes mellitus patients (T2DM; Montvida et al. 2018). However, while the intended effect of GLI in diabetes is to increase insulin release following K_{ATP} channel inhibition of pancreatic β-cells, an untoward off-target effect of GLI on vascular K_{ATP} channels likely leads to decreased muscle blood flow (\dot{Q}_m) and thus O₂ and substrate delivery (Banitt et al., 1996; Bank et al., 2000; Bijlstra et al., 1996; Holdsworth et al. 2015, 2016, 2017; Keller et al. 2004; Rocha et al. 2020; Saito et al., 1996). In addition, whether acting on cardiac and/or vascular myocytes, sulfonylurea medications increase the risk for adverse cardiovascular events (Abdelmoneim et al. 2016, Simpson et al. 2006, 2015), developing heart

failure (McAlister et al. 2008, Kristiansen et al. 2011), and all-cause mortality (Simpson et al. 2015).

Aside from pharmacological intervention, increasing physical activity (i.e., exercise rehabilitation) is recommended for patients with cardiovascular disease to slow/reverse disease progression and, specifically for T2DM patients, increase insulin sensitivity and enhance blood glucose regulation (Colberg et al. 2016). However, the potential side effect of sulphonylurea medication impairing vascular regulation of \dot{Q}_m during exercise (i.e., K_{ATP} channel inhibition via GLI leading to vasoconstriction) may ultimately exacerbate exercise intolerance that is characteristic of T2DM and other cardiovascular diseases. Importantly, maximal aerobic capacity ($\dot{V}O_2max = \dot{Q}_{max} \times$ maximal $a-vO_2$ difference; where \dot{Q}_{max} represents maximal cardiac output) is lower in T2DM patients compared to non-diabetic individuals (Schneider et al. 1984; Wilkerson et al. 2011) and is contingent on coordinated changes in pulmonary, cardiovascular, and metabolic systems to deliver oxygenated blood to contracting skeletal muscle and subsequently match metabolic demands via oxidative phosphorylation. Inability of aerobic metabolism to meet the energetic demands of exercise leads to the utilization of glycolytic energy pathways and subsequent production of fatigue-related metabolites (Wilson et al. 1977; Hogan et al. 1992; Richardson et al. 1998). Furthermore, oxygen utilization ($\dot{V}O_2$) at any moment, and especially $\dot{V}O_2max$, is established by the converging of convective (Fick Principle: $\dot{V}O_2 = \dot{Q}_m \times CaO_2 - CvO_2$) and diffusive (Fick's Law of Diffusion: $\dot{V}O_2 = DO_2 \times PO_2$; where PO_2 is the driving pressure for O_2 flux and DO_2 is the diffusive O_2 conductance) O_2 transport (Wagner 1992, 1996).

At the microvascular level where O_2 and substrate offloading/exchange occurs, convective O_2 transport results from the spatial heterogeneity of blood vessels distributing bulk blood flow (\dot{Q}_m) and the utilization of O_2 by contracting myocytes (arterial-venous O_2 difference, CaO_2-

CvO_2) while diffusive O₂ transport is determined, in part, by the particulate nature of blood and the modest RBC-capillary surface area available for microvascular-myocyte O₂ flux (i.e., percentage of capillaries flowing, RBC flux and RBC velocity) and thus a significant O₂ pressure gradient is present between RBCs and myocytes (Federspiel & Popel, 1986; Groebe & Thews, 1990; Honig & Gayeski 1993; Golub & Pittman, 2005). Utilizing these equations (Fick Principle and Fick's Law of Diffusion), our laboratory has combined phosphorescence quenching (PO_{2mv}, microvascular PO₂), labeled microsphere (tissue specific \dot{Q}_m) techniques, and arterial blood gases to estimate convective and diffusive O₂ conductances during twitch contractions (Behnke et al. 2003; McDonough et al. 2005). In addition, the recent ability to measure the PO₂ nearest the contracting myocyte (interstitial PO₂, PO_{2is}) during the rest-contraction transient demonstrated that a significant resistance to transcapillary O₂ flux exists in mixed-fiber type muscle (PO_{2mv} - PO_{2is} of ~16-20 mmHg) and that DO₂ must increase in order to facilitate increasing $\dot{V}O_2$ during contractions (i.e., \uparrow transcapillary $\dot{V}O_2 = \uparrow DO_2 \times [PO_2mv - PO_2is]$; Hirai et al. 2018). However, skeletal muscle is comprised of varying fiber types and oxidative capacities (Delp & Duan, 1996) which, when factoring changes in fiber compositions and mitochondrial content with aging, disease and/or exercise training, may influence the magnitude of the transcapillary pressure gradients and thus DO₂ for a given metabolic demand ($\dot{V}O_2$). Therefore the first aim of this dissertation (Chapter 2) was to describe the magnitudes of transcapillary pressure gradients across a continuum of fiber types and oxidative capacities, and thus allowing PO_{2mv} to be calculated from PO_{2is} (i.e., $PO_2mv = PO_2is + \text{transcapillary } PO_2$) and be used to estimate convective and diffusive O₂ conductances in future investigations (Chapters 3 and 4).

To date, vascular K_{ATP} channel function in males has been shown to support bulk skeletal muscle blood flow (\dot{Q}_m ; functional and reactive hyperemia), O₂ delivery-utilization matching (PO₂

$\alpha \dot{Q}O_2/\dot{V}O_2$), and $\dot{V}O_{2max}$ during treadmill running (Banitt et al., 1996; Bank et al., 2000; Bijlstra et al., 1996; Holdsworth et al. 2015, 2016, 2017; Keller et al. 2004; Lu et al. 2013; Rocha et al. 2020; Saito et al., 1996). Nonetheless, even though many activities of daily living are performed at some submaximal level to avoid reaching $\dot{V}O_{2max}$ and subsequent exhaustion, thus providing a more clinically relevant assessment of patient quality of life, the effect of K_{ATP} channel inhibition via GLI on submaximal exercise tolerance has not been assessed. Notably, at the onset of submaximal heavy-intensity sustainable exercise $\dot{V}O_2$ increases but reaches a steady-state; whereas in the severe-intensity exercise domain $\dot{V}O_2$ increases to $\dot{V}O_{2max}$ and exercise cessation. This metabolic threshold between heavy- and severe-intensity exercise (critical speed (CS; running) or critical power (CP; cycling)) has been defined in health and disease (reviewed by Jones et al. 2010; Poole et al. 2016; Poole, Behnke & Musch 2020) and has been assessed via multiple constant speed runs-to-exhaustion (i.e., speed-duration relationship) in male rats emphasizing the recruitment of fast-twitch muscles above CS (Copp et al. 2010). As such, because $\dot{Q}m$ is decreased following GLI during treadmill running at speeds below and above CS, especially within oxidative muscles (Holdsworth et al. 2015), vascular K_{ATP} channel function likely supports submaximal exercise tolerance (CS) as well as $\dot{V}O_{2max}$.

Lastly, although evidence supports a greater K_{ATP} channel function in cardiac myocytes protecting against ischemic damage and limiting infarct size in a sex-dependent manner (Brown et al., 2005; Johnson et al., 2006), potential sex differences in vascular smooth muscle K_{ATP} channel function in skeletal muscle remain unknown. Crucially, vascular smooth muscle K_{ATP} channel content appears to be reduced, yet still functional, in T2DM patients (Rajkovic et al. 2020) while females experience a higher relative rate of adverse cardiovascular events (heart failure, ischaemic stroke, cardiovascular death, etc.) compared to men (Malmborg et al. 2020).

Additionally, the lower risk for developing coronary artery disease in nondiabetic young and older females (<60 years) is absent with diabetic patients (Kalyani et al. 2014), suggesting that the etiology of diabetes, or even potential interactions of diabetic medication (i.e., sulphonylureas), has a greater impact on the female vasculature.

Thus the present dissertation sought to: i) establish the support of convective and/or diffusive O₂ transport mediated by vascular K_{ATP} channels within contracting fast-twitch oxidative skeletal muscle, ii) bridge the GLI-mediated changes in O₂ transport, and consequent reductions in $\dot{V}O_2$, to whole-body exercise at submaximal (CS) and maximal ($\dot{V}O_{2max}$) intensities leading to exhaustion (Chapter 3), and iii) determine potential sex differences in skeletal muscle vascular K_{ATP} channel function between male and female rats, and following ovariectomy (female vs. ovariectomized female; pre- and post-menopausal models) (Chapter 4).

References

- Abdelmoneim AS, Eurich DT, Senthilselvan A, Qiu W & Simpson SH (2016). Dose-response relationship between sulphonylureas and major adverse cardiovascular events in elderly patients with type 2 diabetes. *Pharmacoepidemiology and Drug Safety* **25**, 1186-1195.
- Aziz Q, Thomas AM, Gomes J, Ang R, Sones WR, Li Y, Ng KE, Gee L & Tinker A (2014). The ATP-sensitive potassium channel subunit, Kir6.1, in vascular smooth muscle plays a major role in blood pressure control. *Hypertension* **64**, 523–529.
- Bijlstra PJ, den Arend JACJ, Lutterman JA, Russel FGM, Thien T & Smits P (1996). Blockade of vascular ATP-sensitive potassium channels reduces the vasodilator response to ischaemia in humans. *Diabetologia* **39**, 1562–1568.
- Banitt PF, Smits P, Williams SB, Ganz P & Creager MA (1996). Activation of ATP-sensitive potassium channels contributes to reactive hyperemia in humans. *Am J Physiol* **271**, H1594-8.
- Bank AJ, Sih R, Mullen K, Osayamwen M & Lee PC (2000). Vascular ATP-Dependent Potassium Channels, Nitric Oxide, and Human Forearm Reactive Hyperemia. *Cardiovasc Drugs Ther* **14**, 23-29.
- Behnke BJ, McDonough P, Padilla DJ, Musch TI & Poole DC (2003). Oxygen exchange profile in rat muscles of contrasting fibre types. *J Physiol* **549**, 597-605.
- Brown DA, Lynch JM, Armstrong CJ, Caruso NM, Ehlers LB, Johnson MS & Moore RL (2005). Susceptibility of the heart to ischaemia-reperfusion injury and exercise-induced cardioprotection are sex-dependent in the rat. *J Physiol* **564**, 619-630.
- Colberg SR, Sigal RJ, Yardley JE, Riddell MC, Dunstan DW, Dempsey PC, Horton ES, Castorino K & Tate DF (2016). Physical Activity/Exercise and Diabetes: A Position Statement of the American Diabetes Association. *Diabetes Care* **39**, 2062-2079.
- Copp SW, Hirai DM, Musch TI & Poole DC (2010). Critical speed in the rat: implications for hindlimb muscle blood flow distribution and fibre recruitment. *J Physiol* **588**, 5077-5087.
- Delp MD & Duan C (1996). Composition and size of type I, IIA, IID/X, and IIB fibers and citrate synthase activity of rat muscle. *J Appl Physiol* **80**, 261-270.
- Fedderspiel WJ & Popel AS (1986). A theoretical analysis of the effect of the particulate nature of blood on oxygen release in capillaries. *Microvasc Res* **32**, 164–189.
- Flagg TP, Enkvetchakul D, Koster JC & Nichols CG (2010). Muscle K_{ATP} Channels: Recent Insights to Energy Sensing and Myoprotection. *Physiol Rev* **90**, 799-829.
- Foster MV & Coetzee WA (2016). K_{ATP} Channels in the Cardiovascular System. *Physiol Rev* **96**, 177-252.

- Golub AS & Pittman RN (2005). Erythrocyte-associated transients in PO₂ revealed in capillaries of rat mesentery. *Am J Physiol Heart Circ Physiol* **288**, H2735–H2743.
- Groebe K & Thews G (1990). Calculated intra- and extracellular PO₂ gradients in heavily working red muscle. *Am J Physiol Heart Circ Physiol* **259**, H84–H92.
- Hirai DM, Craig JC, Colburn TD, Eshima H, Kano Y, Sexton WL, Musch TI & Poole DC (2018). Skeletal muscle microvascular and interstitial PO₂ from rest to contractions. *J Physiol* **596**, 869–883.
- Hogan MC, Arthur PG, Bebout DE, Hochachka PW & Wagner PD (1992). Role of O₂ in regulating tissue respiration in dog muscle working in situ. *J Appl Physiol* **73**, 728–36.
- Holdsworth CT, Copp SW, Ferguson SK, Sims GE, Poole DC & Musch TI (2015). Acute inhibition of ATP-sensitive K⁺ channels impairs skeletal muscle vascular control in rats during treadmill exercise. *Am J Physiol Heart Circ Physiol* **308**, H1434–42.
- Holdsworth CT, Ferguson SK, Colburn TD, Fees AJ, Craig JC, Hirai DM, Poole DC & Musch TI (2017). Vascular K_{ATP} channels mitigate severe muscle O₂ delivery-utilization mismatch during contractions in chronic heart failure rats. *Respir Physiol Neurobiol* **238**, 33–40.
- Holdsworth CT, Ferguson SK, Poole DC & Musch TI (2016). Modulation of rat skeletal muscle microvascular O₂ pressure via K_{ATP} channel inhibition following the onset of contractions. *Respir Physiol Neurobiol* **222**, 48–54.
- Honig CR & Gayeski TE (1993). Resistance to O₂ diffusion in anemic red muscle: roles of flux density and cell PO₂. *Am J Physiol Heart Circ Physiol* **265**, H868–H875.
- Isenberg G, Vereecke J, van der Heyden G & Carmeliet E (1983). The shortening of the action potential by DNP in guinea-pig ventricular myocytes is mediated by an increase of a time-independent K conductance. *Pflügers Arch* **397**, 251–259.
- Johnson MS, Moore RL & Brown DA (2006). Sex differences in myocardial infarct size are abolished by sarcolemmal K_{ATP} channel blockade in rat. *Am J Physiol Heart Circ Physiol* **290**, H2644–H2647.
- Jones AM, Vanhatalo A, Burnley M, Morton RH & Poole DC (2010). Critical power: implications for determination of VO_{2max} and exercise tolerance. *Med Sci Sports Exerc* **42**, 1876–1890.
- Kalyani RR, Lazo M, Ouyang P, Turkbey E, Chevalier K, Brancati F, Becker D & Vaidya Dhananjay (2014). Sex Differences in Diabetes and Risk of Incident Coronary Artery Disease in Healthy Young and Middle-Aged Adults. *Diabetes Care* **37**, 830–838.
- Keller DM, Ogoh S, Greene S & Raven PB (2004). Inhibition of K_{ATP} channel activity augments baroreflex-mediated vasoconstriction in exercising human skeletal muscle. *J Physiol* **561**, 273–282.

- Kristiansen SB, Løfgren B, Nielsen JM, Støttrup NM, Buhl ES, Nielsen-Kudsk JE, Nielsen TT, Rungby J, Flyvbjerg A & Bøtker HE (2011). Comparison of two sulfonylureas with high and low myocardial K(ATP) channel affinity on myocardial infarct size and metabolism in a rat model of type 2 diabetes. *Diabetologia* **54**, 451-458.
- Lu S, Xiang L, Clemmer JS, Gowdey AR, Mittwede PN & Hester RL (2013). Impaired vascular K_{ATP} function attenuates exercise capacity in obese Zucker rats. *Microcirculation* **20**, 662-669.
- Malmborg M, Schmiegelow MDS, Norgaard CH, Munch A, Gerds T, Schou M, Kistorp C, Torp-Pedersen C, Hlatky MA & Gislason G (2020). Does type 2 diabetes confer higher relative rates of cardiovascular events in women compared with men? *Eur Heart J* **41**, 1346-1353.
- McAlister FA, Eurich DT, Majumdar SR & Johnson JA (2008). The risk of heart failure in patients with type 2 diabetes treated with oral agent monotherapy. *Eur J Heart Fail* **10**, 703-708.
- McDonough P, Behnke BJ, Padilla DJ, Musch TI & Poole DC (2005). Control of microvascular oxygen pressures in rat muscles comprised of different fibre types. *J Physiol* **563**, 903-913.
- Miki T, Suzuki M, Shibasaki T, Uemura H, Sato T, Yamaguchi K, Koseki H, Iwanaga T, Nakaya H, Seino S. Mouse model of Prinzmetal angina by disruption of the inward rectifier Kir6.1. *Nat Med.* 2002 May;8(5):466-72. doi: 10.1038/nm0502-466. PMID: 11984590
- Noma A (1983). ATP-regulated K⁺ channels in cardiac muscle. *Nature* **305**, 147–148.
- Quayle JM, Nelson MT & Standen NB (1997). ATP-sensitive and inwardly rectifying potassium channels in smooth muscle. *Physiol Rev* **77**, 1165-1232.
- Poole DC, Burnley M, Vanhatalo A, Rossiter HB & Jones AM (2016). Critical Power: An Important Fatigue Threshold in Exercise Physiology. *Med Sci Sports Exerc* **48**, 2320-2334.
- Rajkovic J, Peric M, Stanisic J, Novakovic R, Djokic V, Rakocevic J, Tepavcevic S, Labudovic-Borovic M, Gostimirovic M, Heinle H & Gojkovic-Bukarica L (2020). The Role of the Adenosine Triphosphate-Sensitive Potassium Channels in Pinacidil-induced Vasodilation of the Human Saphenous Vein in Patients With and Without Type 2 Diabetes Mellitus. *J Physiol Pharmacol* **71**, 125-135.
- Richardson RS, Noyszewski EA, Leigh JS & Wagner PD (1998). Lactate efflux from exercising human skeletal muscle: role of intracellular PO₂. *J Appl Physiol* **85**, 627–634.
- Rocha MP, Campos MO, Mattos JD, Mansur DE, Rocha HNM, Secher NH, Nobrega ACL & Fernandes IA (2020). K_{ATP} channels modulate cerebral blood flow and oxygen delivery during isocapnic hypoxia in humans. *J Physiol* **598**, 3343-3356.
- Saito Y, McKay M, Eraslan A & Hester RL (1996). Functional hyperemia in striated muscle is reduced following blockade of ATP-sensitive potassium channels. *Am J Physiol Heart Circ Physiol* **270**, H1649–H1654.

- Schneider SH, Amorosa LF, Khachadurian AK & Ruderman NB (1984). Studies on the mechanism of improved glucose control during regular exercise in type 2 (non-insulin-dependent) diabetes. *Diabetologia* **26**, 355-360.
- Simpson SH, Lee J, Choi S, Vandermeer B, Abdelmoneim AS & Featherstone TR (2015). Mortality risk among sulfonylureas: a systematic review and network meta-analysis. *Lancet Diabetes Endocrinol* **3**, 43-51.
- Simpson SH, Majumdar SR, Tsuyuki RT, Eurich DT & Johnson JA (2006). Dose-response relation between sulphonylurea drugs and mortality in type 2 diabetes mellitus: a population-based cohort study. *CMAJ* **174**, 169-174.
- Trube G & Hescheler J (1984). Inward-rectifying channels in isolated patches of the heart cell membrane: ATP-dependence and comparison with cell-attached patches. *Pflügers Arch* **401**, 178–184.
- Van der Heyden G, Vereecke J, Isenberg G, Callewaert G & Carmeliet E (1983). Metabolic inhibition and the cardiac ventricular action potential: voltage clamp analysis using single cells. *Arch Int Pharmacodyn Ther* **263**, 331–332.
- Wagner PD (1992). Gas exchange and peripheral diffusion limitation. *Med Sci Sports Exerc* **24**, 54-58.
- Wagner PD (1996). Determinants of maximal oxygen transport and utilization. *Annu Rev Physiol* **58**, 21-50.
- Wilkerson DP, Poole DC, Jones AM, Fulford J, Mawson DM, Ball CI & Shore AC (2011). Older type 2 diabetic males do not exhibit abnormal pulmonary oxygen uptake and muscle oxygen utilization dynamics during submaximal cycling exercise. *Am J Physiol Regul Integr Comp Physiol* **300**, R685-R692.
- Wilson DF, Erecinska M, Drown C & Silver IA (1977). Effect of oxygen tension on cellular energetics. *Am J Physiol Cell Physiol* **233**, C135-140.
- Yamada M, Isomoto S, Matsumoto S, Kondo C, Shindo T, Horio Y & Kurachi Y (1987). Sulphonylurea receptor 2B and Kir6.1 form a sulphonylurea-sensitive but ATP-insensitive K⁺ channel. *J Physiol* **499**, 715–720, 1997.

Chapter 2 - Transcapillary PO₂ gradients in contracting muscles across the fibre type and oxidative continuum

Trenton D. Colburn^a, Daniel M. Hirai^c, Jesse C. Craig^d, Scott K. Ferguson^e, Ramona E. Weber^a,
Kiana M. Schulze^a, Brad J. Behnke^a, Timothy I. Musch^{a,b}, David C. Poole^{a,b}

^aDepartment of Kinesiology, ^bDepartment of Anatomy and Physiology, Kansas State University
Manhattan, KS

^cDepartment of Health and Kinesiology, Purdue University, West Lafayette, IN

^dDepartment of Internal Medicine, University of Utah, Salt Lake City, UT

^eDepartment of Kinesiology and Exercise Sciences, University of Hawaii, Hilo, HI

Summary

In mixed fibre type skeletal muscle transcapillary PO_2 gradients ($\text{PO}_{2\text{mv}}-\text{PO}_{2\text{is}}$; microvascular and interstitial, respectively) drive O_2 flux across the blood-myocyte interface where the greatest resistance to that O_2 flux resides. Herein we assessed a broad spectrum of fibre type and oxidative capacity rat muscles across the rest-to-contractions (1 Hz, 120 s) transient to test the novel hypotheses that: i) slow-twitch $\text{PO}_{2\text{is}}$ would be greater than fast-twitch, ii) muscles with greater oxidative capacity have greater $\text{PO}_{2\text{is}}$ than glycolytic counterparts, and iii) whether $\text{PO}_{2\text{mv}}-\text{PO}_{2\text{is}}$ at rest is maintained during contractions across all muscle types. $\text{PO}_{2\text{mv}}$ and $\text{PO}_{2\text{is}}$ were determined via phosphorescence quenching in soleus (SOL; 91% type I+IIa fibres and CSA: $\sim 21 \mu\text{mol min}^{-1} \text{g}^{-1}$), peroneal (PER; 33% and $\sim 20 \mu\text{mol min}^{-1} \text{g}^{-1}$), mixed (MG; 9% and $\sim 26 \mu\text{mol min}^{-1} \text{g}^{-1}$) and white gastrocnemius (WG; 0% and $\sim 8 \mu\text{mol min}^{-1} \text{g}^{-1}$) across the rest-contractions transient. $\text{PO}_{2\text{mv}}$ was higher than $\text{PO}_{2\text{is}}$ in each muscle ($\sim 6-13 \text{ mmHg}$; $p < 0.05$). SOL $\text{PO}_{2\text{is}}$ area was greater than the fast-twitch muscles during contractions ($p < 0.05$). Oxidative muscles had greater $\text{PO}_{2\text{is}}$ nadir (9.4 ± 0.8 , 7.4 ± 0.9 , and 6.4 ± 0.4 ; SOL, PER, MG respectively) than WG ($3.0 \pm 0.3 \text{ mmHg}$, $p < 0.05$). The magnitude of $\text{PO}_{2\text{mv}}-\text{PO}_{2\text{is}}$ at rest decreased during contractions in MG only (~ 11 to 7 mmHg ; Time x ($\text{PO}_{2\text{mv}}-\text{PO}_{2\text{is}}$) Interaction, $p < 0.05$). These data support that, since transcapillary PO_2 gradients during contractions are maintained in all muscle types, increased O_2 flux must occur via enhanced intracapillary diffusing conductance, which is most extreme in highly oxidative fast-twitch muscle.

Introduction

Sustained skeletal muscle contractile function and, thus, exercise tolerance, requires adequate energy production via oxidative metabolism. Most mammalian species maintain minimal muscle O₂ stores (i.e., myoglobin concentration <1 mM, Reynaferje, 1962; Hickson et al. 1981; Nemeth & Lowry, 1984; Terrados et al. 1990; Bekedam et al. 2009). Therefore, a rapid increase of pulmonary O₂ uptake ($\dot{V}O_2$) coupled to red blood cell (RBC)-mediated transport to muscle tissue and existence of an appropriate driving pressure across the microvascular-myocyte interface is crucially important. The successful integration of these systems (pulmonary-cardiovascular-metabolic) to match O₂ utilization with O₂ delivery in the muscle (i.e., $\dot{Q}O_2/\dot{V}O_2$ ratio which establishes the partial pressure of O₂, PO₂), is dependent, in part, on the transmural PO₂ gradient and the diffusive properties of the blood-myocyte interface.

Thus, according to Fick's law of diffusion, $\dot{V}O_2 = DO_2 (\Delta PO_2)$, where $\dot{V}O_2$ corresponds to the O₂ flux across a given membrane/barrier, O₂ movement is dictated by changes in the O₂ diffusing conductance of that barrier (DO₂) and the pressure difference between the relevant compartments (ΔPO_2). In skeletal muscle there are structural and functional barriers to transcapillary O₂ flux. The particulate nature of blood combined with the modest fraction of capillary wall that facilitates O₂ flux at any given instant results in the effective capillary surface area being at least two orders of magnitude less than that of mitochondria (Federspiel & Popel, 1986; Groebe & Thews, 1990; Honig & Gayeski, 1993; Golub & Pittman, 2005). This will necessitate a significant transcapillary PO₂ gradient (i.e., PO₂_{mv}-PO₂_{is}, microvascular and interstitial, respectively) (Hirai et al. 2018, 2019). Importantly, there is no O₂ carrier to facilitate transportation from the microvascular space into the interstitial space that immediately surrounds the muscle sarcolemma (known as the carrier-free region, CFR) (Honig & Gayeski, 1993). Given

that blood-myocyte O₂ flux only occurs via that portion of the capillary wall in intimate approximation to the RBC (Federspiel & Popel, 1986) there is an attendant high O₂ flux density (i.e. flux per unit area) that increases with muscle $\dot{V}O_2$ during contractions. Thus, examining the extra-myocyte PO₂ profile from RBC to sarcolemma will provide important information regarding the effective resistance to trans-membrane and trans-compartmental O₂ resistance.

Our laboratory has utilised the latest phosphorescence quenching techniques to reveal a significant PO₂ drop in that small physical space between the microvascular and interstitial compartments of the mixed fibre type spinotrapezius muscle (i.e., PO_{2mv}-PO_{2is}; Hirai et al. 2018). Thus, rapid contraction-induced increases in myocyte $\dot{V}O_2$ incur commensurate falls in PO_{2is} and PO_{2mv}, such that increases in transcapillary O₂ flux ($\dot{V}O_2$) must be achieved via elevated effective DO₂. However, in rat hindlimb muscles spanning the fibre type continuum (slow-twitch and fast-twitch) but with differential oxidative capacities it remains unknown whether, at rest or during contractions: 1) slow-twitch fibres support a greater interstitial-myocyte driving pressure (PO_{2is}) compared to fast-twitch fibres, 2) muscles with greater oxidative capacity have greater PO_{2is} than their predominantly glycolytic counterparts, and 3) whether PO_{2mv}-PO_{2is} is maintained throughout contractions in a similar fashion (i.e., the magnitude of PO_{2mv}-PO_{2is} is not different during contractions from that at rest) across all muscle fibre types.

Therefore, given the pronounced fibre type PO_{2mv} (Behnke et al. 2003; Ferguson et al. 2015; McDonough et al. 2005) and vasomotor control (Behnke et al. 2011) differences in rat hindlimb muscles, we hypothesized (Hypothesis #1) that PO_{2is} of slow-twitch muscle would be greater at rest and during contractions demonstrating superior $\dot{Q}O_2/\dot{V}O_2$ matching (i.e., slower rate of fall (τ ; time constant) and mean response time (MRT)) compared to fast-twitch muscle. We further hypothesized (Hypothesis #2) that, in fast-twitch muscles, those with higher oxidative

capacity would maintain greater $\text{PO}_{2\text{is}}$ throughout contractions despite having faster kinetics (τ and MRT) characteristic of greater O_2 utilization. Lastly, by comparison with extant $\text{PO}_{2\text{mv}}$ data (Behnke et al. 2003; Ferguson et al. 2015), we tested the hypothesis (Hypothesis #3) that a significant transcapillary PO_2 gradient ($\text{PO}_{2\text{mv}}-\text{PO}_{2\text{is}}$) would be maintained throughout contractions in muscles spanning the fibre-type and oxidative spectrum. This latter hypothesis, if correct, would support a mechanistic link between oxidative potential and transcapillary DO_2 within individual muscles (i.e., increased transcapillary DO_2 to meet increasing metabolic demands ($\dot{\text{V}}\text{O}_2$) of contractions in the absence of increased $\text{PO}_{2\text{mv}}-\text{PO}_{2\text{is}}$ compared to rest, per Fick's law of diffusion, $\dot{\text{V}}\text{O}_2 = \text{DO}_2 \times (\text{PO}_{2\text{mv}}-\text{PO}_{2\text{is}})$).

Methods

Ethical Approval

All procedures and protocols were approved by the Kansas State University Institutional Animal Care and Use Committee (IACUC No. 3762) following guidelines established by the National Institutes of Health. Experiments were also conducted in accordance with the ethical standards mandated by the *Journal of Physiology* (Grundy, 2015). Rats were maintained in Association for the Assessment and Accreditation of Laboratory and Animal Care accredited animal facilities under a 12:12 h light:dark cycle with food and water provided *ad libitum*.

Muscles selected for Fibre-type and Oxidative capacity continuum

The interstitial space PO₂ data presented in the current manuscript is the culmination of multiple ongoing investigations. All data were collected with the same procedures and described in detail below (see *Phosphorescence quenching determination of PO_{2mv} and PO_{2is}*). Selection of muscles in the present investigation (soleus, SOL; peroneal, PER; mixed gastrocnemius, MG; and white gastrocnemius, WG) was based on their fibre-type composition and oxidative enzyme capacity (Delp & Duan, 1996) and muscle recruitment patterns from low-to-high intensity exercise (SOL < PER/MG < WG). The SOL muscle is comprised principally of slow-twitch fibres (84% type I, 7% type IIa and 9% type IId/x) with a citrate synthase activity of ~21 µmol min⁻¹ g⁻¹ (CSa; used herein as a marker of oxidative capacity) that is utilized for posture, plantar flexion and ankle stabilization. PER and MG muscles are comprised of predominately fast-twitch fibres with a high oxidative capacity. PER (14% type I, 19% type IIa, 22% type IId/x and 45% type IIb fibres) is an ankle evertor with a CSa of ~20 µmol min⁻¹ g⁻¹. The MG (3% type I, 6% type IIa, 34% type IId/x and 57% type IIb fibres) is a powerful plantar flexion muscle with a CSa of ~26 µmol min⁻¹ g⁻¹.

Lastly, the WG represents fast-twitch glycolytic muscle (8% type II^{d/x} and 92% type II^b fibres; CSA: ~8 µmol min⁻¹ g⁻¹) that is more heavily recruited at high speed/intensity (Armstrong & Laughlin, 1985; Copp et al. 2010).

The PO₂_{mv} data herein come from previous studies within our laboratory investigating fibre-type differences in the rat hindlimb musculature where electrically induced muscle contractions were applied with electrodes sutured to the muscle surface (Behnke et al. 2003 and Ferguson et al. 2015; with WG data collected during Ferguson et al. 2015); as was performed for all novel PO₂_{is} data.

Phosphorescence quenching determination of PO₂_{mv} and PO₂_{is}

In all experiments, phosphorescence quenching was performed in young Sprague-Dawley rats (<7 months old; Charles Rivers Laboratories; Boston, MA, USA) to assess microvascular and interstitial PO₂. The composition of male and female rats are presented in Figures 1 and 2A-D. Previous data investigating sex differences in PO₂_{is} revealed no differences in the control condition (Craig et al. 2018, 2019b); therefore, male/female PO₂ data were combined for any given data set. Phosphorescence signal overlap precludes the simultaneous measurement of PO₂_{mv} and PO₂_{is} in the same muscle (Dunphy et al. 2002; Esipova et al. 2011) and pharmacological protocols assessing channel blockade following the current PO₂_{is} control data (blockade data not shown) precluded the surgical exposure of hindlimb muscles for both limbs and assessment of each muscle (i.e. SOL, PER, MG and WG) within the same animal. Therefore, the current study reports data as separate animals with unpaired statistical comparisons.

Surgical instrumentation. Rats were initially anesthetized with a 5% isoflurane-O₂ mixture and maintained on ~2% isoflurane-O₂ mixture (Butler Animal Health Supply) throughout

the surgical exposure of hindlimb muscles. Core body temperature was maintained ~38°C, assessed via rectal thermometer, on a heating pad. Following an incision on the ventral lateral surface of the neck, the right carotid artery was isolated and cannulated (PE-10 connected to PE-50; Intra-Medic polyethylene tubing; BD, Franklin Lakes, NJ, USA) and connected to a pressure transducer for continuous mean arterial pressure (MAP; PowerLab/LabChart data acquisition system, AD Instruments) measurements and infusion of microvascular phosphorescence probes (R2 and G2). Following an incision on the ventral surface of the tail, the caudal artery was isolated and cannulated (PE-10 connected to PE-50) for blood sampling and infusion of pentobarbital sodium anesthesia. Arterial blood samples were collected following the final contraction protocol of each muscle for determination of O₂ saturation, systemic haematocrit and plasma lactate (Nova Stat Profile M; Nova Biomedical, Waltham, MA, USA).

Following catheter placement, incisions were made to carefully remove overlying skin and fascia to expose the biceps femoris. The semitendinosus was separated from the biceps femoris and the lateral saphenous vein was sutured at the ankle before reflecting the biceps femoris, exposing MG and WG muscles. For SOL and PER measurements, the MG was reflected while maintaining origin and insertion attachments. Rats were then transitioned to pentobarbital sodium anesthesia (~20 mg/kg body wt) given arterially while concentrations of isoflurane were decreased and subsequently discontinued. Toe pinch and palpebral reflexes were checked regularly to monitor the level of anesthesia, supplementing pentobarbital sodium as necessary (0.03-0.05 mL diluted to 0.3 mL with heparinized saline). The left foot was braced and secured to fix the ankle and knee joints at 90° angles. Using 6-0 silk sutures, platinum iridium wire electrodes were secured to the proximal (cathode) and distal (anode) surface regions of each muscle. Exposed muscle tissue was superfused with warmed (~38°C) Krebs-Hensleit bicarbonate-buffered solution equilibrated

with 5% CO₂-95% N₂ (pH 7.4). All exposed tissue surrounding the sutured electrodes were covered with Saran Wrap (Dow Brands, Indianapolis, IN) to minimize tissue dehydration.

Experimental protocol. The microvascular phosphorescent probes Oxyphor R2 (Pd-meso-tetra(4-carboxyphenyl)porphyrin dendrimer) and Oxyphor G2 (Pd-*meso*-tetra-(4-carboxyphenyl)-porphoryin) were infused arterially (15-20 mg kg⁻¹ dissolved in 0.4 mL of saline) while the interstitial space probe Oxyphor G4 (Pd-*meso*-tetra-(3,5-dicarboxyphenyl)-tetrabenzoporphyrin) was injected into the muscle (~10 µl/injection; 10 µM) and subsequently covered with Saran Wrap to protect the muscle from ambient air. Notably, these highly soluble probes do not permeate biological membranes in skeletal muscle (Dunphy et al. 2002; Poole et al 2004; Esipova et al. 2011) and therefore remain in the compartment of interest for PO₂ measurements.

At least 15 min was allowed for Oxyphors R2 and G2 to bind to albumin (Lo et al. 1997; Wilson et al. 2006) and distribute evenly in the plasma of systemic vasculature as well as for G4 to diffuse and stabilize within the interstitial space following microinjections (Craig et al. 2018, 2019a,b; Hirai et al. 2018; Smith et al. 2007). The muscle surface temperature was measured via infrared surface thermometer during interstitial assessments to ensure that proper k_Q and τ₀ settings of the frequency domain phosphorimeter (PMOD 5000; Oxygen Enterprises, Philadelphia, PA) were used. The common end of the light guide was positioned ~2-4 mm superficial to the lateral surface of exposed muscle tissue and in a field absent of large vessels to ensure the microvascular and interstitial regions being measured were principally of capillary-myocyte interface. Importantly, the largest contributor to vascular volume is capillary volume (~85%; Behnke et al. 2001; Poole et al. 1997).

$\text{PO}_{2\text{mv}}$ (4-8 V) and $\text{PO}_{2\text{is}}$ (6-8 V) were measured via phosphorescence quenching (see below) at rest and during 120-s of twitch contractions (1 Hz, 2-ms pulse duration; Grass stimulator model S88, Quincy, MA) and recorded at 2-s intervals. Following contractions PO_2 was monitored to ensure microvascular control was preserved and values returned to baseline. Following data collection, rats were euthanized via pentobarbital sodium overdose ($> 100 \text{ mg kg}^{-1}$ i.p. or $> 50 \text{ mg kg}^{-1}$ i.a.) followed by pneumothorax.

PO₂ Measurement and Curve-fitting

The Stern-Volmer relationship was used in calculating PO_2 . Direct measurement of phosphorescence lifetime yielded PO_2 via the following equation:

$$\text{PO}_2 = [\tau^0/\tau - 1] / (k_Q \times \tau^0)$$

Where k_Q is the quenching constant and τ^0 and τ are the phosphorescence lifetimes in the absence of O_2 and at the ambient O_2 concentration, respectively. In tissues at 32.3°C (muscle surface temperature: $\sim 31^\circ\text{C}$) the parameters for G4 were as follows: k_Q of $258 \text{ mmHg}^{-1} \text{ s}^{-1}$ and τ^0 of $226 \mu\text{s}$ (Esipova et al 2011). Parameters for $\text{PO}_{2\text{mv}}$ were utilized presuming blood to be temperature regulated by core temperature (38°C). R2 parameters were k_Q : $409 \text{ mmHg}^{-1} \text{ s}^{-1}$ and τ^0 : $601 \mu\text{s}$ (Lo et al. 1997). G2 parameters were k_Q : $273 \text{ mmHg}^{-1} \text{ s}^{-1}$ and τ^0 : $251 \mu\text{s}$ (Dunphy et al. 2002). Muscle temperature does not change appreciably during the contraction protocol used herein (Craig et al. 2019), therefore the phosphorescence lifetime is affected exclusively by the O_2 partial pressure.

Data for the initial fall in PO_2 (i.e. primary PO_2 response) were obtained via curve-fitting $\text{PO}_{2\text{is}}$ data points with computer software (SigmaPlot 12.5, Systat Software, San Jose, CA) while data regarding secondary responses (undershoot of PO_2 ($\Delta_2\text{PO}_2$)) were calculated manually (see

below). Using the two-component model below, the primary PO₂ responses were constrained to the primary amplitude (Δ_1) as to not overestimate magnitude and rate of PO₂ fall. The following two-component model was used to fit data over time:

$$\text{Two-component: } \text{PO}_2(t) = \text{PO}_2_{\text{BL}} - \Delta_1 \text{PO}_2 (1 - e^{-(t-\text{TD}_1)/\tau_1}) + \Delta_2 \text{PO}_2 (1 - e^{-(t-\text{TD}_2)/\tau_2})$$

Where PO₂(t) is the PO₂ at any given time point t, PO₂(BL) corresponds to pre-contracting resting baseline PO₂, Δ_1 and Δ_2 are the amplitudes for the first and second component respectively, TD₁ and TD₂ are the time delays for each component, and τ_1 and τ_2 are the time constants (i.e., time to reach 63% of the final response value) for each component. Appropriate fits were determined via: 1) the coefficient of determination, 2) sum of the squared residuals, 3) visual inspection and analysis of the model fits to the data and the residuals. Mean response time (MRT) is the overall kinetics of the primary response and calculated as TD₁ + τ_1 . The secondary response ($\Delta_2 \text{PO}_2$) was taken as the difference between end contractions (PO₂_{end}) and nadir (PO₂_{nadir}), where PO₂_{nadir} was calculated as [PO₂_{BL} - $\Delta_1 \text{PO}_2$] and PO₂_{end} was a 10 s average of raw data (i.e. 112-120 s). Area under the curves (PO₂_{area}) were integrated by summing each 2 s measurement across the 120 s contraction protocol.

Statistical Analyses

Arterial blood samples were compared between groups via One-Way ANOVA with Bonferroni correction for multiple comparisons. Central haemodynamic and PO₂ kinetic parameters were compared using unpaired Student's *t*-tests. PO₂ profiles were assessed via Two-Way ANOVA (Time x Compartment) with Tukey's *post hoc* analyses. Data are reported as mean \pm standard deviation (SD) with statistical significance accepted at p < 0.05.

Results

Of the six PER $\text{PO}_{2\text{mv}}$ measurements obtained, one animal was removed due to a coefficient of determination greater than 2 standard deviations from the group mean. The remaining $\text{PO}_{2\text{mv}}$ and $\text{PO}_{2\text{is}}$ of all animals were used in making statistical comparisons between muscles (SOL, PER, MG, and WG) and compartments ($\text{PO}_{2\text{mv}}$ vs $\text{PO}_{2\text{is}}$).

Arterial Blood Samples and Central Haemodynamics

Data for arterial O_2 saturation, systemic hematocrit and lactate concentration for $\text{PO}_{2\text{mv}}$ and $\text{PO}_{2\text{is}}$ are presented in Table 1. MAP was significantly higher during $\text{PO}_{2\text{mv}}$ measurements compared to $\text{PO}_{2\text{is}}$ measurements in SOL (116 ± 13 vs 101 ± 14), MG (113 ± 14 vs 102 ± 11) and WG (114 ± 9 vs 99 ± 10 mmHg; $p < 0.05$ for all). Nonetheless, there is no significant effect of MAP on $\text{PO}_{2\text{mv}}$ until MAP falls below 70 mmHg (Behnke et al. 2006) and equivalent $\Delta\text{PO}_{2\text{mv}}$ - $\text{PO}_{2\text{is}}$ has been shown with these MAPs (Hirai et al. 2018). Therefore, no differences in central haemodynamic responses were expected to influence PO_2 comparisons between the microvascular and interstitial compartments.

Interstitial PO_2 : Influence of Muscle Fibre Type and Oxidative Capacity

Mean $\text{PO}_{2\text{is}}$ profiles (Figure 1) and kinetics parameter data (Table 2) are presented for SOL, PER, MG and WG at rest and during 120 s of twitch contractions. Resting $\text{PO}_{2\text{is}}$ was greater in slow-twitch SOL and the postural fast-twitch oxidative PER muscles compared to fast-twitch MG and WG muscles (SOL and PER > MG > WG; $p < 0.05$). Following the onset of contractions, the postural SOL and PER muscles fell to $\text{PO}_{2\text{is nadir}}$ and $\text{PO}_{2\text{is end}}$ levels not different from each other ($p > 0.05$ for both), however SOL fell at a slower rate (τ and $\Delta_1\text{PO}_{2\text{is}}/\tau$; $p < 0.05$). SOL $\text{PO}_{2\text{is}}$

also fell at a slower rate (τ and MRT) compared to fast-twitch MG and WG muscles while maintaining a significantly higher interstitial-myocyte O₂ driving pressure throughout (i.e., PO_{2is}_{nadir} and PO_{2is}_{end}; p < 0.05).

Within fast-twitch fibre muscles, the more oxidative PER and MG had a greater interstitial-myocyte O₂ driving pressure at rest and throughout contractions (PO_{2is}_{BL}, PO_{2is}_{nadir}, and PO_{2is}_{end}; p < 0.05 for all) than the glycolytic WG, with greater absolute and relative fall in PO_{2is} (Δ_1 PO_{2is} and Δ_1 PO_{2is}/ τ , respectively; p < 0.05 for all). In addition, integrating the area under the curves (Figure 1, PO₂_{area} shown in Figure 4) revealed a graded reduction in total PO_{2is} during contractions when transitioning from slow-twitch oxidative to fast-twitch glycolytic muscle (SOL > PER > MG > WG; p < 0.05).

Transcapillary O₂ Gradients in Muscles of Differing Fibre-type and Oxidative Capacity

Mean PO_{2mv} of extant data (Behnke et al. 2003 and Ferguson et al. 2015) and PO_{2is} are presented in Figures 2A-D, along with the transcapillary pressure gradient between the microvascular and interstitial compartments (PO_{2mv}-PO_{2is}). In all muscles, there was a significant pressure gradient at rest (~6-13 mmHg) that was maintained throughout contractions (Figures 2A-D, Figure 3 and Table 2: PO₂_{BL}, PO₂_{nadir}, and PO₂_{end}, p < 0.05 for all). Interestingly, there were no significant differences in Δ_1 PO₂ between microvascular and interstitial compartments (p > 0.05) except for the locomotive fast-twitch oxidative MG where there was a greater reduction in PO_{2mv} (10.7 ± 3.9 vs 7.0 ± 2.2 mmHg, p < 0.05). In addition, there was a Time x (PO_{2mv}-PO_{2is}) interaction during MG contractions where the pressure gradient, and thus driving pressure for transcapillary O₂ flux, was reduced (Figure 2C; p < 0.001). Accordingly, Figure 4 demonstrates that the difference in total available O₂ driving pressure (PO_{2mv}-PO_{2is} PO₂_{area}) during contractions

between microvascular and interstitial compartments of MG and PER is approximately half that of their slow-twitch oxidative counterpart (i.e. SOL).

In Figure 4, the PO_2 area in the microvascular compartment demonstrates the significantly greater driving pressure, and thus O_2 availability, in the slow-twitch SOL muscle compared to the fast-twitch fibre muscles ($\text{SOL} > \text{PER} = \text{MG} = \text{WG}$). This single step reduction from slow-twitch to fast-twitch fibres contrasts the graded reduction present in the interstitial space ($\text{SOL} > \text{PER} > \text{MG} > \text{WG}$; all $p < 0.05$). The difference between PO_{2mv} and PO_{2is} (i.e. transcapillary PO_2) represents the contrasting muscle-specific O_2 pressure gradients across the capillary wall, with fast-twitch oxidative PER and MG muscles having ~31-54% lower transcapillary driving pressure than slow-twitch SOL and fast-twitch WG.

Discussion

The present investigation is the first to resolve the profile of skeletal muscle interstitial PO₂ during the rest-contractions transition across a broad spectrum of muscle fibre types and oxidative capacities. Consequently, these data resolve a significant transcapillary pressure gradient (PO₂_{mv}-PO₂_{is}) thereby revealing the presence of a significant resistance to O₂ flux in all muscles examined at rest and during contractions regardless of fibre type and oxidative capacity. Importantly, for oxidative metabolism to support contractile function and exercise tolerance, the tightly coordinated increase in O₂ flux across the microvascular-myocyte interface and into the mitochondria (Fick's Law of Diffusion: $\dot{V}O_2 = DO_2 \times \Delta PO_2_{mv-mito}$), in health, is established through an effectively maintained microvascular PO₂ relative to mitochondrial PO₂ during contractions whilst $\dot{V}O_2$ increases and PO₂ subsequently decreases in all compartments. Furthermore, these data demonstrate that: i) in oxidative muscles, slow-twitch fibre PO₂_{is} falls at a slower rate (i.e. τ and MRT) than fast-twitch fibres while maintaining greater PO₂_{is}, ii) within fast-twitch muscles, a higher oxidative capacity is supplied by a greater interstitial-mitochondrial driving pressure (i.e. PO₂_{is}) than for glycolytic counterparts, and iii) despite varying magnitudes of transcapillary pressure gradients at rest (PO₂_{mv}-PO₂_{is} ~6-13 mmHg), increased O₂ utilization with contractions must be supported by effective increases in transcapillary DO₂ (i.e. RBC flux, velocity, and hematocrit (Hirai et al. 2018, 2019)) as per Fick's law.

Slow-twitch vs. Fast-twitch Interstitial PO₂ (Hypothesis #1)

Slow-twitch fibres are primarily located in postural muscles and those recruited during lower-intensity exercise (i.e. below critical speed (Copp et al. 2010)). Having a greater capillary-to-fibre ratio and greater vasodilatory capacity compared to their fast-twitch counterparts, slow-

twitch fibres evince a significantly longer $\text{PO}_{2\text{mv}}$ time delay and MRT during contractions (Behnke et al. 2003, 2011; McDonough et al. 2005). Herein we demonstrate that this behavior is present within the interstitial space and precedes $\text{PO}_{2\text{is}}$ falling towards its nadir/steady-state (Table 2; $p < 0.05$). Figure 3 shows that the $\text{PO}_{2\text{is}} \text{ nadir}$ for fast-twitch muscles is also significantly lower than the slow-twitch SOL. This greater interstitial-myocyte driving pressure in slow-twitch muscle is interpreted as evidence of a better $\dot{\text{QO}}_{2\text{is}}$ -to- $\dot{\text{VO}}_{2\text{is}}$ matching at rest and through coordinated changes in increased microvascular $\dot{\text{QO}}_2$ during contractions (muscle pump, immediate and prolonged vasodilation (Joyner & Casey, 2015; Laughlin et al. 2012; Thomas & Segal, 2004)) as well as myoglobin-mediated O_2 storage and PO_2 buffering (Type I > IIA > IIX, mostly absent in IIB fibres; Hickson 1981; Ordway & Garry, 2004). Although the fibre and oxidative distribution within and among muscles is generally more distinct in rodents compared to humans (Armstrong & Laughlin 1984, 1985, Edgerton et al. 1975, Johnson et al. 1973), there exists a substantial heterogeneity of fibre types across human muscles (i.e., type I fibres: soleus 88% vs rectus femoris 36%) as a function of depth within a given muscle (greater proportion of type I fibres in deeper regions; Johnson et al. 1973) and across elite athletic populations (i.e., sprinters <30% and distance runners >70% type I fibres; Saltin & Gollnick, 1983). Thus, although the more compartmentalized (rodent) compared to mosaic (human) distribution of fibres and their oxidative capacity, and consequent sharing of capillaries, affects energetic control to exercise (Forbes et al. 2008), the $\dot{\text{QO}}_{2\text{is}}$ -to- $\dot{\text{VO}}_{2\text{is}}$ matching in rodent muscles provides context when interpreting human experiments where gathering such data is technically infeasible at present.

Oxidative Capacity and Fast-twitch Interstitial PO₂ (Hypothesis #2)

During voluntary exercise in humans mean intracellular PO₂ measured during contractions of major locomotor muscles falls to ~3-5 mmHg (Richardson et al. 1995; Mole et al. 1999). However, those measurements represent a mosaic of fibre types and it is known that individual muscles with higher oxidative capacity exhibit greater microvascular \dot{Q}_{O_2} and microvascular-myocyte driving pressures (Behnke et al. 2003; McDonough et al. 2005). The current investigation illustrates that higher PO_{2is}'s are present within oxidative muscles compared to low-oxidative WG (Table 2 and Figure 1), and within fast-twitch muscles the oxidative PER and MG display faster PO_{2is} kinetics (i.e. τ ; Table 2) compared to the primarily glycolytic WG. Faster PO_{2is} kinetics (PER/MG < WG) likely reflect a combination of i) higher oxidative potential ($\dot{V}O_2$) compared to WG and ii) myoglobin-O₂ storage establishing greater PO_{2is} in PER and MG at rest with subsequent O₂ offloading during contractions enhancing the relative rate of PO_{2is} decline (i.e., Δ_1PO_{2is}/τ) in the initial ~30-60 seconds. Importantly, although myoglobin-mediated supply of O₂ for mitochondrial $\dot{V}O_2$ may slow PO_{2is} kinetics upstream, the concentration of mammalian myoglobin is minimal (<1 mM, Reynaferje, 1962; Hickson et al. 1981; Nemeth & Lowry, 1984; Terrados et al. 1990; Bekedam et al. 2009) and the current data suggests that the magnitude of intracellular $\dot{V}O_2$ in oxidative tissue outstrips myoglobin's ability to slow the absolute rate of PO_{2is} decline (i.e., τ and MRT) compared to myoglobin-lacking WG (Hickson 1981; Ordway & Garry, 2004). Myoglobin is thus anticipated to enhance the amount of O₂ available for mitochondria during contractions whilst not contributing significantly to slowing the kinetic response as assessed in the interstitial space.

The initial PO_{2is} decline is followed by a subsequent rise in PO_{2is} resulting from an elevated vascular response (increased \dot{Q}_{O_2} ; Behnke et al. 2011) and potentially transcapillary DO₂

(see *Transcapillary O₂ Diffusing Capacity*) on $\dot{Q}O_{2is}/\dot{V}O_{2is}$ matching (Δ_2PO_{2is} ; SOL/PER/MG > WG, Table 2). Ultimately, greater PO₂ in that compartment nearest the contracting myocyte (i.e. PO_{2is}) could potentially indicate a higher intramyocyte PO₂ and be crucial for limiting the amount of energy produced via glycolytic metabolism and the subsequent increase in fatigue-related metabolites (i.e., H⁺, Pi; Wilson et al. 1977; Hogan et al. 1992). In support of this notion, Richmond et al. (1999) determined, in the mixed fibre spinotrapezius muscle, that the ‘critical PO_{2is}’ is ~2.4–2.9 mmHg when aerobic metabolism becomes limited and glycolytic metabolism (assessed via NADH fluorescence) begins to increase. The WG in the present investigation reached ~3.0 mmHg during contractions which very likely decreased intracellular $\dot{V}O_2$ reflecting the requisite preservation of the interstitial-myocyte driving pressure of O₂.

Transcapillary PO₂ Gradient (Hypothesis #3a)

To support oxidative metabolism O₂ must move from O₂-carrying RBCs across plasma, capillary wall, interstitial space, sarcolemma, cytoplasm and then across the outer mitochondrial membrane. The pathway elements and physical barriers from RBC to sarcolemma are considered to constitute the carrier free region (CFR) where PO₂ gradients are necessary to drive blood-myocyte O₂ flux. Extending upon previous work in mesentery and skin (Tsai et al. 1998; Cabrales et al. 2006; Golub et al. 2007, 2008), Hirai and colleagues (2018) recently demonstrated a transcapillary PO₂ gradient in mixed fibre-type skeletal muscle of moderate oxidative capacity (48% type I+IIa fibres with CSa of 14 $\mu\text{mol min}^{-1} \text{ g}^{-1}$; from Delp & Duan, 1996). Interestingly, the lowest PO_{2is} (~7 mmHg) was still greater than previously measured intramuscular PO₂ during contractions (~3-5 mmHg; Mole et al. 1999; Richardson et al. 1995), highlighting a potential intermediate step in the O₂ cascade where separate microvascular-interstitial and interstitial-

myocyte pressure gradients exist. Data herein further supports the notion of an intermediate step in the O₂ cascade with the lowest PO₂*is* during the rest-contractions transient remaining above 6 mmHg in the more oxidative muscles (Figure 1).

Importantly, maintenance of a transcapillary and potentially interstitial-myocyte PO₂ gradient (see Figure 5) may be influenced by the metabolic demands of fast-twitch versus slow-twitch, and high-oxidative compared to low-oxidative muscles, relative to the supply of microvascular O₂ ($\dot{Q}O_2mv$). $\dot{Q}O_2mv$ increases immediately following the onset of contractions (<4 s) (reviewed by Joyner & Casey, 2015; Laughlin et al. 2012; Thomas & Segal 2004). Specifically, RBC flux in mixed fibre muscle increases in concert with $\dot{V}O_2mv$ which maintains PO₂*mv* (~4-16 s) and even PO₂*is* (~6-8 s) close to resting before falling precipitously to its nadir/steady-state levels (Behnke et al. 2001, 2002; Craig et al. 2018; Hirai et al. 2018; Kindig et al. 2002). In the microvascular compartment across the differing muscle compositions herein, slow-twitch SOL had a significantly longer time delay (TD) compared to fast-twitch muscles (Table 2). Assessing the TD (i.e., maintained $\dot{Q}O_2/\dot{V}O_2$ ratio) in microvascular PO₂, compared to the interstitial compartment, may provide insight into resting arterial saturation/extraction and RBC dynamics (thus O₂ diffusing conductance) immediately following contractions onset, especially when increases in $\dot{Q}O_2$ matches immediate (Behnke et al. 2002) or delayed (Grassi, 2005; Richardson et al. 2015) increases in $\dot{V}O_2$. Specifically, the slow twitch SOL had equivalent delays in both compartments suggesting that O₂ delivery into the microvascular compartment ($\dot{Q}O_2mv$) increased such that O₂ utilization from the blood ($\dot{V}O_2mv$, equal to $\dot{Q}O_2is$) increased in proportion to O₂ being utilized from the interstitial compartment ($\dot{V}O_2is$). Within fast-twitch oxidative muscle, however, PO₂*is* fell before PO₂*mv* in the PER yet had a longer TD in the MG. The ability of PO₂*is* to be maintained close to resting longer than PO₂*mv* in the MG suggests that RBC flux (and thus

DO_2 conductance) within the MG increased more rapidly than the PER. Beyond the initial few seconds, the MG had a significantly smaller transcapillary pressure gradient compared to rest (Time x ($\text{PO}_{2\text{mv}}-\text{PO}_{2\text{is}}$) interaction), further suggesting increased transcapillary DO_2 .

Figures 2A-D demonstrate that, even despite the transcapillary resistance to O_2 flux, the ability for $\dot{\text{QO}}_2$ into the microvascular compartment to match the increased $\dot{\text{VO}}_2$ out of the microvascular compartment in individual contracting muscles is paralleled in the interstitial space regardless of muscle fibre type and oxidative capacity (i.e., $\text{PO}_{2\text{mv}}-\text{PO}_{2\text{is}}$ is not significantly increased). Additionally, in fast-twitch oxidative muscle, the resistance to transcapillary O_2 flux may be reduced (Figures 2C and 4, also see *Transcapillary O₂ Diffusing Capacity* below) therefore revealing a greater proportional contribution of elevated transcapillary DO_2 to increase transcapillary O_2 flux during contractions. Previous studies have demonstrated augmented blood flow and elevated $\text{PO}_{2\text{mv}}$ utilizing exogenous nitric oxide donors such as sodium nitroprusside and nitrate/nitrite supplementation in health and disease (Colburn et al. 2017, Craig et al. 2018, 2019b, Ferguson et al. 2013a,b, 2015, 2016a,b, Ferreira et al. 2006a, Glean et al. 2015). Whether enhancing $\dot{\text{QO}}_{2\text{mv}}$ increases $\text{PO}_{2\text{is}}$ to a similar degree or widens $\text{PO}_{2\text{mv}}-\text{PO}_{2\text{is}}$ therefore increasing transcapillary driving pressure and decreasing the proportional reliance on transcapillary DO_2 for increasing O_2 flux, remains to be investigated. In studies where blood flow and O_2 delivery are altered (i.e., enzyme/channel inhibition studies and/or disease), the ability to measure blood flow and $\text{PO}_{2\text{is}}$ simultaneously, and subsequently to estimate muscle $\dot{\text{VO}}_2$, will enhance our understanding of the influence of extracellular PO_2 on controlling myocyte $\dot{\text{VO}}_2$, metabolism and contractile function.

Transcapillary O₂ Diffusing Capacity (Hypothesis #3b)

Comparing total PO_{2is} following the onset of contractions with respect to PO_{2mv} (Figure 4) provides the opportunity to assess how $\dot{V}O_2$ (increased consumption decreasing intracellular PO₂ and O₂ resistance), relative to $\dot{Q}O_2$ (high flux density increasing O₂ resistance), impacts the pressure gradient between microvascular and interstitial compartments. PO_{2mv} falls more slowly than PO_{2is} (i.e. greater τ and lesser $\Delta PO_2is/\tau$) in slow-twitch SOL and fast-twitch PER of similar oxidative capacity (~20-21 $\mu\text{mol min}^{-1} \text{ g}^{-1}$; Table 2) transiently increasing the PO_{2mv}-PO_{2is} gradient (Figures 2A-B). The greater total transcapillary driving pressure difference in SOL (Microvascular-Interstitial PO₂ area, Figure 4) suggests that the transient increase in PO_{2mv}-PO_{2is} was consequent to faster vasodilation and high $\dot{Q}O_2mv$ flux density limiting transcapillary O₂ diffusing conductance (Behnke et al. 2011, Dawson et al. 1987). Fast-twitch oxidative muscles (PER and MG) conversely exhibited lower total transcapillary O₂ driving pressure emphasizing a proportionally greater transcapillary DO₂. However, the more oxidative fast-twitch MG (~26 $\mu\text{mol min}^{-1} \text{ g}^{-1}$) begins from a lower resting PO_{2is} and falls at the same rate as PO_{2mv} supporting a greater $\dot{V}O_2$ throughout (Table 2 and Figure 2C), effectively reducing resistance to transcapillary O₂ flux immediately at contraction onset (i.e. decreased PO_{2mv}-PO_{2is}). Greater transcapillary PO₂ in the low-oxidative WG compared to PER and MG may mark the i) presence of low capillary:fibre surface area for transcapillary O₂ flux (Anderson & Henriksson, 1977; Dawson et al. 1987; Saltin & Gollnick, 1983) and/or ii) absence of a myoglobin O₂ store at rest (greater PO_{2mv}-PO_{2is}) which, if present, would be expected to desaturate rapidly during contractions to support mitochondrial O₂ provision and increase the relative fall in PO_{2is} (i.e., $\Delta_1 PO_2is/\tau$) as it facilitates intramyocytic DO₂. Therefore, increased DO_{2mv-mito} of contracting myoglobin-deficient fast-twitch muscle may extend the whole path of the carrier free region (CFR) in fast-twitch glycolytic (i.e. WG) yet

be largely localized to the narrow distance between microvascular and interstitial compartments within its myoglobin-containing oxidative counterparts (PER and MG; smaller PO_2mv - PO_2is). These interpretations extend further our mechanistic interpretation of increased O_2 diffusing conductance within contracting fast-twitch compared to slow-twitch muscle using PO_2mv and blood flow measurements (Ferreira et al. 2006; McDonough et al. 2005).

Implications for Exercise Training and Disease Conditions

Maximal aerobic capacity ($\dot{\text{V}}\text{O}_{2\text{max}}$) and submaximal exercise tolerance (critical speed) are reduced in disease (i.e., heart failure with reduced (HFrEF) and preserved (HFpEF) ejection fraction (Craig et al. 2019a; Mezzani et al. 2010, Poole et al. 2011, 2018), diabetes (Regensteiner et al. 1995), and COPD (Chiappa et al. 2008; Neder et al. 2000a)) and aging (Neder et al. 2000b; Ogawa et al. 1992). Specifically, PO_2mv (Behnke et al. 2004, 2005, 2007; Ferreira et al. 2006a; Padilla et al. 2007) and PO_2is (Craig et al. 2019b) are reduced in HFrEF and diabetes which lowers intramuscular PO_2 initiating increases in fatigue-related metabolites via increased reliance on glycolytic metabolism (Hogan et al. 1992; Wilson et al. 1977). Exercise training elevates mixed fibre PO_2mv (Hirai et al. 2014) and enhances $\dot{\text{Q}}\text{O}_{2\text{mv}}$ kinetics (Hirai et al. 2015; Laughlin & Roseguini, 2008) and myoglobin content in rats (Hickson et al. 1981) in a fibre type specific manner. These training-induced adaptations to O_2 delivery and storage likely permit tighter metabolic regulation of contracting PO_2is and intramuscular PO_2 . Considering the reduction in PO_2is of slow-twitch, but not fast-twitch glycolytic, muscle in HFrEF (Craig et al. 2019a), whether disease or aging impairs, or exercise training enhances, transcapillary PO_2 gradients (i.e., impairs/improves the total driving pressure for transcapillary O_2 flux) and transcapillary DO_2 (i.e.,

removes/enhances the proportional reliance on transcapillary DO₂ for O₂ flux) in a fibre type-specific manner warrants further investigation.

Experimental Considerations

The current investigation employed a large established data set of microvascular and interstitial PO₂ measurements under the same anesthesia and contraction protocols that afforded three key advantages: limiting surgical time, avoiding signal overlap of phosphorescence probes and reduction of animal numbers consistent with IACUC mandates. Namely, the availability of PO₂ measurements from separate animals in existing studies ensured that the preparations in each instance remained fresh and stable and were not compromised by extended elapsed time. Specifically, PO₂*is* measurement across multiple muscles entails surgical exposure and localized interstitial injections and blood gas sampling. To follow this with surgical access of opposing limb muscles, systemic infusion of phosphorescence probes, PO₂*mv* measurements and further blood gas sampling (Hirai et al. 2018) would have extended the protocol such that cardiovascular stability may be compromised. In light of these considerations, the current methodology aligns best with the IACUC mandates of both reduction and refinement.

Since interpretation of PO₂ changes from rest to exercise in any given compartment (i.e., microvascular or interstitial) and among separate muscles are dependent on adjustments in $\dot{Q}O_2$ and $\dot{V}O_2$, changes in intracellular $\dot{V}O_2$ during contractions could influence the measured PO₂ (i.e., WG). We therefore utilized previous blood flow data (Behnke et al. 2003, McDonough et al. 2005), capillary haematocrit at rest and during contractions (16 and 20%, respectively, Kindig et al 2002), together with current PO₂*mv* and O₂ saturation levels based on the O₂ dissociation curve (SOL: 35/17, PER: 23/6, MG: 24/6, and WG: 19/12%, rest/contractions, respectively) in order to infer,

to the best of our ability, changes in muscle $\dot{V}O_2$ during contractions (Table 3). Calculated increases in $\dot{V}O_{2mv}$ from rest to submaximal contractions were not different among fast-twitch muscles ($\Delta\dot{V}O_{2mv} \sim 7 \text{ ml O}_2 \text{ min}^{-1} 100g^{-1}$), with slow-twitch SOL having the greatest increase ($\Delta\dot{V}O_{2mv} \sim 11 \text{ ml O}_2 \text{ min}^{-1} 100g^{-1}$). Yet, the $\dot{Q}O_{2mv}/\dot{V}O_{2mv}$ matching during contractions was greatest in slow-twitch SOL (1.084) versus fast-twitch muscles, with WG (1.058) numerically greater compared to PER/MG (1.031). As mentioned previously, the WG likely reached a ‘critical PO_2is ’ which limited further increases in intracellular $\dot{V}O_2$ and demonstrated the smallest reduction in O_2 saturation (-7% versus -17-18% of the oxidative muscles). However, it is the $\dot{Q}O_{2mv}/\dot{V}O_{2mv}$ during contractions compared to that at rest which addresses vascular adjustments in supply ($\dot{Q}O_{2mv}$) to different levels of demand ($\dot{V}O_{2mv}$) between muscles. This assessment revealed that, in addition to limited intracellular $\dot{V}O_2$ (and thus $\dot{V}O_{2mv}$) of the WG, this low-oxidative muscle also had the smallest perturbation in $\Delta\dot{Q}O_{2mv}/\dot{V}O_{2mv}$ (-0.020 versus -0.065 in SOL/PER/MG) highlighting that, compared to the more oxidative muscles, O_2 in the WG microvascular compartment was unable to diffuse into the interstitial space even when the O_2 was available (i.e., low capillary:fibre ratio and surface area for O_2 flux keeping PO_{2mv} and O_2 saturation elevated despite very low PO_2is ; Anderson & Henriksson, 1977; Dawson et al. 1987, Saltin & Gollnick, 1983). Thus, these calculations support the interpretations to the proportional reliance on sustained transcapillary O_2 driving pressures ($PO_{2mv}-PO_2is$ of slow-twitch oxidative and fast-twitch glycolytic) and/or enhanced diffusive O_2 conductance (fast-twitch oxidative MG, and potentially PER) contributing to the present transcapillary PO_2 gradients throughout the transition to increased metabolic demands (Figure 4).

Conclusions

These data are the first to demonstrate a significant transmural PO₂ gradient between microvascular and interstitial compartments in muscles spanning the fibre type and oxidative capacity continuum. The significant PO₂ gradient between red blood cell and adjacent sarcolemma (referred to as the “carrier free region”, CFR) present at rest is maintained throughout submaximal twitch contractions (Hypothesis #3). Since the magnitude of the transcapillary PO₂ gradient is maintained in slow-twitch SOL the interstitial-myocyte driving pressure for O₂ flux (i.e. PO_{2is}) of slow-twitch fibres is greater, and falls at a slower rate, compared to fast-twitch muscle (Hypothesis #1), as demonstrated previously in the microvascular compartment. Fast-twitch muscles with greater oxidative capacity maintain a higher PO_{2is} than their low-oxidative glycolytic counterpart to support greater O₂ metabolism (Hypothesis #2). Accordingly, there is a graded reduction in total interstitial O₂ driving pressure throughout the rest-contraction transient (PO_{2 area}) from slow-twitch oxidative to fast-twitch glycolytic. As dictated by Fick’s law of diffusion for O₂ flux across the capillary wall ($\dot{V}O_2 = DO_2 \times (PO_{2mv} - PO_{2is})$), increases in O₂ flux ($\dot{V}O_2$) must result from increases in effective diffusing conductance (DO₂; primarily capillary red blood cell haemodynamics and distribution). In the case of fast-twitch oxidative muscle, the transcapillary DO₂ must increase further in the face of decreased PO_{2mv}-PO_{2is}. Therefore, there is an apparent interplay between the functional influence of physical properties within muscles of differing fibre composition (i.e., capillarity and vascular reactivity) and intracellular oxidative potential (i.e., high $\dot{V}O_{2is}$ in fast-twitch muscle or decreased $\dot{V}O_{2is}$ in critically low O₂ environments) in establishing PO_{2is} during contractions. This dynamic interplay manifests in either sustaining the transcapillary O₂ driving pressures present at rest (PO_{2mv}-PO_{2is} of slow-twitch oxidative and fast-twitch glycolytic) and/or further enhancing diffusive O₂ conductance (decreasing PO_{2mv}-PO_{2is} in fast-

twitch oxidative MG, and potentially PER) to increase O₂ flux into the space nearest the contracting myocyte.

References

- Anderson P & Henriksson J (1977). Capillary supply of the quadriceps femoris muscle on man: adaptive response to exercise. *J Physiol* **270**, 677-690.
- Armstrong RB & Laughlin MH (1984). Exercise blood flow patterns within and among rats after training. *Am J Physiol* **246**, H59-68.
- Armstrong RB & Laughlin MH (1985). Rat muscle blood flows during high-speed locomotion. *J Appl Physiol* **59**, 1322-1328.
- Behnke BJ, Armstrong RB & Delp MD (2011). Adrenergic control of vascular resistance varies in muscles composed of different fiber types: influence of the vascular endothelium. *Am J Physiol Regul Integr Comp Physiol* **301**: R783-R790.
- Behnke BJ, Barstow TJ, Kindig CA, McDonough P, Musch TI & Poole DC (2002). Dynamics of oxygen uptake following exercise onset in rat skeletal muscle. *Respir Phys & Neurobiol* **133**: 229-239.
- Behnke BJ, Delp MD, Dougherty PJ, Musch TI & Poole DC (2005). Effects of aging on microvascular oxygen pressures in rat skeletal muscle. *Respir Physiol Neurobiol* **146**, 259-268.
- Behnke BJ, Delp MD, McDonough P, Spier SA, Poole DC & Musch TI (2004). Effects of chronic heart failure on microvascular oxygen exchange dynamics in muscles of contrasting fiber type. *Cardiovascular Research* **61**: 325-332.
- Behnke BJ, Delp MD, Poole DC & Musch TI (2007). Aging potentiates the effect of congestive heart failure on muscle microvascular oxygenation. *J Appl Physiol* **103**, 1757-1763.
- Behnke BJ, Kindig CA, Musch TI, Koga S & Poole DC (2001). Dynamics of microvascular oxygen pressure across the rest-exercise transition in rat skeletal muscle. *Respir Physiol* **126**: 53-63.
- Behnke BJ, McDonough P, Padilla DJ, Musch TI & Poole DC (2003). Oxygen exchange profile in rat muscles of contrasting fibre types. *J Physiol* **549.2**, 597-605.
- Behnke BJ, Padilla DJ, Ferreira LF, Delp MD, Musch TI & Poole DC (2006). Effects of arterial hypotension on microvascular oxygen exchange in contracting skeletal muscle. *J Appl Physiol* **100**, 1019-1026.
- Bekedam MA, van Beek-Harmsen BJ, van Mechelen W, Boonstra A & van der Laarse WJ (2009). Myoglobin concentration in skeletal muscle fibers of chronic heart failure patients. *J Appl Physiol* **107**, 1138-1143.
- Cabralles P, Tsai AG, Johnson PC & Intaglietta M (2006). Oxygen release from arterioles with normal flow and no-flow conditions. *J Appl Physiol* **100**, 1569-1576.
- Chiappa GR, Borghi-Silva A, Ferreira LF, Carrascosa C, Oliveira CC, Maia J, Gimenes AC, Queiroga Jr F, Berton D, Ferreira EM, Nery LE & Neder JA (2008). Kinetics of muscle deoxygenation are accelerated at the onset of heavy-intensity exercise in patients with COPD: relationship to central cardiovascular dynamics. *J Appl Physiol* **104**, 1341-1350.

Colburn TD, Ferguson SK, Holdsworth CT, Craig JC, Musch TI & Poole DC (2017). Effect of sodium nitrite on local control of contracting skeletal muscle microvascular oxygen pressure in healthy rats. *J Appl Physiol* **122**, 153-160.

Copp SW, Hirai DM, Musch TI & Poole DC (2010). Critical speed in the rat: implications for hindlimb muscle blood flow distribution and fibre recruitment. *J Physiol* **588.24**, 5077-5087.

Craig JC*, Colburn TD*, Caldwell JT, Hirai DM, Tabuchi A, Baumfalk DR, Behnke BJ, Ade CJ, Musch TI & Poole DC (2019a). Central and peripheral factors mechanistically linked to exercise intolerance in heart failure with reduced ejection fraction. *Am J Physiol Heart Circ Physiol* **317**, H434-H444.

Craig JC, Colburn TD, Hirai DM, Schettler MJ, Musch TI & Poole DC (2018). Sex and nitric oxide bioavailability interact to modulate interstitial PO₂ in healthy rat skeletal muscle. *J Appl Physiol* **124**, 1558-1566.

Craig JC, Colburn TD, Hirai DM, Musch TI & Poole DC (2019b). Sexual dimorphism in the control of skeletal muscle interstitial PO₂ of heart failure rats: effects of dietary nitrate supplementation. *J Appl Physiol* **126**, 1184-1192.

Dawson JM, Tyler KR & Hudlicka O (1987). A comparison of the microcirculation in rat fast glycolytic and slow oxidative muscles at rest and during contractions. *Microvasc Res* **33**, 167-182.

Delp MD & Duan C (1996). Composition and size of type I, IIA, IID/X, and IIB fibers and citrate synthase activity of rat muscle. *J Appl Physiol* (1985) **80**: 261-270.

Dunphy I, Vinogradov SA & Wilson DF (2002). Oxyphor R2 and G2: phosphors for measuring oxygen by oxygendifependent quenching of phosphorescence. *Anal Biochem* **310**, 191-198.

Edgerton VR, Smith JL & Simpson DR (1975). Muscle fibre type populations of human leg muscles. *Histochem J* **7**, 259-266.

Esipova TV, Karagodov A, Miller J, Wilson DF, Busch TM & Vinogradov SA (2011). Two new ‘protected’ oxyphors for biological oximetry: properties and application in tumor imaging. *Anal Chem* **83**, 8756-8765.

Fedderspiel WJ & Popel AS (1986). A theoretical analysis of the effect of the particulate nature of blood on oxygen release in capillaries. *Microvasc Res* **32**, 164-189.

Ferguson SK, Glean AA, Holdsworth CT, Wright JL, Fees AJ, Colburn TD, Stabler T, Allen JD, Jones AM, Musch TI & Poole DC (2016a). Skeletal muscle vascular control during exercise: impact of nitrite infusion during nitric oxide synthase inhibition in healthy rats. *J Cardiovasc Pharmacol Ther* **21**, 201-208.

Ferguson SK, Hirai DM, Copp SW, Holdsworth CT, Allen JD, Jones AM, Musch TI & Poole DC (2013a). Effects of nitrate supplementation via beetroot juice on contracting rat skeletal muscle microvascular oxygen pressure dynamics. *Respir Physiol Neurobiol* **187**, 250-255.

Ferguson SK, Hirai DM, Copp SW, Holdsworth CT, Allen JD, Jones AM, Musch TI & Poole DC (2013b). Impact of dietary nitrate supplementation via beetroot juice on exercising muscle vascular control in rats. *J Physiol* **591**, 547-557.

- Ferguson SK, Holdsworth CT, Colburn TD, Wright JL, Craig JC, Fees AJ, Jones AM, Allen JD, Musch TI & Poole DC (2016b). Dietary nitrate supplementation: impact on skeletal muscle vascular control in exercising rats with chronic heart failure. *J Appl Physiol* **121**: 661-669.
- Ferguson SK, Holdsworth CT, Wright JL, Fees AJ, Allen JD, Jones AM, Musch TI & Poole DC (2015). Microvascular oxygen pressures in muscles comprised of different fiber types: impact of dietary nitrate supplementation. *Nitric Oxide* **48**, 38-43.
- Ferreira LF, Hageman KS, Hahn SA, Williams J, Padilla DJ, Poole DC & Musch TI (2006a). Muscle microvascular oxygenation in chronic heart failure: role of nitric oxide availability. *Acta Physiol* **188**, 3-13.
- Ferreira LF, McDonough P, Behnke BJ, Musch TI & Poole DC (2006b). Blood flow and O₂ extraction as a function of O₂ uptake in muscles composed of different fiber types. *Respir Physiol Neurobiol* **153**, 237-249.
- Forbes SC, Paganini AT, Slade JM, Towse TF & Meyer RA (2008). Phosphocreatine recovery kinetics following low- and high-intensity exercise in human triceps surae and rat posterior hindlimb muscles. *Am J Physiol Reg Integr Comp Physiol* **296**, R161-170.
- Gayeski TE & Honig CR (1986). O₂ gradients from sarcolemma to cell interior in red muscle at maximal VO₂. *Am J Physiol Heart Circ Physiol* **251**, H789-H799.
- Glean AA, Ferguson SK, Holdsworth CT, Colburn TD, Wright JL, Fees AJ, Hageman KS, Poole DC & Musch TI (2015). Effects of nitrite infusion on skeletal muscle vascular control during exercise in rats with chronic heart failure. *Am J Physiol Heart Circ Physiol* **309**, H1354-H1360.
- Golub AS, Barker MC & Pittman RN (2007). PO₂ profiles near arterioles and tissue oxygen consumption in rat mesentery. *Am J Physiol Heart Circ Physiol* **293**, H1097-H1106.
- Golub AS, Barker MC & Pittman RN (2008). Microvascular oxygen tension in the rat mesentery. *Am J Physiol Heart Circ Physiol* **294**, H21-H28.
- Golub AS & Pittman RN (2005). Erythrocyte-associated transients in PO₂ revealed in capillaries of rat mesentery. *Am J Physiol Heart Circ Physiol* **288**, H2735-H2743.
- Grassi B (2005). Delayed Metabolic Activation of Oxidative Phosphorylation in Skeletal Muscle at Exercise Onset. *Med Sci Sports Exerc* **37**, 1567-1573.
- Groebel K & Thews G (1990). Calculated intra- and extracellular PO₂ gradients in heavily working red muscle. *Am J Physiol Heart Circ Physiol* **259**, H84-H92.
- Grundy D (2015). Principles and standards for reporting animal experiments in The Journal of Physiology and Experimental Physiology. *J Physiol* **593**, 2547-2549.
- Heinonen I, Koga S, Kallikoski KK, Musch TI & Poole DC (2015). Heterogeneity of muscle blood flow and metabolism: influence of exercise, aging and disease states. *Exerc Sport Sci Rev* **43**, 117-1224.
- Hickson RC (1981). Skeletal muscle cytochrome c and myoglobin, endurance, and frequency of training. *J Appl Physiol Respirat Environ Exercise Physiol* **51**: 746-749.

- Hirai DM, Colburn TD, Craig JC, Hotta, Kano Y, Musch TI & Poole DC (2019). Skeletal muscle interstitial O₂ pressures: bridging the gap between the capillary and myocyte. *Microcirculation*. 2019; 26:e12497.
- Hirai DM, Copp SW, Holdsworth CT, Ferguson SK, McCullough DJ, Behnke BJ, Musch TI & Poole DC (2014). Skeletal muscle microvascular oxygenation dynamic in heart failure: exercise training and nitric oxide-mediated function. *Am J Physiol Heart Circ Physiol* **306**, H690-H698.
- Hirai DM, Craig JC, Colburn TD, Eshima H, Kano Y, Sexton WL, Musch TI & Poole DC (2018). Skeletal muscle microvascular and interstitial PO₂ from rest to contractions. *J Physiol* **596**, 869-883.
- Hirai DM, Musch TI & Poole DC (2015). Exercise training in chronic heart failure: improving skeletal muscle O₂ transport and utilization. *Am J Physiol Heart Circ Physiol* **309**, H1419-H1439.
- Hogan MC, Arthur PG, Bebout DE, Hochachka PW & Wagner PD (1992). Role of O₂ in regulating tissue respiration in dog muscle working in situ. *J Appl Physiol* (1985) **73**, 728-736.
- Honig CR & Gayeski TE (1993). Resistance to O₂ diffusion in anemic red muscle: roles of flux density and cell PO₂. *Am J Physiol Heart Circ Physiol* **265**, H868–H875.
- Johnson MA, Polgar J, Weightman D & Appleton D (1973). Data on the distribution of fibre types in thirty-six human muscles. An autopsy study. *J Neurol Sci* **18**, 111-129.
- Joyner MJ & Casey DP (2015). Regulation of increased blood flow (hyperemia) to muscles during exercise: a hierarchy of competing physiological needs. *Physiol Rev* **95**, 549-601.
- Kindig CA, Richardson TE & Poole DC (2002). Skeletal muscle capillary hemodynamics from rest to contractions: implications for oxygen transfer. *J Appl Physiol* **92**, 2513-2520.
- Laughlin MH, Davis MJ, Secher NH, van Lieshout JJ, Arce-Esquivel AA, Simmons GH, Bender SB, Padilla J, Bache RJ, Merkus D & Duncker DJ (2012). Peripheral Circulation. *Compr Physiol* **2**, 321-447.
- Laughlin MG & Roseguini B (2008). Mechanisms for exercise training-induced increases in skeletal muscle blood flow capacity: differences with interval sprint training versus aerobic endurance training. *J Physiol Pharmacol* **59**, 71-88.
- Lo LW, Vinogradov SA, Koch CJ & Wilson DF (1997). A new, water soluble, phosphor for oxygen measurements in vivo. *Adv Exp Med Biol* 428, 651-656.
- McDonough P, Behnke BJ, Padilla DJ, Musch TI & Poole DC (2005). Control of microvascular oxygen pressures in rat muscles comprised of different fibre types. *J Physiol* **563**, 903-913.
- McDonough P, Behnke BJ, Kindig CA & Poole DC (2001). Rat microvascular PO₂ kinetics during the exercise-off transient. *Exp Physiol* **86**, 349-356.
- Mezzani A, Corrà U, Giordano A, Colombo S, Psaroudaki M & Gianuzzi P (2010). Upper intensity limit for prolonged aerobic exercise in chronic heart failure. *Med Sci Sports Exerc* **42**, 633-639.

- Molé PA, Chung Y, Tran TK, Sailasuta N, Hurd R & Jue T (1999). Myoglobin desaturation with exercise intensity in human gastrocnemius muscle. *Am J Physiol Regul Integr Comp Physiol* **277**, R173–R180.
- Neder JA, Jones PW, Nery LE & Whipp BJ (2000a). Determinants of the Exercise Endurance Capacity in Patients with Chronic Obstructive Pulmonary Disease: The Power-Duration Relationship. *Am J Respir Crit Care Med* **162**, 497-504.
- Neder JA, Jones PW, Nery LE & Whipp BJ (2000b). The effect of age on the power/duration relationship and the intensity-domain limits in sedentary men. *Eur J Appl Physiol* **82**, 326-332.
- Nemeth PM & Lowry OH (1984). Myoglobin Levels in Individual Human Skeletal Muscle Fibers of Different Type. *J Histochem Cytochem* **32**, 1211-1216.
- Ogawa T, Spina RJ, Martin III WH, Kohrt WM, Schechtman KB, Holloszy JO & Ehsani AA (1992). Effects of Aging, Sex, and Physical Training on Cardiovascular Responses to Exercise. *Circulation* **86**, 494-503.
- Ordway GA & Garry DJ (2004). Myoglobin: an essential hemoprotein in striated muscle. *J Exp Biol* **207**, 3441-3446.
- Padilla DJ, McDonough P, Behnke BJ, Kano Y, Hageman SK, Musch TI & Poole DC (2007). Effects of Type II diabetes on muscle microvascular oxygen pressures. *Respir Physiol Neurobiol* **156**, 187-195.
- Poole DC, Behnke BJ, McDonough P, McAllister RM & Wilson DF (2004). Measurement of muscle microvascular oxygen pressures: compartmentalization of phosphorescent probe. *Microcirculation* **11**, 317-326.
- Poole DC, Hirai DM, Copp SW & Musch TI (2012). Muscle oxygen transport and utilization in heart failure: implications for exercise (in)tolerance. *Am J Physiol Heart Circ Physiol* **302**, H1050-H1063.
- Poole DC & Mathieu-Costello O (1997). Effect of pulmonary emphysema on diaphragm capillary geometry. *J Appl Physiol* **82**, 599-606.
- Poole DC, Richardson RS, Haykowsky MJ, Hirai DM & Musch TI (2018). Exercise limitations in heart failure with reduced and preserved ejection fraction. *J Appl Physiol* **124**, 208-224.
- Regensteiner JG, Sippel J, McFarling ET, Wolfel EE & Hiatt WR (1995). Effects of non-insulin dependent diabetes on maximal exercise performance. *Med Sci Sports Exerc* **27**, 875-881.
- Reynafarje B (1962). Myoglobin content and enzymatic activity of muscle and altitude adaptation. *J Appl Physiol* **17**, 301-305.
- Richardson RS, Noyszewski EA, Kendrick KF, Leigh JS & Wagner PD (1995). Myoglobin O₂ desaturation during exercise. Evidence of limited O₂ transport. *J Clin Invest* **96**, 1916–1926.
- Richardson RS, Wary C, Wray DW, Hoff J, Rossiter HB, Layec G & Carlier PG (2015). MRS Evidence of Adequate O₂ Supply in Human Skeletal Muscle at the Onset of Exercise. *Med Sci Sports Exerc* **47**, 2299-2307.

- Richmand KN, Shonat RD, Lynch RM & Johnson PC (1999). Critical PO₂ of skeletal muscle in vivo. *Am J Physiol Heart Circ Physiol* **277**, H1831-H1840.
- Roca J, Agusti AG, Alonso A, Poole DC, Viegas C, Barbera JA, Rodriguez-Roisin R, Ferrer A & Wagner PD (1992). Effects of training on muscle O₂ transport at VO_{2max}. *J Appl Physiol* **73**, 1067-1076.
- Saltin B & Gollnick PD (1983). Skeletal muscle adaptability: significance for metabolism and performance. In: Peachy LD, Adrian RH, Geiger SR, editors. *Handbook of Physiology, Skeletal Muscle*. Bethesda, USA: American Physiological Society, pp. 555-631.
- Smith LM, Golub AS & Pittman RN (2002). Interstitial PO₂ determination by phosphorescence quenching microscopy. *Microcirculation* **9**, 389-395.
- Terrados N, Jansson E, Sylven C & Kaijser L (1990). Is hypoxia a stimulus for synthesis of oxidative enzymes and myoglobin? *J Appl Physiol* **68**, 2369-2372.
- Thomas GD & Segal SS (2004). Neural control of muscle blood flow during exercise. *J Appl Physiol* **97**, 731-738.
- Tsai AG, Friesenecker B, Mazzoni MC, Kerger H, Buerk DG, Johnson PC & Intaglietta M (1998). Microvascular and tissue oxygen gradients in the rat mesentery. *Proc Natl Acad Sci USA* **95**, 6590-6595.
- Wilson DF, Lee WMF, Makonnen S, Finikova O, Apreleva S & Vinogradov SA (2006). Oxygen pressures in the interstitial space and their relationship to those in the blood plasma in resting skeletal muscle. *J Appl Physiol* **101**, 1648-1656.
- Wilson DF, Erecinska M, Drown C & Silver IA (1977). Effect of oxygen tension on cellular energetics. *Am J Physiol Cell Physiol* **233**: C135-C140.

Table 2.1. Arterial blood samples following microvascular and interstitial PO₂ measurements

	Soleus		Peroneal		Mixed Gastrocnemius		White Gastrocnemius	
	PO _{2mv}	PO _{2is}	PO _{2mv}	PO _{2is}	PO _{2mv}	PO _{2is}	PO _{2mv}	PO _{2is}
Arterial pH	7.40 ± 0.06	7.41 ± 0.05	7.38 ± 0.05	7.44 ± 0.04	7.42 ± 0.06	7.41 ± 0.03	7.40 ± 0.08	7.42 ± 0.04
O₂ Saturation (%)	93.6 ± 4.8	87.2 ± 12.9	91.6 ± 6.2	91.1 ± 2.1	95.3 ± 3.2 ‡	91.4 ± 3.5	93.9 ± 5.3	89.7 ± 4.2
Systemic Haematocrit (%)	35.4 ± 5.8	31.1 ± 4.3	34.5 ± 6.1	35.6 ± 1.1	36.3 ± 6.2	34.1 ± 4.3	40.0 ^	34.1 ± 2.9
Lactate (mM)	1.4 ± 0.4	1.0 ± 0.5	0.9 ± 0.3 ‡	2.4 ± 0.5 *	1.6 ± 0.2	1.4 ± 0.3 #	1.8 ± 0.2	1.4 ± 0.6 #

Data are mean ± SD and compared via One-Way ANOVA with Bonferroni correction for multiple comparisons. See Figures 2A-D for the sample size of each group. ‡ p < 0.05 vs PO_{2is}; * p < 0.05 vs SOL; # p < 0.05 vs PER; ^ p < 0.05 vs MG. ^ Systemic Haematocrit analysis was only available for one White Gastrocnemius PO_{2mv}.

Table 2.2. Microvascular and interstitial PO₂ kinetics parameters following the onset of twitch contractions

	Soleus		Peroneal		Mixed Gastrocnemius		White Gastrocnemius	
	PO _{2mv}	PO _{2is}	PO _{2mv}	PO _{2is}	PO _{2mv}	PO _{2is}	PO _{2mv}	PO _{2is}
PO _{2 BL} (mmHg)	29.8 ± 5.1 ‡	20.0 ± 5.3	23.9 ± 4.4 ‡*	18.3 ± 6.2	24.2 ± 3.6 ‡*	13.3 ± 2.7 *#	21.8 ± 3.6 ‡*	8.9 ± 3.3 *#†
Δ ₁ PO ₂ (mmHg)	9.9 ± 2.7	10.5 ± 3.3	12.2 ± 3.2	10.9 ± 3.8	10.7 ± 3.9 ‡	7.0 ± 2.2 *#	5.2 ± 1.1 *#†	5.9 ± 2.7 *#
TD (s)	14.6 ± 5.6	13.7 ± 3.7	9.0 ± 3.5 ‡*	3.9 ± 3.0 *	5.8 ± 5.4 *	8.1 ± 2.5 *#	4.2 ± 1.2 *#	4.1 ± 1.6 *†
τ (s)	23.6 ± 7.5 ‡	16.8 ± 1.3	14.1 ± 1.8 ‡*	10.8 ± 2.6 *	13.2 ± 5.0 *	12.7 ± 3.8 *	14.7 ± 5.0 *	16.9 ± 4.6 #†
MRT (s)	38.3 ± 9.7 ‡	30.5 ± 7.5	23.1 ± 3.8 ‡*	14.7 ± 3.1 *	19.0 ± 6.5 *	20.8 ± 5.6 *#	18.9 ± 6.1 *	21.0 ± 5.2 *#
PO _{2 nadir}	19.9 ± 4.6 ‡	9.4 ± 3.9	11.7 ± 5.0 ‡*	7.4 ± 3.3	13.5 ± 1.3 ‡*	6.3 ± 1.5 *	16.7 ± 2.5 ‡†	3.0 ± 1.4 *#†
Δ ₂ PO ₂ (mmHg)	0.6 ± 0.5 ‡	1.1 ± 0.8	1.7 ± 1.9 *	2.1 ± 1.4 *	- 0.1 ± 0.2 ‡*#	0.8 ± 0.6 #	0.7 ± 0.9 †	0.5 ± 0.4 *#†
PO _{2 end} (mmHg)	20.4 ± 4.6 ‡	10.5 ± 4.2	13.4 ± 5.2 ‡*	9.5 ± 3.4	13.4 ± 1.4 ‡*	7.1 ± 1.7 *#	17.4 ± 1.7 ‡†	3.5 ± 1.6 *#†
Δ ₁ PO ₂ /τ (mmHg/s)	0.47 ± 0.25 ‡	0.71 ± 0.36	0.87 ± 0.17 *	1.05 ± 0.40 *	0.82 ± 0.20 ‡*	0.60 ± 0.26 #	0.38 ± 0.12 #†	0.35 ± 0.14 *#†

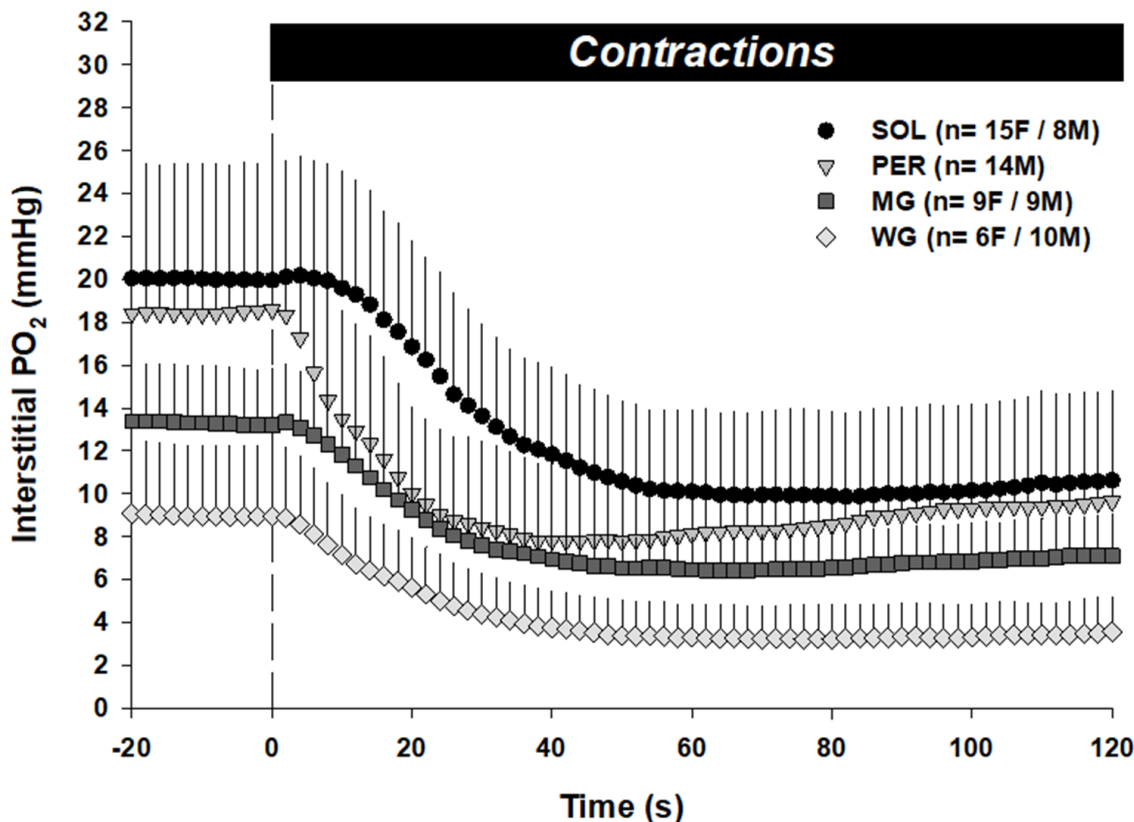
PO_{2mv}, microvascular PO₂; PO_{2is}, interstitial PO₂; PO_{2 BL}, resting baseline PO₂; Δ₁PO₂ and Δ₂PO₂, amplitude of the first and second components, respectively; TD, time delay; τ, time constant; MRT, mean response time; PO_{2 nadir}, lowest response prior to secondary rise in PO₂; PO_{2 end}, PO₂ at the end of contractions; Δ₁PO₂/τ, rate of PO₂ fall. Data are mean ± SD and compared via unpaired Student's *t*-tests. See Figures 2A-D for the sample size of each group. ‡ p < 0.05 vs PO_{2is}; * p < 0.05 vs SOL; # p < 0.05 vs PER; † p < 0.05 vs MG.

Table 2.3. Microvascular oxygen transport from rest to contractions

	O ₂ Sat (%)	Hct (%)	Q̇m (ml min ⁻¹ 100g ⁻¹)	Q̇O _{2mv} (ml O ₂ min ⁻¹ 100g ⁻¹)	VŌ _{2mv} (ml min ⁻¹ 100g ⁻¹)	DO _{2mv-mito} (ml O ₂ min ⁻¹ mmHg ⁻¹ 100g ⁻¹)	Q̇O _{2mv} /VŌ _{2mv}
SOL Rest	35	16	27	5.35	4.65	0.156	1.149
SOL End	17	20	85	16.83	15.52	0.761	1.084
PER Rest	23	16	8	1.58	1.45	0.061	1.095
PER End	6	20	46	9.11	8.83	0.659	1.031
MG Rest	24	16	6	1.19	1.08	0.045	1.098
MG End	6	20	42	8.31	8.06	0.602	1.031
WG Rest	19	16	8	1.58	1.47	0.067	1.078
WG End	12	20	45	8.91	8.42	0.484	1.058

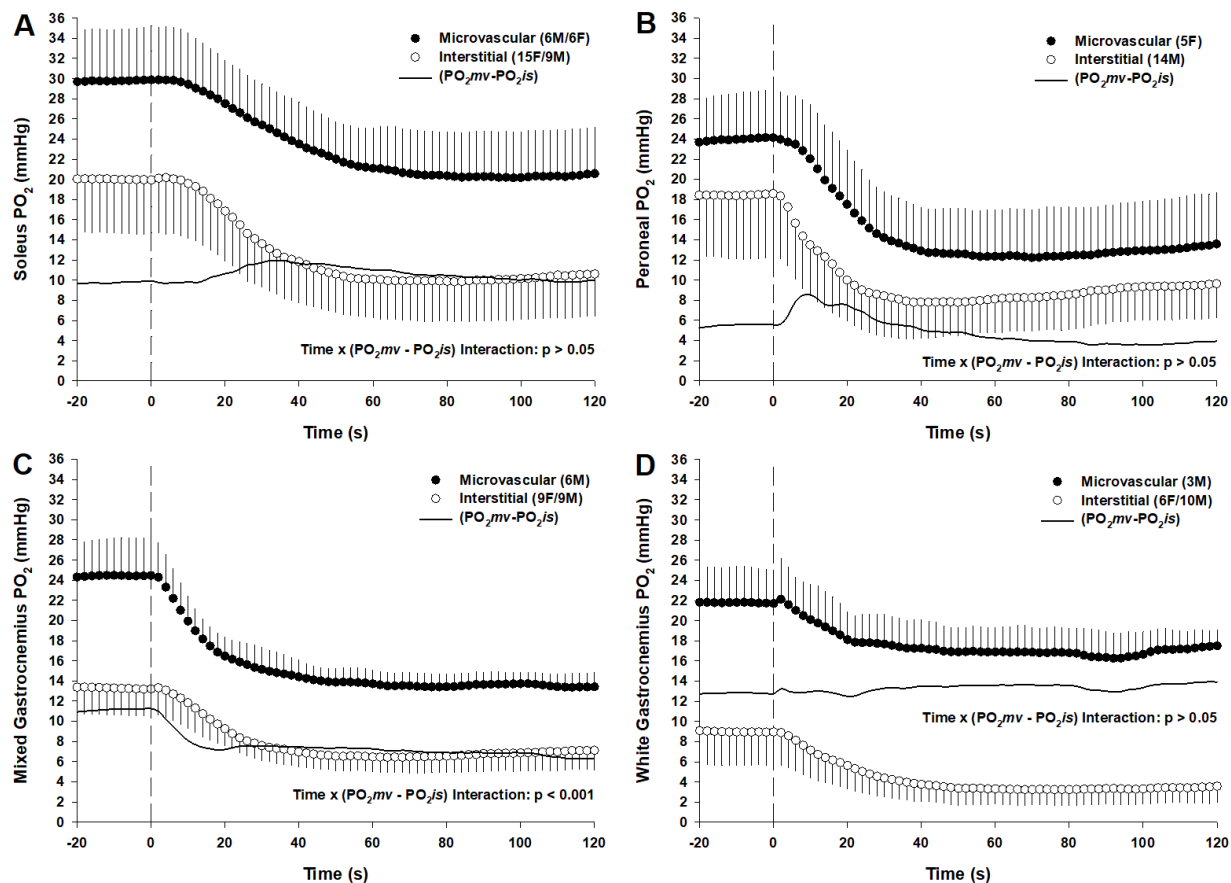
Microvascular oxygen delivery ($\dot{Q}O_{2mv}$), utilization ($\dot{V}O_{2mv}$) and diffusing conductance ($DO_{2mv-mito}$) at rest and at the end of 120 s of twitch contractions. The Fick equation was used to calculate $\dot{V}O_{2mv}$ (i.e., $\dot{V}O_{2mv} = \dot{Q}m \times (CaO_2 - CvO_2)$) assuming the present PO_{2mv} is analogous to venous PO_2 (McDonough et al. 2001) and, by extension from the O_2 dissociation curve, venous blood O_2 content (Roca et al. 1992). Thus venous O_2 contents (CvO_2) were calculated $[(1.34 \text{ ml } O_2 \text{ (gHb)}^{-1} \times (Hct/3) \times \%O_2 \text{ Saturation}) + (PO_{2mv} \times 0.003)]$ based on the constructed rat O_2 dissociation curve with Hill coefficient (n) of 2.6 to obtain O_2 saturation ($O_2 \text{ Sat}$) from the present PO_{2mv} (see Table 2), an O_2 carrying capacity of $1.34 \text{ ml } O_2 \text{ (gHb)}^{-1}$, haemoglobin (Hb) concentration using capillary haematocrit at rest and during contractions (Kindig et al. 2002), and a P_{50} of 38 (the PO_2 at which Hb is 50% saturated with O_2). $\dot{Q}O_{2mv}$ (i.e., $\dot{Q}O_{2mv} = \dot{Q}m \times CaO_2$) and $\dot{V}O_{2mv}$ utilizing extant blood flow ($\dot{Q}m$; Behnke et al. 2003, McDonough et al. 2005) and capillary haematocrit during rest and contractions (Hct; Kindig et al. 2002). $DO_{2mv-mito}$ was defined as $\dot{V}O_{2mv}/PO_{2mv}$ and provides an index of diffusive O_2 transport per unit of O_2 driving pressure. $\dot{Q}O_{2mv}/\dot{V}O_{2mv}$ emphasizes the degree of O_2 delivery relative to O_2 utilization (i.e., higher values suggesting greater muscle perfusion per unit of intramyocyte $\dot{V}O_2$).

Figure 2.1. Interstitial PO₂ from rest to contractions in muscles of differing fibre type and oxidative capacity



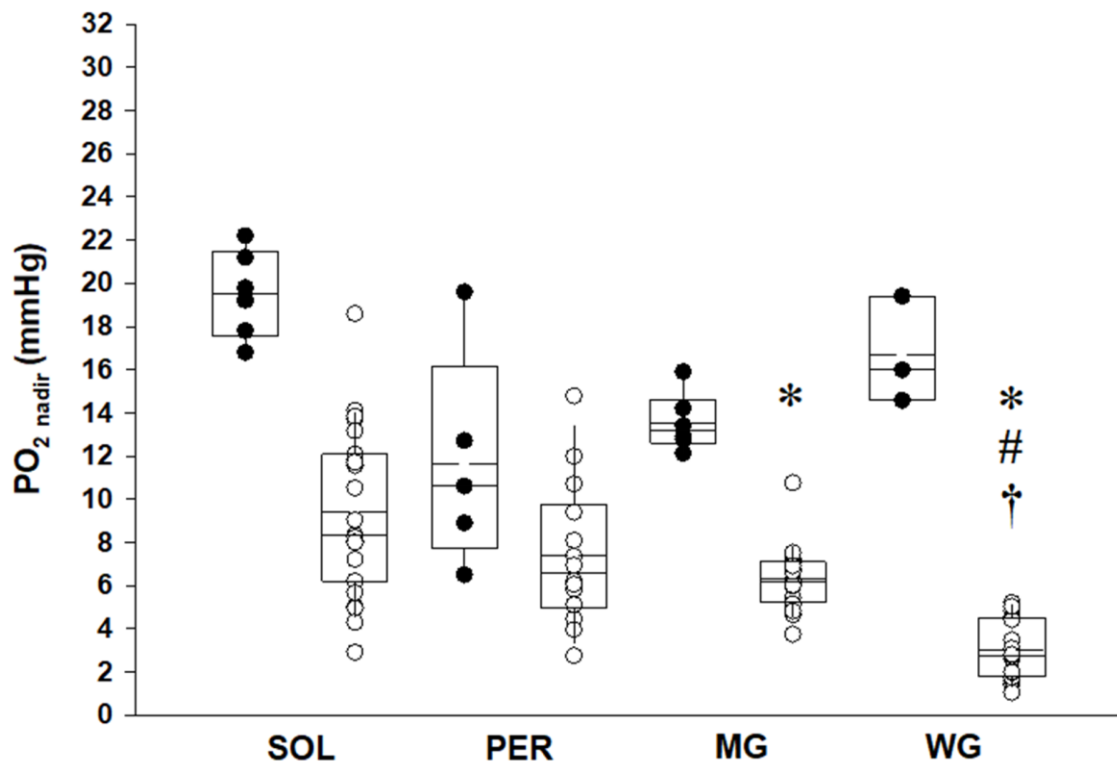
Note the significantly greater PO₂is of slow-twitch oxidative soleus (SOL; circle; CSa $\sim 21 \mu\text{mol min}^{-1} \text{ g}^{-1}$) muscle compared to fast-twitch oxidative peroneal (PER; downward triangle; CSa $\sim 20 \mu\text{mol min}^{-1} \text{ g}^{-1}$) and mixed gastrocnemius (MG; square; CSa $\sim 26 \mu\text{mol min}^{-1} \text{ g}^{-1}$) muscles. Additionally, within fast-twitch muscles, PER and MG remained greater than the glycolytic white gastrocnemius (WG; diamond; CSa $\sim 8 \mu\text{mol min}^{-1} \text{ g}^{-1}$). Time zero depicts the onset of twitch contractions. Data are mean \pm SD. Citrate synthase activity (CSa) data are from Delp & Duan (1996).

Figures 2.2A-D. Microvascular and interstitial PO₂ and transcapillary PO₂ from rest to contractions



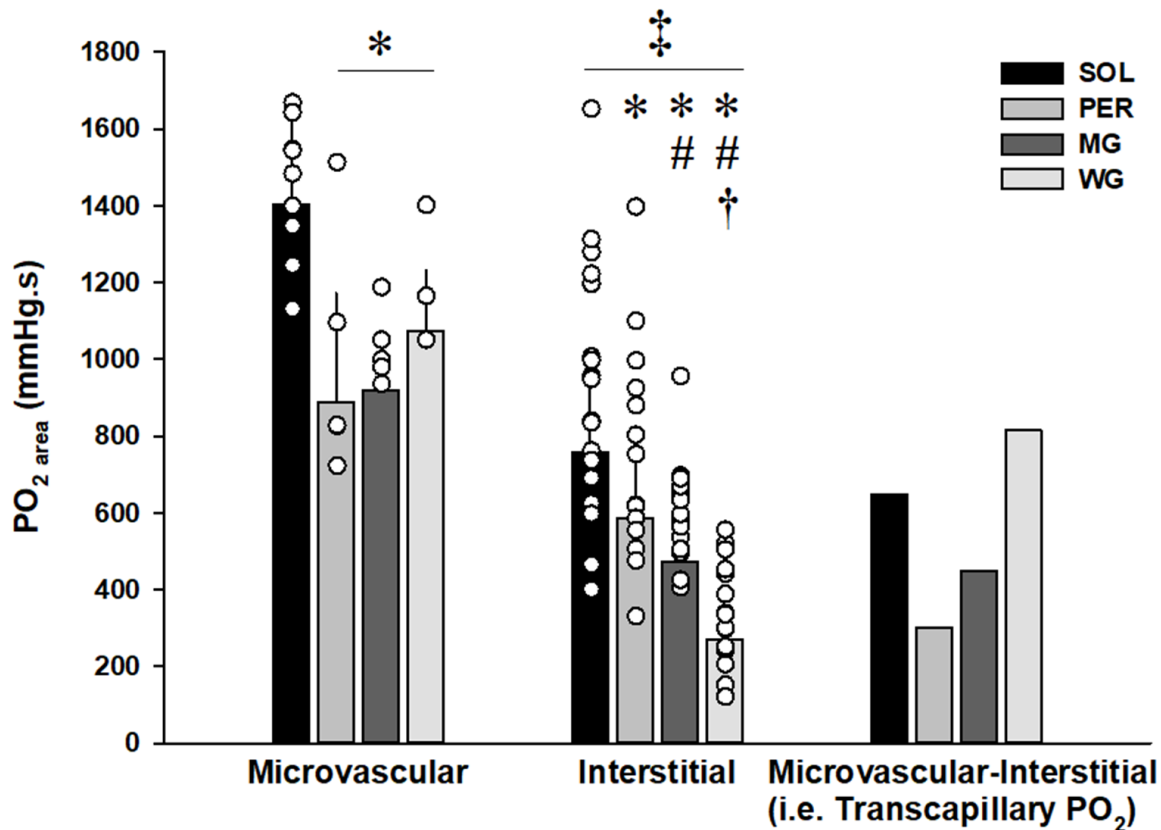
The transcapillary pressure gradient for O₂ (PO₂_{mv}-PO₂_{is}) at rest is maintained throughout twitch contractions. According to Fick's Law of Diffusion [$\dot{V}O_2 = DO_2 \times (PO_2mv - PO_2is)$], increased metabolic demand ($\dot{V}O_2$) necessitates increased diffusing conductance (DO₂) across the capillary wall during maintained, or decreased, PO₂_{mv}-PO₂_{is}. Time zero depicts the onset of twitch contractions. The bolded line (PO₂_{mv}-PO₂_{is}) is the difference between mean PO₂ of microvascular (closed circle) and interstitial (open circle) compartments. Note the reduction in PO₂_{mv}-PO₂_{is} following the onset of contractions in MG (Time x (PO₂_{mv}-PO₂_{is}) Interaction), highlighting further increases in transcapillary DO₂ to accommodate the increased myocyte $\dot{V}O_2$. Data are mean \pm SD with the PO₂_{mv} and PO₂_{is} of each muscle compared across time via Two-Way ANOVA (Time x Compartment) with Tukey's *post hoc* analyses.

Figure 2.3. Microvascular and interstitial PO_2 nadir following the onset of contractions



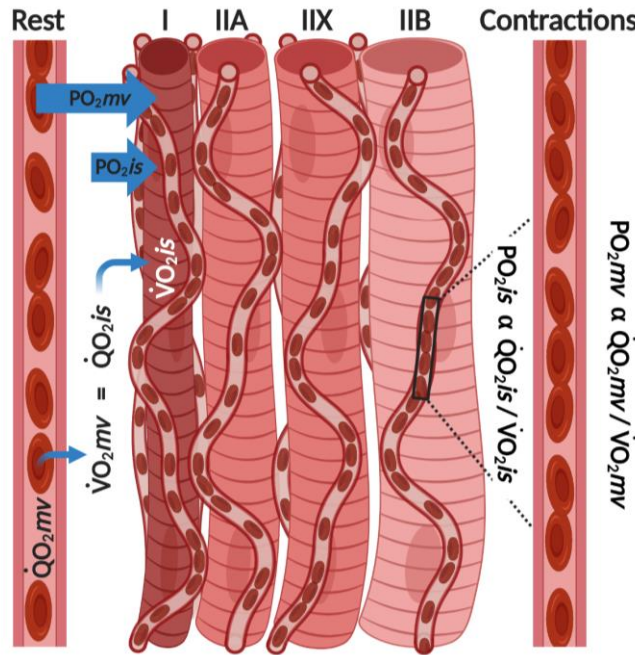
Even at the lowest portion of the rest-contraction transient, interstitial (open) PO_2 is significantly lower than the microvascular (closed) compartment in all muscles ($p < 0.05$). Interstitial PO_2 nadir exhibits a decline transitioning from slow-twitch oxidative to fast-twitch glycolytic muscle. Data are individual responses with box plots and compared via unpaired Student's t -tests. * $p < 0.05$ vs SOL; # $p < 0.05$ vs PER; † $p < 0.05$ vs MG.

Figure 2.4. Transcapillary pressure gradient for O₂ flux



PO₂ area was determined by integrating the area under the PO_{2mv} and PO_{2is} curves throughout the 120 s of twitch contractions. The difference between microvascular and interstitial PO₂ area denotes the total transcapillary driving pressure for O₂ flux (i.e. transcapillary PO₂) throughout the rest-contraction transient. Note the profound reduction in transcapillary PO₂ of fast-twitch oxidative PER and MG compared to slow-oxidative SOL (likely driven via high O₂ flux density) and fast-twitch glycolytic WG (via low intracapillary DO₂; Dawson et al. 1987). Data are mean \pm SD and compared via unpaired Student's *t*-tests. † p < 0.05 vs PO_{2is}; * p < 0.05 vs SOL; # p < 0.05 vs PER; ‡ p < 0.05 vs MG.

Figure 2.5. The flow of O₂ from red blood cell to myocyte



This schematic represents the flow of O₂ from the microvasculature down into skeletal muscle with O₂ delivery (\dot{QO}_2)-to-utilization (\dot{VO}_2) matching establishing O₂ partial pressures ($PO_2 \propto \dot{QO}_2 / \dot{VO}_2$). Red blood cells (RBC) transport O₂ (O₂ bound to haemoglobin) through the microvascular compartment (\dot{QO}_2mv) where, at the RBC-capillary interface, O₂ diffuses across the capillary wall into the interstitium (\dot{VO}_2mv). As there is no haeme-storage for O₂ in the interstitial space, the O₂ flux into the interstitium (\dot{VO}_2mv) must equal O₂ leaving the interstitium (\dot{QO}_2is) and also O₂ entering the myocyte (\dot{VO}_2is ; i.e., $\dot{QO}_2mv > \dot{VO}_2mv = \dot{QO}_2is = \dot{VO}_2is$). Total intramyocyte \dot{VO}_2 is the sum of \dot{VO}_2is and O₂ utilized from myoglobin-O₂ stores (I > II A > II X, absent in II B; Hickson et al. 1981). The driving pressure for O₂ flux (i.e., PO_2) is the mass balance between \dot{QO}_2 and \dot{VO}_2 for each compartment, with transcapillary O₂ flux at any given moment resulting from the coordinated balance between the pressure gradient ($PO_2mv - PO_2is$) and diffusing conductance (DO_2) between RBC and sarcolemma, per Fick's Law of Diffusion: Transcapillary $\dot{VO}_2 = DO_2 \times (PO_2mv - PO_2is)$. With a mosaic distribution pattern of myofibres and shared capillaries *in vivo*, fibre type differences are depicted regarding cross sectional area (Delp & Duan, 1996) and capillary:fibre ratio (Saltin & Gollnick, 1983) and capillary haematocrit when transitioning from rest to contractions (~16 to 20%; Kindig et al. 2002).

Chapter 3 - Vascular ATP-sensitive K⁺ channels support maximal aerobic capacity and critical speed via convective and diffusive O₂ transport

Trenton D. Colburn^a, Ramona E. Weber^a, K. Sue Hageman^b, Jacob T. Caldwell^a, Kiana M. Schulze^a, Carl J. Ade^a, Brad J. Behnke^a, David C. Poole^{a,b}, Timothy I. Musch^{a,b}

^aDepartment of Kinesiology, ^bDepartment of Anatomy and Physiology, Kansas State University Manhattan, KS, 66506, USA

Summary

Vascular ATP-sensitive K^+ (K_{ATP}) channels support skeletal muscle blood flow and microvascular oxygen delivery-to-utilization matching during exercise, however, oral sulphonylurea treatment in diabetes inhibits pancreatic K_{ATP} channels to enhance insulin release. Herein we tested the hypotheses that i) systemic K_{ATP} channel inhibition via glibenclamide (GLI; 10 mg kg⁻¹ i.p.) would decrease cardiac output at rest (echocardiography), maximal aerobic capacity ($\dot{V}O_{2max}$) and the speed-duration relationship (i.e. lower critical speed (CS)) during treadmill running and ii) local K_{ATP} channel inhibition (5 mg kg⁻¹ GLI superfusion) would decrease blood flow (15 μ m microspheres), interstitial space oxygen pressures (PO_{2is} ; phosphorescence quenching) and convective and diffusive O_2 transport ($\dot{Q}O_2$ and $D\dot{O}_2$, respectively; Fick Principle and Law of Diffusion) in contracting fast-twitch oxidative mixed gastrocnemius muscle (MG: 9% type I+IIa fibres). At rest, GLI slowed LV relaxation (2.11±0.59 vs 1.70±0.23 cm s⁻¹) and decreased heart rate (321±23 vs 304±22 bpm, both $P < 0.05$) while cardiac output remained unaltered (219±64 vs 197±39 ml min⁻¹, $P > 0.05$). During exercise, GLI reduced $\dot{V}O_{2max}$ (71.5±1.0 vs 68.0±1.5 ml kg⁻¹ min⁻¹) and CS (35.9±0.9 vs 31.9±1.1 m min⁻¹, both $P < 0.05$). Local K_{ATP} channel inhibition decreased MG blood flow (49±9 vs 34±4 ml min⁻¹ 100g tissue⁻¹) and PO_{2is} nadir (5.9±0.3 vs 4.7±0.4 mmHg) during twitch contractions. Furthermore, MG $\dot{V}O_2$ was reduced via impaired $\dot{Q}O_2$ and $D\dot{O}_2$ ($P < 0.05$ for each). Collectively, these data support that vascular K_{ATP} channels help sustain submaximal exercise tolerance in healthy rats. For patients taking sulfonylureas K_{ATP} channel inhibition may exacerbate exercise intolerance.

Introduction

Sulphonylureas are the most popular second-line anti-diabetic drug prescribed to patients with Type 2 diabetes mellitus (T2DM, Montvida et al. 2018), enhancing insulin release from pancreatic beta cells by inhibition of ATP-sensitive potassium (K_{ATP}) channels. This is true irrespective of the increased risk of adverse cardiovascular events (Abdelmoneim et al. 2016, Simpson et al. 2006, 2015), developing heart failure (HF; McAlister et al. 2008, Kristiansen et al. 2011) and all-cause mortality (Simpson et al. 2015). K_{ATP} channels are metabolic sensors that are also present in neural, vascular (endothelial) and muscle (smooth, cardiac and skeletal) tissue, contributing significantly to the hyperpolarization of membrane potentials via K^+ efflux and subsequent reductions in calcium ion influx. Attention to this category of K^+ channels, and their physiological significance in metabolic control during exercise, has increased with the use of genetic knockout/down models (Flagg et al. 2010). However, the use of genetically altered animal models may result in unknown/unrelated systemic modifications and confound the translatability of K_{ATP} channel function to humans (Kane et al. 2004).

Current data in animal and human studies modulating K_{ATP} channel function with inhibitors (i.e. glibenclamide (GLI), tolbutamide) and activators (pinacidil) suggest that normal K_{ATP} channel function plays a significant role in limiting myocardial damage following ischaemic events in sedentary and exercise trained animals (cardiac; Brown et al. 2005a,b), enhance reactive and functional hyperemia to skeletal muscle (vascular; Banitt et al. 1996, Bijlstra et al. 1996, Hammer, Ligon, & Hester 2001, Holdsworth et al. 2015, Keller et al. 2004, Lu et al. 2013, Saito et al. 1996; but not all, Farouque & Meredith 2003), and reduce skeletal muscle tension between contractions (myocyte; Gong et al. 2000, Matar et al. 2000). Whereas systemic administration of GLI has been shown to decrease exercising limb blood flow (Holdsworth et al. 2015, Keller et al.

2004) and maximal aerobic capacity ($\dot{V}O_{2max}$; Lu et al. 2013), it remains unknown whether these cardiovascular impairments are mediated through reductions in cardiac function, vascular function within skeletal muscle, or both. As adequate energy production via oxidative metabolism dictates contractile function during fatiguing activity and depends on heterogeneous oxygen transport within muscle (Hogan et al. 1992, Wilson et al. 1977, Richardson et al. 1998), maximal oxygen uptake ($\dot{V}O_{2max} = \dot{Q}_{max} \times \text{maximal a-vO}_2 \text{ difference}$) relies on a prodigious increase in cardiac output (\dot{Q}) combined with a highly effective red blood cell distribution and O_2 extraction within active skeletal muscle (arterial-venous O_2 content) (reviewed by Laughlin et al. 2012, Poole & Jones 2012). Notwithstanding the importance of $\dot{V}O_{2max}$, the ability to sustain high intensity exercise and daily physical tasks are more appropriately determined via a submaximal threshold (i.e. critical speed or critical power) where oxidative metabolism meets metabolic demand below this threshold but, above this threshold, increases in fast-twitch fibre recruitment, fatigue-related metabolite production, and O_2 consumption lead to $\dot{V}O_{2max}$ and task failure (Copp et al. 2010, Jones et al. 2008, Monod & Scherrer, 1965, Poole et al. 1988, 2016). Importantly, it remains unknown how vascular K_{ATP} channels contribute to O_2 transport within highly oxidative fast-twitch muscles and their role in supporting fatiguing exercise, especially as the proportional contribution of these channels to the overall vascular response may increase in disease (Holdsworth et al. 2017).

Therefore the current investigation was designed to assess the effect of systemic K_{ATP} channel inhibition via GLI on i) resting cardiac function, ii) maximal aerobic capacity ($\dot{V}O_{2max}$) and iii) submaximal exercise tolerance (CS). Local K_{ATP} channel inhibition via GLI superfusion was used to assess iv) skeletal muscle blood flow (\dot{Q}_m) and v) interstitial space O_2 pressures (PO_{2is} ; established by O_2 delivery-to-utilization matching immediately proximal to myocytes)

within contracting fast-twitch muscle of high oxidative capacity. Incorporating the Fick principle ($\dot{V}O_2 = \dot{Q}_m \times (CaO_2 - CvO_2)$) and law of diffusion ($\dot{V}O_2 = DO_2 \times \Delta PO_2$), direct measurements were used to estimate convective ($\dot{Q}O_2$) and diffusive (DO_2) O_2 conductances within microvascular and interstitial compartments where the convergence of $\dot{Q}O_2$ and DO_2 establish $\dot{V}O_2$ (Wagner 1992, 1996). Considering vascular function and exercise assessments of K_{ATP} channels have been performed in male rats (Holdsworth et al. 2015, 2016, 2017, Lu et al. 2013) when females may be more adversely affected by sulphonylurea treatment (Brown et al. 2005b, Johnson et al. 2006) the current investigation sought to bridge the translatability of K_{ATP} channel function to females. It was hypothesized that K_{ATP} channel inhibition would impair resting cardiac output and decrease $\dot{V}O_{2max}$ and CS. It was further hypothesized that local K_{ATP} channel inhibition would reduce skeletal muscle blood flow and PO_{2is} during twitch contractions, and slow the recovery of PO_{2is} following contractions, effectively decreasing $\dot{V}O_2$ by impairing O_2 conductance ($\dot{Q}O_2$ and DO_2). Data in support of these hypotheses would reveal a heretofore under-appreciated peripheral vascular role for K_{ATP} channels in the maintenance of O_2 delivery and contractile function.

Methods

Ethical Approval

All protocols and procedures were approved by the Institutional Animal Care and Use Committee of Kansas State University and conducted according to the guidelines and ethical standards put forth by the National Institutes of Health and Journal of Physiology (Grundby, 2015). Ten female Sprague-Dawley rats (~8 months old during terminal experiments) were maintained in Association for the Assessment and Accreditation of Laboratory and Animal Care accredited animal facilities on a 12:12 h light:dark cycle with food and water provided *ad libitum*. Vaginal lavages were conducted for a minimum of 10 days to monitor menstrual cycles (Marcondes et al. 2002, Smith et al. 2017) with all testing performed during the proestrus phase. In the initial 14-21 days, while menstrual cycles were monitored, acclimation to running was conducted on a custom-built treadmill for ~5 min day⁻¹ at ~25 m min⁻¹ up a 5% incline. During the final acclimation days treadmill speed was increased progressively in the last 2-3 min up to 50-60 m min⁻¹ to familiarize the rats with high speed running (Copp et al. 2010, Craig et al. 2019a, Poole et al. 2020). Importantly, these brief duration acclimation runs do not elicit training adaptations (Dudley et al. 1982, Armstrong & Laughlin 1984, Musch et al. 1992)

Drug Dosing

K_{ATP} channel inhibition was administered via the pharmacological sulphonylurea derivative glibenclamide (GLI: 494 g mol⁻¹, 5-chloro-N-{4-[N-(cyclohexylcarbamoyl)sulfamoyl]phentyl}-2-methoxybenzamide, Sigma-Aldrich, St. Louis, MO). For acute systemic inhibition via an intraperitoneal injection on experimental days, a 10 ml stock solution was made by GLI dissolved in 9 ml saline (0.9% NaCl), 900 µl NaOH (0.1 M), and

100 μ l DMSO and briefly sonicated. The amount of GLI dissolved in solution was determined on experimental days to obtain a final 1 ml dose of 10 mg kg⁻¹ (Lu et al. 2013). For local inhibition via superfusion, the stock solution utilized distilled water in place of saline and GLI was dissolved to obtain a final 5 mg kg⁻¹ dose, with 0.5 ml GLI stock solution diluted in 2.5 ml of warmed Krebs-Hensleit bicarbonate-buffered solution equilibrated with 5% CO₂-95% N₂ (pH 7.4; in mM, 4.7 KCl, 2.0 CaCl₂, 2.4 MgSO₄, 131 NaCl and 22 NaHCO₃).

GLI injections (10 mg kg⁻¹, i.p.) occurred ~30-60 min prior to echocardiographic assessment and treadmill exercise testing ($\dot{V}O_{2max}$ and CS; Lu et al. 2013) to align with peak plasma concentration (i.e., ~60-85 min after oral administration of 10 mg kg⁻¹ GLI, Li et al. 2012). Thus, each rat underwent at least six GLI injections over ~7-8 weeks. During interstitial PO₂ measurements, inhibition was administered locally via GLI superfusion (5 mg kg⁻¹ in Krebs-Hensleit solution, Holdsworth et al. 2017).

Echocardiography determination of LV function

Transthoracic echocardiography was performed with a commercially available system (Logiq S8; GE Health Care, Milwaukee, WI) using an 18 MHz linear transducer (L8-18i). Rats were anesthetized initially on 5% isoflurane-O₂ mixture and then maintained on 1.5-2% isoflurane-O₂ mixture while positioned supine on a heating pad (42°C) to maintain core temperature. Standard two-dimensional and M-mode images were obtained from the midpapillary level with frame rates >50 frames s⁻¹. Ventricular dimensions were obtained from M-mode measurements over four consecutive cardiac cycles. Left ventricular internal dimensions were measured at end diastole (LVIDd) and end systole (LVIDs). Fractional shortening (FS) was calculated from LV chamber diameters: FS = [(LVIDd – LVIDs)/LVIDd] x 100. Left end-systolic (LVESV) and end-diastolic

(LVEDV) volumes were estimated using the Teichholz formula: LV volume = [7.0/(2.4 + LV dimension)] x LV dimension³. Stroke volume (SV) was calculated as: SV = LVEDV – LVESV. Ejection fraction (EF) was calculated using LV volume measurements: EF = [(LVEDV – LVESV)/LVEDV] x 100. Rates of contraction (+V) and relaxation (-V) of the posterior LV wall were also measured in M-mode by integrating the slope from end-diastolic and end-systolic internal diameter locations used for assessing LVIDd and LVIDs. Heart rate (HR) was estimated using the average contraction and relaxation times across the four cardiac cycles: HR = 60 / (contraction time + relaxation time). Cardiac output (CO) was calculated using HR and SV values: CO = HR x SV.

Determination of Maximal Oxygen Uptake and Critical Speed

Maximal oxygen uptake ($\dot{V}O_{2max}$) tests were performed in a plexiglass metabolic chamber placed on the treadmill (Musch et al. 1988) and connected to O₂ (model S-3A/I) and CO₂ (model CD-3A; AEI Technologies; Pittsburg, PA) analyzers. Gas measurements were performed in real time and recorded in the final 5-10 s of each stage. Treadmill speed was initially set to 25 m min⁻¹ for two minutes, increased to 40 m min⁻¹ for an additional two minutes, and then increased progressively ~5 m min⁻¹ each minute until the rat was unable to maintain pace with the treadmill or no further increases in $\dot{V}O_2$ were recorded despite increases in speed. High reproducibility of $\dot{V}O_{2max}$ measurements has been established previously in our laboratory (Copp et al. 2009).

Following $\dot{V}O_{2max}$ testing, the speed-duration relationship was determined via the multiple constant-speed method (Copp et al. 2010, Craig et al. 2019a). Critical speed tests consisted of 5 runs-to-exhaustion at predetermined speeds estimated to elicit exhaustion between 2 and 20 min. Each test began with a 2 min warm-up at 20 m min⁻¹, followed by 1 min of quiet

rest, and then rapid increase in treadmill speed (<10 s) toward the target speed to be maintained for the duration of the test. Timing began when the investigator adjusting treadmill speed verified the attainment of the target speed. When rats drifted toward the back of the running lane a separate investigator provided encouragement via manual bursts of air toward the hindlimbs. Tests were terminated immediately when rats were unable to keep up with the treadmill speed despite apparent exertion and encouragement. The termination of all tests were determined by the same investigators who were blinded to the overall exercise time. Successful runs-to-exhaustion were verified by the absence of a righting reflex (i.e. unwilling/unable to right themselves within 2 s of being placed on their backs). The initial run was set at 60 m min^{-1} and subsequent speeds were selected at $\sim 5 \text{ m min}^{-1}$ increments to obtain the appropriate range of run durations (i.e., 2-20 min). When successful constant-speed tests were completed, the speed-duration parameters were determined by 1) the hyperbolic speed-time model ($\text{time} = D' / (\text{speed} - CS)$, where the asymptote of this curve is CS and the curvature constant is D'; and 2) the linear 1/time model ($\text{speed} = D' \times 1/\text{time} + CS$), where speed is plotted as a function of the inverse of time (s) to exhaustion, D' is the slope, and CS is the intercept of the regression line (Copp et al. 2010, 2013, Poole et al. 2016). To mitigate any potential influence of training (increased CS) or weight gain (decreased CS) on the speed-duration relationship, the slowest of the constant-speed runs were performed early (i.e., run 2-4) under control conditions and the final runs overall consisted of control and GLI runs at the slowest speeds. Preliminary data showed that times-to-exhaustion of the slowest speed under control conditions, and thus CS, were either maintained or decreased compared to the initial slowest run. Therefore the shorter of the two was used to model the speed-duration relationship.

Phosphorescence quenching determination of PO₂is

On the final day of experimentation, rats were anesthetized initially on 5% isoflurane-O₂ mixture and maintained on 2-2.5% isoflurane-O₂ mixture for the duration of carotid and caudal (tail) artery catheterizations and surgical exposure of hindlimb muscles. Rats were placed on a heating pad to maintain core temperature ~37-38°C, measured via rectal thermometer. Following a midline incision of the skin covering the neck, the right carotid artery was isolated and cannulated (PE-10 connected to PE-50; Intra-Medic polyethylene tubing; BD, Franklin Lakes, NJ, USA) for continuous measurements of mean arterial pressure (MAP) and heart rate (HR), and infusion of fluorescent-labelled microspheres for blood flow measurements (see *Fluorescent microsphere assessment of blood flow*). The caudal artery was cannulated for infusion of pentobarbital sodium anesthesia and blood sampling (i.e., blood gases and blood flow reference sample). Arterial blood samples were collected following the final contraction protocol for determination of O₂ saturation, systemic haematocrit and plasma lactate (Nova Stat Profile M; Nova Biomedical, Waltham, MA, USA).

Following catheterization, an incision was made above the lateral malleolus of the left hindlimb and overlaying skin and fascia reflected to expose the biceps femoris. Upon tying off the lateral great saphenous artery (6-0 silk suture) the distal portion of the biceps femoris was reflected to expose the mixed gastrocnemius (MG). The MG muscle was selected for its fast-twitch fibre composition (97% type IIA+IID/X+IIB), oxidative capacity (citrate synthase: ~25 µmol/min/g; Armstrong & Phelps 1984, Delp & Duan 1996), and most importantly its recruitment at and above the fatigue threshold (i.e., critical speed; Copp et al. 2010). The MG was left attached to its anatomical origin and insertion while variations in muscle length were minimized throughout the experimental protocol with knee and ankle joints stabilized ~90° angles. Rats were then

progressively transitioned off isoflurane and onto pentobarbital sodium anesthesia (50 mg ml^{-1}) with depth of anesthesia continuously monitored via toe pinch and corneal sensitivity reflexes, and additional anesthesia provided as necessary (0.03-0.05 ml of 50 mg ml^{-1} diluted to 0.3 ml of heparinized saline). Platinum iridium electrodes were attached (6-0 silk suture) to the proximal (cathode) and distal (anode) regions of the muscles to produce electrically induced muscle contractions. Surrounding exposed tissue was covered with Saran Wrap (Dow Brands, Indianapolis, IN) to reduce tissue dehydration and exposure to superfused solutions. Exposed muscle was superfused regularly with warmed Krebs-Henseleit bicarbonate buffered solution equilibrated with 5% CO₂-95% N₂.

Experimental protocol. Two separate contraction bouts were performed on the MG under control (Krebs-Henseleit) and K_{ATP} channel inhibition (5 mg kg^{-1} GLI in Krebs-Henseleit) superfused conditions. GLI superfusion was performed second, due to the long half-life of GLI, and with > 20 min of recovery between contraction bouts to prevent any potential priming effect of repeated contraction bouts on PO_{2is} profiles. Interstitial space PO₂ (PO_{2is}) was measured via phosphorescence quenching at rest and during 180 s twitch contractions (1 Hz, 7 V, 2 ms pulse duration; Grass stimulator model S88, Quincy, MA) and recorded at 2 s intervals (Craig et al. 2018, 2019a,b, Hirai et al. 2018a). Recovery PO_{2is} was measured for an additional 240 s to ensure that PO_{2is} returned and stabilized at baseline prior to subsequent GLI superfusion and contractions. With PO_{2is} measured continuously, GLI was superfused (3 ml total volume) onto the MG for 180 s and allowed an additional 180 s before the same contraction protocol was repeated (i.e., total of > 23 min elapsed between contraction bouts).

Measurement of interstitial PO₂. A frequency domain phosphorometer (PMOD 5000; Oxygen Enterprises, Philadelphia, PA) was used to measure PO_{2is} as described previously (Craig

et al. 2018, 2019a,b, Hirai et al. 2018a). The Oxyphor G4 (Pd-*meso*-tetra-(3,5-dicarboxyphenyl)-tetrabenzoporphyrin) was injected locally (two to four 10 μl injections at 10 μM concentration) with a 29 gauge needle, with care taken to avoid any visible vasculature. Following injection, the muscle was covered in Saran Wrap and allowed > 20 min to allow the G4 to thoroughly diffuse throughout the interstitial space. This oxyphor is well suited for use in biological tissues because it does not cross membranes and is stable across the physiological pH range (Esipova et al. 2011). Muscle surface temperature was measured via noncontact infrared thermometer, since this oxyphor is temperature sensitive. The exposed MG temperatures was $31.6 \pm 0.2^\circ\text{C}$. Previous studies have shown that the present twitch contraction protocol does not significantly change muscle temperature (Craig et al. 2018, 2019a).

Phosphorescence quenching applies the Stern-Volmer relationship (Rumsey et al. 1988; Esipova et al. 2011) describing the quantitative O_2 dependence of the phosphorescent probe G4 via the equation $\text{PO}_{2is} = [(\tau_0/\tau) - 1]/(k_Q \cdot \tau_0)$, where k_Q is the quenching constant and τ and τ_0 are the phosphorescence lifetimes at the ambient O_2 concentration and in the absence of O_2 , respectively. For G4 in tissue at $\sim 32^\circ\text{C}$, k_Q is $\sim 258 \text{ mmHg/s}$ and τ_0 is $\sim 226 \mu\text{s}$ (Esipova et al. 2011). Because muscle temperature does not change appreciably throughout the contraction protocol used herein (Craig et al. 2018, 2019a), the phosphorescence lifetime is determined exclusively by the O_2 partial pressure. Following G4 injection, the common end of the bifurcated light guide was positioned 3–4 mm above the exposed muscle surface. All PO_{2is} measurements were performed in a dark room to minimize extraneous exposure to light.

Analysis of interstitial PO_2 kinetics. Contracting PO_{2is} responses were analyzed using 30 s of resting data and the 180 s contraction bouts using a monoexponential plus time delay model

(one component) or a monoexponential plus time delay with a secondary component (two component) model when necessary,

One component

$$PO_2is_t = PO_2is_{BL} - \Delta_1 PO_2is(1 - e^{-(t - TD)/\tau})$$

Two component

$$PO_2is_t = PO_2is_{BL} - \Delta_1 PO_2is(1 - e^{-(t - TD)/\tau}) + \Delta_2 PO_2is(1 - e^{-(t - TD_2)/\tau_2})$$

where PO_2is_t represents the PO_2is at any point in time, PO_2is_{BL} is the baseline before the onset of contractions, $\Delta_1 PO_2is$ and $\Delta_2 PO_2is$ are the primary and secondary amplitudes, TD and TD_2 are the time delays before the fall and secondary rise in PO_2is , and τ and τ_2 are the time constants (i.e., the time required to reach 63% of the amplitude) for the primary and secondary amplitudes. The mean response time (MRT) was calculated as the sum of the model derived TD and τ . When the secondary component model was necessary, the primary amplitude was constrained to the nadir value in order to maximize the accuracy of the primary response kinetics (Craig et al. 2018, 2019a,b). The goodness of model fit was determined using the following criteria: 1) coefficient of determination, 2) sum of the squared residuals, and 3) visual inspection and analysis of the model fits to the data and the residuals. Because $\Delta_2 PO_2is$ (i.e., undershoot of PO_2is ; $\Delta_2 PO_2is = PO_2is_{end} - PO_2is_{nadir}$) was often nonexponential in nature, $\Delta_2 PO_2is$ was determined manually by calculating the difference between the PO_2is at the end of contractions (PO_2is_{end} , average of 172-180 s) minus the nadir value of PO_2is during contractions ($PO_2is_{nadir} = PO_2is_{BL} - \Delta_1 PO_2is$). Rate of PO_2is recovery was calculated in eight rats as the time taken to reach 63% of the overall response (i.e., T63) between PO_2is_{end} and recovery PO_2is (average of 232-240 s).

Fluorescent microsphere determination of blood flow

The microsphere technique was used to determine MG blood flow as described previously (Deveci et al. 1999, Musch et al. 1986, Van Oosterhout et al. 1993). Two fluorescent microspheres (blue-green (430/465nm) and red (580/605nm), Invitrogen FluoSpheres polystyrene microspheres, ThermoFisher Scientific) were injected in random order at the end of MG and MG GLI contractions. Following 180 s contractions, blood withdrawal from the tail catheter was initiated at 0.25 ml min^{-1} while $0.25\text{-}0.30 \times 10^6$ $15.5 \mu\text{m}$ diameter fluorescent microspheres were injected into the aortic arch via the carotid artery catheter. Muscle contractions and blood withdrawal were terminated 30 s after the microsphere injection. Following the final contraction protocol, rats were euthanized via pentobarbital sodium overdose ($>100 \text{ mg kg}^{-1}$, i.a.), proper catheter placement in the aortic arch was confirmed, and tissues (left and right kidneys, left and right mixed gastrocnemei) dissected and stored (-80°C) for later analyses. For the final analyses, kidney and muscle tissues were weighed and placed directly in 15 ml screw cap polypropylene tubes with a conical base. Five ml of 2 M KOH in 99% ethanol with 0.5% Tween-80 were added to the tubes, vortexed, and placed in a dry heating block (60°C) with intermittent vortexing until tissue digestion was complete. Tubes were then centrifuged at 3,000 rpm (1,500 g) for 15 min. Supernatant was carefully aspirated until $<500 \mu\text{l}$ remained to minimize the possibility of accidental microsphere loss. One ml of deionized H₂O was added and tubes quickly vortexed to resuspend the remaining pellet, followed by the addition of 9 ml ethanoic Tween-80, vortexing and another 15 min of centrifuging. Tubes were aspirated as previously described before 5 ml of 100 mM phosphate buffer (pH 7.0) was added to neutralize the pellet and solution, followed by 4 ml of absolute ethanol. The tubes were further vortexed, centrifuged, and aspirated to $<300 \mu\text{l}$. To ensure complete resuspension of microspheres, the tubes were vortexed again before being placed in an

oven (60°C) to evaporate to 100-150 µl. To improve solvent extraction from the microspheres, which would be less efficient in a dry pellet, the tubes were periodically removed from the oven and vortexed. To dissolve the polystyrene microspheres and release the fluorescent dye, 2 ml of solvent (di(ethylene glycol) ethyl ether acetate, 98%; Sigma-Aldrich Corporation, St. Louis, MO, USA) was added and vortexed several times over 3-5 min and left for 30 min before being sonicated (5 min) in a water bath to ensure complete dye extraction. Once the solvent was added, all remaining steps were conducted in dim lighting to prevent signal decay prior to fluorescent intensity measurements. After sonication the tubes were centrifuged once more (10 min) before supernatant was pipetted (300 µl) into 96 well plates in quadruplicates for the measurement of fluorescent intensity (SpectraMax i3 Multi-Mode Platform, Molecular Devices, San Jose, CA). Total tissue blood flows were calculated according to the reference sample method (Ishise et al. 1980, Musch & Terrell, 1992) and expressed mass specifically in $\text{ml min}^{-1} 100 \text{ g tissue}^{-1}$. Adequate mixing of microspheres prior to infusion were determined by <20% difference in left and right kidney and/or muscle blood flows.

Muscle oxygen consumption

The Fick equation was used to calculate microvascular oxygen consumption ($\dot{\text{V}}\text{O}_{2\text{mv}}$) with the assumptions that microvascular PO_2 ($\text{PO}_{2\text{mv}}$) can be calculated from interstitial measurements (i.e., $\text{PO}_{2\text{mv}} = \text{PO}_{2\text{is}} + \text{transcapillary PO}_2$; Colburn et al. 2020a) and is an appropriate analogue for venous PO_2 (McDonough et al. 2001) and, by extension from the O_2 dissociation curve, venous blood O_2 content (Roca et al. 1992). Therefore mixed venous O_2 content (CvO_2) was calculated from $\text{PO}_{2\text{mv}}$ using the rat O_2 dissociation curve (constructed using the Hill coefficient (n) of 2.6, the measured [Hb], P_{50} (the PO_2 at which Hb is 50% saturated with O_2) of 38 mmHg, and an O_2

carrying capacity of 1.34 ml O₂ (gHb)⁻¹). Arterial O₂ content (CaO₂) was measured directly via arterial blood sample and, when combined with blood flow (\dot{Q}_m) and CvO₂ values, was used to calculate $\dot{V}O_{2mv}$ via the principle of mass balance using the Fick Equation (i.e., $\dot{V}O_{2mv} = \dot{Q}_m \times (CaO_2 - CvO_2)$). Microvascular O₂ diffusion conductance (DO_{2mv}) was defined as $\dot{V}O_{2mv}/PO_{2mv}$ which provides an index of diffusive O₂ transport per unit of driving pressure. Interstitial O₂ diffusion conductance (DO_{2is} = $\dot{V}O_{2is}/PO_{2is}$) was assessed utilizing the present PO_{2is} and calculated $\dot{V}O_{2mv}$ (i.e., $\dot{V}O_{2is}$ was presumed equal to $\dot{V}O_{2mv}$ considering the absence of storage for O₂ in the interstitial fluid and, thus, O₂ leaving the microvascular compartment must equal O₂ leaving the interstitial compartment).

Statistical Analyses

The effect of systemic GLI on resting LV function, exercise parameters ($\dot{V}O_{2max}$, CS and D'), and local GLI superfusion on contracting MG measurements (MAP, HR, PO_{2is} kinetics parameters, \dot{Q}_m , microvascular $\dot{Q}O_2$ and $\dot{V}O_2$ and microvascular and interstitial DO₂) were assessed using two-tail paired t-tests. PO_{2is} profiles were assessed via Two-Way repeated measure ANOVA (Time x Drug) with Tukey's *post hoc* analyses. Data are presented as mean \pm SD. Significance was accepted at P < 0.05.

Results

Two rats were unwilling to complete all runs needed to assess the speed-duration relationship, therefore comparisons between control and K_{ATP} channel inhibition were conducted on eight rats.

Resting Echocardiography

Left ventricular (LV) echocardiographic measurements are presented in Table 1. Compared to control, GLI did not alter LVEDV (0.83 ± 0.08 vs 0.83 ± 0.06 , P = 0.976) nor LVESV (0.15 ± 0.07 vs 0.19 ± 0.09 ml, P = 0.172) and thus stroke volume remained unchanged (0.68 ± 0.19 vs 0.65 ± 0.11 ml, P = 0.354). LV fractional shortening (47 ± 6 vs 42 ± 5 , P = 0.084) and ejection fraction (83 ± 5 vs $78 \pm 6\%$, P = 0.088) were also not significantly altered. However, the rate of LV relaxation (2.11 ± 0.59 vs 1.70 ± 0.23 , P = 0.048), but not contraction (2.76 ± 0.49 vs 2.44 ± 0.43 cm s⁻¹, P = 0.079), was significantly slowed resulting in a decreased heart rate (321 ± 23 vs 304 ± 22 bpm, P = 0.043) during maintained cardiac output (219 ± 64 vs 197 ± 39 ml min⁻¹, P = 0.105).

Maximal Aerobic Capacity and Speed-duration relationship

Table 2 and Figures 1 and 2 demonstrate that GLI reduced $\dot{V}O_{2max}$ (71.5 ± 3.1 vs 67.9 ± 4.8 ml min⁻¹ kg⁻¹, P = 0.034) and CS (35.9 ± 2.4 vs 31.9 ± 3.1 m min⁻¹, P = 0.020) whereas D' remained unchanged (98 ± 16 vs 91 ± 25 m, P = 0.532).

Blood Sample Analysis and Central Haemodynamics During Phosphorescence Quenching

Arterial pH (7.39 ± 0.01), O₂ saturation ($90.7 \pm 0.9\%$), haematocrit ($34.9 \pm 1.3\%$) and lactate concentration (1.5 ± 0.2 mM) were assessed following the GLI contraction. GLI superfusion did not alter MAP or HR (both $P > 0.346$) therefore MAP (101 ± 3 and 98 ± 3 mmHg; $P = 0.096$) and HR (352 ± 11 and 354 ± 15 bpm; $P = 0.831$) were not different at the start of control and GLI contractions, respectively.

MG Blood Flow and Interstitial PO₂

GLI superfusion impaired MG blood flow during contractions (52 ± 25 vs 34 ± 13 ml min⁻¹ 100 g⁻¹; $P = 0.015$). The effect of GLI superfusion on PO_{2is} during the rest-contraction transient is presented in Table 3 and Figure 3. GLI reduced MG PO_{2is} BL (-1.1 ± 1.1 mmHg; $P = 0.020$). At the onset of contractions, there was a shortening in TD ($P = 0.005$) with a statistically nonsignificant change in τ (14.1 ± 2.7 vs 12.2 ± 3.0 ; $P = 0.053$) yet a faster overall PO_{2is} fall (MRT: 22.2 ± 4.7 vs 17.3 ± 4.3 s, $P = 0.002$) to a lower PO_{2is} nadir (5.9 ± 0.9 vs 4.7 ± 1.1 , $P = 0.013$) but not different PO_{2is} end (7.3 ± 1.5 vs 6.1 ± 1.4 mmHg; $P = 0.073$) compared to control (see Figure 3; all 2 s measurements, Two-Way repeated measures ANOVA with Tukey's *post hoc* analyses, $P < 0.062$). Following contractions, GLI PO_{2is} recovered slower (T63: 95 ± 19 vs 118 ± 20 s, $P = 0.047$) but to a similar end recovery PO_{2is} (14.6 ± 4.0 vs 15.3 ± 6.5 mmHg; $P = 0.556$) during the observed window.

MG Muscle Oxygen Delivery, Consumption, and Diffusive Conductance

Compared to control, Figure 4 illustrates that GLI decreased MG oxygen delivery (\dot{Q}_{O_2mv} : 6.4 ± 1.1 vs 4.2 ± 0.6 ml O₂ min⁻¹ 100 g⁻¹; $P = 0.015$) and oxygen consumption from the

microvascular compartment ($\dot{V}O_2mv$: 5.8 ± 1.0 vs 3.9 ± 0.5 ml O₂ min⁻¹ 100 g⁻¹; P = 0.016). Consequently, microvascular (DO₂*mv*: 0.40 ± 0.07 vs 0.30 ± 0.04 ; P = 0.023) and interstitial diffusive conductances (DO₂*is*: 0.80 ± 0.13 vs 0.66 ± 0.08 ml O₂ min⁻¹ mmHg⁻¹ 100 g⁻¹; P = 0.040) were significantly reduced. Furthermore, DO₂*is* was significantly greater than DO₂*mv* (P = 0.0002 and 0.0001, control and GLI respectively), with the reduction in DO₂*mv* following GLI (-22 ± 7%) trending towards being proportionally greater than the reduction in DO₂*is* (-15 ± 6%; P = 0.070).

Discussion

The main original finding of this investigation is that, in female rats, glibenclamide (GLI)-induced impairment of maximal (i.e., maximal oxygen uptake, $\dot{V}O_{2max}$) and submaximal (i.e., critical speed, CS) exercise can be attributed, in part, to reductions in peripheral vascular K_{ATP} channel function. Systemic GLI administration did not change cardiac output at rest, assessed via doppler echocardiography. However, the slowed LV relaxation and reduced heart rate at rest following GLI highlights a peripheral insult to K_{ATP} channels that is likely compensated, in part, by baroreflex-mediated changes in left ventricular function. Accordingly, local inhibition of vascular K_{ATP} channels during contractions resulted in decreased blood flow and interstitial space O_2 delivery-to-utilization matching (i.e., PO_{2is}) of fast-twitch oxidative skeletal muscle and slowed the recovery of PO_{2is} following cessation of contractions. Using the Fick principle and law of diffusion, estimations of MG convective and diffusive conductances ($\dot{Q}O_2$ and DO_2 , respectively), and thus $\dot{V}O_2$, were impaired following GLI. Therefore the exercise intolerance that is symptomatic of patient populations (i.e., diabetes, heart failure), which have a greater proportion of, and blood flow to, fast-twitch fibres, may be exacerbated by oral sulphonylurea medications impairing vascular K_{ATP} channel-mediated vasodilation.

K_{ATP} Channel Function on Maximal Aerobic Capacity and Speed-Duration Relationship

Consistent with our hypothesis, systemic K_{ATP} channel inhibition impaired maximal aerobic capacity ($\dot{V}O_{2max}$) and submaximal exercise tolerance (CS). Lu and colleagues previously demonstrated impaired $\dot{V}O_{2max}$ (~54 to 36 ml O_2 min^{-1} kg^{-1} , ~33%) in rats following GLI injections (2013); however, utilizing a comparatively steeper ramp protocol, the current data exhibited higher baseline $\dot{V}O_{2max}$ and a far smaller effect of GLI (~5%, Table 2). This discrepancy

likely stems directly from the slower ramp protocol wherein longer durations at submaximal speeds would be expected to enhance glycogen depletion in skeletal muscle leading to exhaustion at lower $\dot{V}O_2$ levels. Supporting the need for steeper ramp protocols, Richardson et al. (1993) demonstrated greater $\dot{V}O_{2\text{max}}$ and maximum work rate within 13-15 min of knee extension exercise compared to those previously measured using a slower, lengthier ramp protocol (~40-60 min; Anderson & Saltin, 1985). Accordingly, GLI-induced reductions in HR in the face of elevated MAP occurred at slower speeds, but not at 60 m min^{-1} (Holdsworth et al. 2015). Coupled with decreased hindlimb muscle blood flows throughout all speeds, this suggests that vascular control of O_2 delivery is impaired especially at submaximal speeds while metabolite build-up at supra-CS speeds may activate group III/IV afferents to increase HR at near maximal speed/intensity (Holdsworth et al. 2015). This notion is highlighted in the current investigation (Figure 1) where GLI-induced reductions in CS were greater than those seen in $\dot{V}O_{2\text{max}}$ (~12 vs ~5%, respectively).

K_{ATP} Channel Function on Cardiac Function

Assessed via Doppler ultrasound under anesthesia, GLI significantly reduced the rates of LV relaxation and HR (Table 1) but not cardiac output. Decreased HR has been demonstrated in GLI treated rats during conscious rest which occurred simultaneously with increased MAP and decreased sympathetic activity to hindlimb muscles (Colburn et al. 2020b). Although resting cardiac function is not expected to relate directly to cardiac function during high-intensity exercise (Figure 1), we believe that the present changes in LV relaxation and HR at rest help to emphasize a peripheral insult following systemic K_{ATP} channel inhibition (Colburn et al. 2020b, Holdsworth et al. 2015, 2016) that manifests changes in cardiac function likely to minimize MAP increases (Colburn et al. 2020b) and/or decrease the work of the heart during elevated MAP. Additionally,

as direct K_{ATP} channel inhibition of cardiomyocytes would enhance contractility and hinder relaxation (Flagg et al. 2010, Kane et al. 2005, Zingman et al. 2007), it is most likely that the primary effect of systemic GLI administration herein results from a peripheral, and not cardiomyocyte-mediated, alteration in K_{ATP} channel function (i.e., vascular K_{ATP} channel inhibition leading to vasoconstriction and increased MAP with a baroreceptor-mediated secondary reduction in sympathetic activity to decrease cardiac output, Colburn et al. 2020b). These adjustments in cardiac function are likely removed at near-maximal intensity when sympathetic activity is enhanced and HR is not different between control and GLI conditions (Holdsworth et al. 2015). However, future experimental designs where possible should measure SV and cardiac output during high-intensity exercise to assess the primary, or secondary, effect of K_{ATP} channel inhibition on cardiac function. Nevertheless, reductions in $\dot{V}O_{2max}$ herein are considered to result, in part, from $\dot{Q}O_2:\dot{V}O_2$ mismatch at the level of skeletal muscle and impaired systemic arterial-venous O₂ difference (i.e., $\dot{V}O_{2max} = \dot{Q}O_{2max} \times$ maximal a-vO₂ difference).

K_{ATP} Channel Function on Skeletal Muscle Blood Flow and PO_{2is}

To assess the contribution of vascular K_{ATP} channels supporting skeletal muscle O₂ transport, and thus oxidative phosphorylation, the current investigation measured the interstitial space driving pressure of O₂ (PO_{2is}) during the rest-contractions transient during submaximal contractions, muscle blood flow (\dot{Q}_m) at the end of contractions, and PO_{2is} during recovery. Following local GLI administration, PO_{2is} in the MG fast-twitch oxidative muscle fell faster (i.e., MRT) and to a lower PO_{2is} (PO_{2is nadir}; Table 3, Figure 3) when \dot{Q}_m was reduced. Interestingly, because PO_{2is BL} was also reduced following GLI, the magnitude of PO_{2is} fall (i.e., Δ_1 PO_{2is}) was unaltered, possibly due to a lowering of intracellular $\dot{V}O_2$ to preserve interstitial-myocyte PO₂ and

prevent muscle damage, as proposed by Richmond et al. (1999). Therein the ‘critical PO₂’, the point at which PO_{2is} ceased to continue falling and NADH fluorescence signal increased, was ~2.4-2.9 mmHg for mixed-fibre spinotrapezius muscle and may be greater in the more oxidative MG (citrate synthase activity: ~26 vs ~14 $\mu\text{mol min}^{-1} \text{ g}^{-1}$; Delp & Duan, 1996). While the exact contribution of lowered $\dot{\text{V}}\text{O}_2$ (Figure 4) is unable to be separated completely between low $\dot{\text{Q}}\text{O}_2$ - (via decreased $\dot{\text{Q}}m$ which lowered PO_{2is} and sped the fall in PO_{2is}) and/or myocyte-mediated $\dot{\text{V}}\text{O}_2$ lowering, the end result is indeed lower $\dot{\text{V}}\text{O}_2$ which would increase the reliance on glycolytic energy sources for contractions and production of fatigue-related metabolites (Hogan et al. 1992, Wilson et al. 1977, Richardson et al. 1998).

In addition, despite recovering to a similar PO_{2is}, GLI significantly slowed the recovery compared to control. All of these findings during local K_{ATP} channel inhibition provide evidence supporting that the reductions in exercise tolerance resulting from systemic GLI administration were due, in part, to impaired O₂ transport at the microvascular level hindering aerobic metabolism within the contracting myocyte (see *Convective and Diffusive Determinants of O₂ Transport* below) and, especially for repeated bouts of physical activity, increasing the amount of time needed to re-establish muscle PO₂ and replenish muscle energy stores (Haseler et al. 1999; Kindig et al. 2005).

Convective and Diffusive Determinants of O₂ Transport

Utilizing direct measurements of $\dot{\text{Q}}m$, arterial O₂ content (CaO₂), and the O₂ pressures nearest the contracting myocytes (PO_{2is}) to calculate PO_{2mv} (PO_{2mv} = PO_{2is} + transcapillary PO₂; Colburn et al. 2020a), the authors conflated the Fick principle ($\dot{\text{V}}\text{O}_2\text{mv} = \dot{\text{Q}}m \times (\text{CaO}_2 - \text{CvO}_2)$; i.e., convective O₂ transport) and Fick’s law of diffusion ($\dot{\text{V}}\text{O}_2\text{mv} = \text{DO}_2\text{mv} \times \text{PO}_2\text{mv}$; i.e., diffusive O₂

transport) to estimate muscle convective O₂ delivery ($\dot{Q}O_{2mv}$), diffusive conductance for O₂ (DO_{2mv}), and the resulting $\dot{V}O_2$ from the microvascular compartment. Importantly, the convergence of the convective and diffusive determinants to O₂ transport describes the rate of O₂ consumption by skeletal muscle (Wagner, 1992, 1996).

In the current investigation, impaired PO_{2is} was due, in part, to reductions in $\dot{Q}m$. As a result, the rate of O₂ able to be consumed from the microvascular compartment was significantly reduced ($\dot{V}O_{2mv} \downarrow 33\%$). As demonstrated in Figure 4, this change in $\dot{V}O_{2mv}$ was not only a consequence of impaired $\dot{Q}O_{2mv}$ ($\downarrow 34\%$) but also lowered microvascular-myocyte diffusing conductance (DO_{2mv} $\downarrow 25\%$). Traditionally interpreted in the context of microvascular-myocyte O₂ transport, DO_{2mv} is altered via changes in capillary haematocrit, RBC flux and RBC velocity (reviewed by Poole et al. 2013, Poole, 2019). More recently, with the advent of PO_{2is} measurements during contractions (Hirai et al. 2018a, Colburn et al. 2020a), interstitial DO₂ (DO_{2is}, interstitial-myocyte) can be estimated presuming that O₂ leaving the microvascular compartment ($\dot{V}O_{2mv}$) equals O₂ leaving the interstitial compartment ($\dot{V}O_{2is}$; i.e., negligible change in storage of O₂ in interstitial fluid) during steady-state contractions and can be calculated from $\dot{V}O_{2mv}$ and the present PO_{2is} (i.e., DO_{2is} = $\dot{V}O_{2mv}/PO_{2is}$ when $\dot{V}O_{2mv} = \dot{V}O_{2is}$). Interestingly, since $\dot{V}O_2$ must be equivalent in both compartments, DO₂ was greater in the interstitial compartment compared to microvascular compartment and both decreased with GLI. However, with GLI, DO₂ was almost reduced to a significantly greater extent when O₂ diffused out of the microvascular compartment compared to the subsequent O₂ diffusion out of the interstitium ($\downarrow 25\%$ and 19% , DO_{2mv} vs DO_{2is}, respectively). These disparate magnitudes of, and potential reductions in, DO₂ between compartments are likely to result from: i) divergent surface areas for O₂ flux (i.e., across capillary wall < into myocyte) and ii) fluid dynamics wherein

impaired buffering of RBCs following GLI (i.e., ↓ percent capillaries flowing, RBC flux and RBC velocity, Hirai et al. 2018b) would yield greater decrements in $\text{DO}_{2\text{mv}}$ than $\text{DO}_{2\text{is}}$ considering interstitial fluid volume is expected to remain relatively constant during contractions and unaffected by GLI. Furthermore, since $\text{PO}_{2\text{mv}}$ for control and GLI conditions were calculated using the same transcapillary PO_2 ($\text{PO}_{2\text{mv}} = \text{PO}_{2\text{is}} + \text{transcapillary PO}_2$), the reduction in $\text{DO}_{2\text{mv}}$ following GLI is potentially underestimated as a result of increased transcapillary PO_2 . Crucially, increased \dot{Q}_m and RBC dynamics increase $\text{DO}_{2\text{mv}}$ and reduce transcapillary PO_2 ($\text{PO}_{2\text{mv}}-\text{PO}_{2\text{is}}$) in the contracting fast-twitch oxidative MG (MG Control: $\uparrow\dot{V}\text{O}_2 = \uparrow\downarrow\text{DO}_2 \times \downarrow[\text{PO}_{2\text{mv}}-\text{PO}_{2\text{is}}]$; Colburn et al. 2020a) whereas the GLI-induced reduction in \dot{Q}_m herein and impaired RBC dynamics (Hirai 2018b) would serve to reduce $\text{DO}_{2\text{mv}}$ compared to control and therefore increasing the actual $\text{PO}_{2\text{mv}}$ following GLI (MG+GLI compared to MG Control: $\downarrow\dot{V}\text{O}_2 = \downarrow\downarrow\text{DO}_2 \times \uparrow[\text{PO}_{2\text{mv}}-\text{PO}_{2\text{is}}]$).

The interplay between convective and diffusive O_2 delivery on muscle $\dot{V}\text{O}_2$ has been assessed directly in healthy skeletal muscle across fibre types (Behnke et al. 2003, McDonough et al. 2005), during handgrip exercise (Rosenberry et al. 2019) and in disease populations during isolated knee extensor and cycling exercise (COPD: Broxterman et al. 2019, HFrEF: Esposito et al. 2010, 2011 (exercise trained)). To our knowledge, the current investigation is the first to assess changes in convective and diffusive O_2 conductance following specific channel/enzyme inhibition and provides evidence that this approach can be utilized in future studies examining O_2 transport in health, dysfunction related to a range of cardiovascular diseases (i.e., diabetes, sickle cell anemia, pulmonary hypertension, heart failure, HF; Ferguson et al. 2018, Hirai et al. 2015, Padilla et al. 2006, 2007), and potential therapeutic interventions aimed at increasing O_2 delivery (i.e.,

nitrate and nitrite supplementation; Colburn et al. 2017, Craig et al. 2019b, Ferguson et al. 2013a,b, 2015, 2016a,b, Glean et al. 2015).

Experimental Considerations

Glycolytic muscle fibres experience the greatest metabolic perturbations during exercise and accordingly contain a greater content of pore-forming K_{ATP} channel subunit Kir6.2 (type IIB > IIX > IIA > I; Banas et al. 2011) which depresses force production and resting tension and limits intracellular calcium-mediated fibre damage (Cifelli et al. 2008, Gong et al. 2003, Thabet et al. 2005). When skeletal muscle K_{ATP} channels are inhibited via GLI, this could potentially lead to greater myocyte contraction and $\dot{V}O_2$. Although augmenting K_{ATP} channels via pinacidil impairs force production and increases the rate of skeletal muscle fatigue *ex vivo*, K_{ATP} channel inhibition via GLI does not decrease skeletal muscle fatigue or alter force production during tetanic contractions yet appears to increase resting muscle tension between contractions and could, therefore, increase $\dot{V}O_2$ accordingly (Matar et al. 2000, Gong et al. 2000). Nonetheless, the topical application of GLI and related disturbance of $\dot{Q}O_2:\dot{V}O_2$ matching (i.e., PO_{2is}) of the fast-twitch oxidative glycolytic MG are, principally, consequent to impaired blood flow (decreased herein, and also in Holdsworth et al. 2015) rather than increased metabolic demand ($\dot{V}O_2$; see Figure 4).

Whereas the present experimental design precluded the assessment of blood flow at rest and during treadmill running (i.e., utilizing fluorescent microspheres to assess resting/running blood flow would prevent blood flow assessment during PO_{2is} in the same rat), prior investigations from our laboratory have demonstrated reduced muscle blood flow following GLI at rest and a wide range of speeds (20, 40 and 60 m min⁻¹, the latter of which yields $\dot{V}O_{2max}$ on the inclined treadmill in rats, Colburn et al 2020b and Holdsworth et al. 2015). Therefore the authors are

assured that skeletal muscle blood flow is reduced following systemic GLI administration herein and during the cardiac assessment via doppler ultrasound.

Clinically, a primary concern of sulphonylurea use in patient populations is the potential for hypoglycaemia. Prior to exercise, hypoglycaemia following GLI-mediated insulin release and systemic glucose uptake would inherently limit exercise duration by limiting blood glucose stores for energy production. To minimize this limitation, the authors performed all exercise testing within 30-90 min of systemic GLI administration to target K_{ATP} channel inhibition and not incur the confounding effects on glucose availability that would result from a longer duration GLI-mediated insulin release (Li et al. 2012). Importantly, while assessing the speed-duration relationship (Table 2 and Figure 2), the curvature constant (D') remained unchanged following K_{ATP} channel inhibition. While CS is better understood and reflects the upper threshold of oxidative phosphorylation to support metabolic demand, D' is considered to reflect principally the contributions of finite non-aerobic energy stores and fatigue-resistant muscular properties supporting exercise above CS (reviewed by Poole et al. 2016). Additionally, exercise measurements were performed every 4 days to target the proestrus phase. Repeated acute doses of GLI, which has a half-life up to 10 h, is not anticipated to have a cumulative effect across testing days. Nevertheless, if a chronic K_{ATP} channel inhibition effect was captured, it would mirror more directly the use of oral sulphonylureas in T2DM patients and the present investigation may actually underestimate the long-term effects of K_{ATP} channel inhibition that is associated with elevated risk for adverse cardiovascular events, developing HF, and all-cause mortality (Abdelmoneim et al. 2016, Kristiansen et al. 2011, McAlister et al. 2008, Simpson et al. 2006, 2015).

Conclusions

These data emphasize the important role that vascular ATP-sensitive K⁺ (K_{ATP}) channels have in supporting exercise tolerance. Crucially, systemic inhibition of K_{ATP} channels via GLI reduces $\dot{V}O_{2max}$ and submaximal exercise tolerance (CS). These impairments during treadmill running are reflected in fast-twitch oxidative glycolytic MG muscle where local inhibition of vascular K_{ATP} channels reduces skeletal muscle blood flow (\dot{Q}_m) and O₂ delivery during twitch contractions (i.e., PO_{2is}). As a result, by reducing convective O₂ ($\dot{V}O_2 = \dot{Q}_m \times$ arterial-venous O₂ content) and diffusive O₂ conductances ($\dot{V}O_2 = DO_2 \times \Delta PO_2$), K_{ATP} channel inhibition lowered muscle $\dot{V}O_2$. Therefore the exercise (in)tolerance of disease patients taking oral sulphonylurea medication may be, in part, due to pharmacologically-mediated impairments in vascular O₂ transport and muscle O₂ utilization.

References

- Abdelmoneim AS, Eurich DT, Senthilselvan A, Qiu W & Simpson SH (2016). Dose-response relationship between sulphonylureas and major adverse cardiovascular events in elderly patients with type 2 diabetes. *Pharmacoepidemiology and Drug Safety* **25**, 1186-1195.
- Andersen P & Saltin B (1985). Maximal perfusion of skeletal muscle in man. *J Physiol* **366**, 233–249.
- Armstrong RB & Laughlin MH (1984). Exercise blood flow patterns within and among rat muscles after training. *Am J Physiol* **246**: H59-68.
- Banas K, Clow C, Jasmin BJ & Renaud JM (2011). The K_{ATP} channel Kir6.2 subunit content is higher in glycolytic than oxidative skeletal muscle fibers. *Am J Physiol Regul Integr Comp Physiol* **301**, R916-R925.
- Banitt PF, Smits P, Williams SB, Ganz P & Creager MA (1996). Activation of ATP-sensitive potassium channels contributes to reactive hyperemia in humans. *Am J Physiol* **271**, H1594-8.
- Behnke BJ, McDonough P, Padilla DJ, Musch TI & Poole DC (2003). Oxygen exchange profile in rat muscles of contrasting fibre types. *J Physiol* **549.2**, 597-605.
- Bijlstra PJ, den Arend JACJ, Lutterman JA, Russel FGM, Thien T & Smits P (1996). Blockade of vascular ATP-sensitive potassium channels reduces the vasodilator response to ischaemia in humans. *Diabetologia* **39**, 1562–1568.
- Brown DA, Chicco AJ, Jew KN, Johnson MS, Lynch JM, Watson PA & Moore RL (2005a). Cardioprotection afforded by chronic exercise is mediated by the sarcolemmal, and not mitochondrial, isoform of the K_{ATP} channel in the rat. *J Physiol* **569**, 913-924.
- Brown DA, Lynch JM, Armstrong CJ, Caruso NM, Ehlers LB, Johnson MS & Moore RL (2005b). Susceptibility of the heart to ischaemia-reperfusion injury and exercise-induced cardioprotection are sex-dependent in the rat. *J Physiol* **564**, 619-630.
- Broxterman RM, Hoff J, Wagner PD & Richardson RS (2020). Determinants of the diminished exercise capacity in patients with chronic obstructive pulmonary disease: looking beyond the lungs. *J Physiol* **598**, 599-610.
- Cifelli C, Boudreault L, Gong B, Bercier JP & Renaud JM (2008). Contractile dysfunctions in ATP-dependent K^+ channel-deficient mouse muscle during fatigue involve excessive depolarization and Ca^{2+} influx through L-type Ca^{2+} channels. *Exp Physiol* **93**, 1126-1138.
- Colburn TD, Ferguson SK, Holdsworth CT, Craig JC, Musch TI & Poole DC (2017). Effect of sodium nitrite on local control of contracting skeletal muscle microvascular oxygen pressure in healthy rats. *J Appl Physiol* **122**, 153-160.

Colburn TD, Hirai DM, Craig JC, Ferguson SK, Weber RE, Schulze KM, Behnke BJ, Musch TI & Poole DC (2020a). Transcapillary PO₂ Gradients in Contracting Muscles Across the Fibre Type and Oxidative Continuum. *J Physiol* **598**, 3187-3202.

Colburn TD, Holdsworth CT, Craig JC, Hirai DM, Montgomery S, Poole DC, Musch TI & Kenney MJ (2020b). ATP-sensitive K⁺ Channel Inhibition in Rats Decreases Kidney and Skeletal Muscle Blood Flow Without Increasing Sympathetic Nerve Discharge. *Respir Physiol & Neurobiol.* **278**, 103444. DOI: 10.1016/j.resp.2020.103444

Copp SW, Davis RT, Poole DC & Musch TI (2009). Reproducibility of endurance capacity and VO₂ peak in male Sprague-Dawley rats. *J Appl Physiol* **106**, 1072–1078.

Copp SW, Hirai DM, Musch TI & Poole DC (2010). Critical speed in the rat: implications for hindlimb muscle blood flow distribution and fibre recruitment. *J Physiol* **588**, 5077-5087.

Copp SW, Holdsworth CT, Ferguson SK, Hirai DM, Poole DC & Musch TI (2013). Muscle fibre-type dependence of neuronal nitric oxide synthase-mediated vascular control in the rat during high speed treadmill running. *J Physiol* **591**, 2885–2896.

Craig JC*, Colburn TD*, Caldwell JT, Hirai DM, Tabuchi A, Baumfalk DR, Behnke BJ, Ade CJ, Musch TI & Poole DC (2019a). Central and peripheral factors mechanistically linked to exercise intolerance in heart failure with reduced ejection fraction. *Am J Physiol Heart Circ Physiol* **317**, H434-H444.

Craig JC, Colburn TD, Hirai DM, Musch TI & Poole DC (2019b). Sexual dimorphism in the control of skeletal muscle interstitial PO₂ of heart failure rats: effects of dietary nitrate supplementation. *J Appl Physiol* **126**, 1184-1192.

Craig JC, Colburn TD, Hirai DM, Schettler MG, Musch TI & Poole DC (2018). Sex and nitric oxide bioavailability interact to modulate interstitial PO₂ in healthy rat skeletal muscle. *J Appl Physiol* **124**, 1558-1566.

Delp MD & Duan C (1996). Composition and size of type I, IIA, IID/X, and IIB fibers and citrate synthase activity of rat muscle. *J Appl Physiol* **80**, 261–270.

Deveci D & Egginton S (1999). Development of the fluorescent microsphere technique for quantifying regional blood flow in small mammals. *Exp Physiol* **84**, 615–630.

Dudley GA, Abraham WM & Terjung RL (1982). Influence of exercise intensity and duration on biochemical adaptations in skeletal muscle. *J Appl Physiol Respirat Environ Exercise Physiol* **53**, 844-850.

Esipova TV, Karagodov A, Miller J, Wilson DF, Busch TM & Vinogradov SA (2011). Two New “Protected” Oxyphors for Biological Oximetry: Properties and Application in Tumor Imaging. *Anal Chem* **83**, 8756-8765.

- Esposito F, Mathieu-Costello O, Shabetai R, Wagner PD & Richardson RS (2010). Limited maximal exercise capacity in patients with chronic heart failure: partitioning the contributors. *J Am Coll Cardiol* **55**, 1945-1954.
- Esposito F, Reese V, Shabetai R, Wagner PD & Richardson RS (2011). Isolated quadriceps training increases maximal exercise capacity in chronic heart failure: the role of skeletal muscle convective and diffusive oxygen transport. *J Am Coll Cardiol* **58**, 1353-1362.
- Farouque HMO & Meredith IT (2003). Effects of inhibition of ATP-sensitive potassium channels on metabolic vasodilation in the human forearm. *Clin Sci (Lond)* **104**, 39-46.
- Ferguson SK, Glean AA, Holdsworth CT, Wright JL, Fees AJ, Colburn TD, Stabler T, Allen JD, Jones AM, Musch TI & Poole DC (2016a). Skeletal muscle vascular control during exercise: impact of nitrite infusion during nitric oxide synthase inhibition in healthy rats. *J Cardiovasc Pharmacol Ther* **21**, 201-208.
- Ferguson SK, Hirai DM, Copp SW, Holdsworth CT, Allen JD, Jones AM, Musch TI & Poole DC (2013a). Effects of nitrate supplementation via beetroot juice on contracting rat skeletal muscle microvascular oxygen pressure dynamics. *Respir Physiol Neurobiol* **187**, 250-255.
- Ferguson SK, Hirai DM, Copp SW, Holdsworth CT, Allen JD, Jones AM, Musch TI & Poole DC (2013b). Impact of dietary nitrate supplementation via beetroot juice on exercising muscle vascular control in rats. *J Physiol* **591**, 547-557.
- Ferguson SK, Harral JW, Pak DI, Redinius KM, Stenmark KR, Schaer DJ, Buehler PW & Irwin DC (2018). Impact of cell-free hemoglobin on contracting skeletal muscle microvascular oxygen pressure dynamics. *Nitric Oxide* **76**, 29-36.
- Ferguson SK, Holdsworth CT, Colburn TD, Wright JL, Craig JC, Fees A, Jones AM, Allen JD, Musch TI & Poole DC (2016b). Dietary nitrate supplementation: impact on skeletal muscle vascular control in exercising rats with chronic heart failure. *J Appl Physiol* **121**, 661-669.
- Ferguson SK, Holdsworth CT, Wright JL, Fees AJ, Allen JD, Jones AM, Musch TI & Poole DC (2015). Microvascular oxygen pressures in muscles comprised of different fiber types: impact of dietary nitrate supplementation. *Nitric Oxide* **48**, 38-43.
- Flagg TP, Enkvetchakul D, Koster JC & Nichols CG (2010). Muscle K_{ATP} channels: recent insights to energy sensing and myoprotection. *Physiol Rev* **90**, 799-829.
- Glean AA, Ferguson SK, Holdsworth CT, Colburn TD, Wright JL, Fees AJ, Hageman KS, Poole DC & Musch TI (2015). Effects of nitrite infusion on skeletal muscle vascular control during exercise in rats with chronic heart failure. *Am J Physiol Heart Circ Physiol* **309**, H1354-H1360.
- Gong B, Miki T, Seino S & Renaud JM (2000). A K_{ATP} channel deficiency affects resting tension, not contractile force, during fatigue in skeletal muscle. *Am J Physiol Cell Physiol* **279**, C1351-C1358.

- Gong B, Legault D, Miki T, Seino S & Renaud JM (2003). K_{ATP} channels depress force production by reducing action potential amplitude in mouse EDL and soleus muscle. *Am J Physiol Cell Physiol* **285**, C1464-C1474.
- Grundy D (2015). Principles and standards for reporting animal experiments in The Journal of Physiology and Experimental Physiology. *J Physiol* **593** 2547–2549.
- Hammer LW, Ligon AL & Hester RL (2001). Differential Inhibition of Functional Dilation of Small Arterioles by Indomethacin and Glibenclamide. *Hypertension* **37**, 599-603.
- Haseler LJ, Hogan MC & Richardson RS (1999). Skeletal muscle phosphocreatine recovery in exercise-trained humans is dependent on O₂ availability. *J Appl Physiol* **86**: 2013–2018.
- Hirai DM, Craig JC, Colburn TD, Eshima H, Kano Y, Sexton WL, Musch TI & Poole DC (2018a). Skeletal muscle microvascular and interstitial PO₂ from rest to contractions. *J Physiol* **596**, 869-883.
- Hirai DM, Craig JC, Colburn TD, Tabuchi A, Hageman KS, Musch TI & Poole DC (2018b). Regulation of Capillary Hemodynamics by K_{ATP} Channels in Resting Skeletal Muscle. *FASEB J* **32**, 581.8.
- Hirai DM, Musch TI & Poole DC (2015). Exercise training in chronic heart failure: improving skeletal muscle O₂ transport and utilization. *Am J Physiol Heart Circ Physiol* **309**, H1419-H1439.
- Hogan MC, Arthur PG, Bebout DE, Hochachka PW & Wagner PD (1992). Role of O₂ in regulating tissue respiration in dog muscle working in situ. *J Appl Physiol* **73**, 728–36.
- Holdsworth CT, Copp SW, Ferguson SK, Sims GE, Poole DC & Musch TI (2015). Acute inhibition of ATP-sensitive K⁺ channels impairs skeletal muscle vascular control in rats during treadmill exercise. *Am J Physiol Heart Circ Physiol* **308**, H1434-42.
- Holdsworth CT, Ferguson SK, Colburn TD, Fees AJ, Craig JC, Hirai DM, Poole DC & Musch TI (2017). Vascular K_{ATP} channels mitigate severe muscle O₂ delivery-utilization mismatch during contractions in chronic heart failure rats. *Respir Physiol Neurobiol* **238**, 33–40.
- Holdsworth CT, Ferguson SK, Poole DC & Musch TI (2016). Modulation of rat skeletal muscle microvascular O₂ pressure via K_{ATP} channel inhibition following the onset of contractions. *Respir Physiol Neurobiol* **222**, 48-54.
- Ishise S, Pogram BL, Yamamoto J, Kitamura Y & Frohlich ED (1980). Reference sample microsphere method: cardiac output and blood flows in conscious rat. *Am J Physiol Heart Circ Physiol* **239**, H443-H449.
- Johnson MS, Moore RL & Brown DA (2006). Sex differences in myocardial infarct size are abolished by sarcolemmal K_{ATP} channel blockade in rat. *Am J Physiol Heart Circ Physiol* **290**, H2644–H2647.

Jones AM, Wilkerson DP, DiMenna F, Fulford J & Poole DC (2008). Muscle metabolic responses to exercise above and below the “critical power” assessed using 31P-MRS. *Am J Physiol Regul Integr Comp Physiol* **294**, R585-593.

Kane GC, Behfar A, Yamada S, Perez-Terzic C, O’Cochlain F, Reyes S, Dzeja PP, Miki T, Seino S & Terzic A (2004). ATP-Sensitive K⁺ Channel Knockout Compromises the Metabolic Benefit of Exercise Training, Resulting in Cardiac Deficits. *Diabetes* **53**, S169-S175.

Kane GC, Liu XK, Yamada S, Olson TM & Terzic A (2005). Cardiac K_{ATP} channels in health and disease. *J Mol Cell Cardiol* **38**, 937-943.

Keller DM, Ogoh S, Greene S & Raven PB (2004). Inhibition of K_{ATP} channel activity augments baroreflex-mediated vasoconstriction in exercising human skeletal muscle. *J Physiol* **561**, 273–282.

Kindig CA, Walsh B, Howlett RA, Stary CM & Hogan MC (2005). Relationship between intracellular PO₂ recovery kinetics and fatigability in isolated single frog myocytes. *J Appl Physiol* **98**: 2316 –2319.

Kristiansen SB, Løfgren B, Nielsen JM, Støttrup NM, Buhl ES, Nielsen-Kudsk JE, Nielsen TT, Rungby J, Flyvbjerg A & Bøtker HE (2011). Comparison of two sulfonylureas with high and low myocardial K(ATP) channel affinity on myocardial infarct size and metabolism in a rat model of type 2 diabetes. *Diabetologia* **54**, 451-458.

Laughlin MH, Davis MJ, Secher NH, van Lieshout JJ, Arce-Esquivel AA, Simmons GH, Bender SB, Padilla J, Bache RJ, Merkus D & Duncker DJ (2012). Peripheral Circulation. *Compr Physiol* **2**, 321-447.

Li Y, Wei Y, Zhang F, Wang D & Wu X (2012). Changes in the pharmacokinetics of glibenclamide in rats with streptozotocin-induced diabetes mellitus. *Acta Pharmaceutica Sinica B* **2**, 198-204.

Lu S, Xiang L, Clemmer JS, Gowdey AR, Mittwede PN & Hester RL (2013). Impaired vascular K_{ATP} function attenuates exercise capacity in obese Zucker rats. *Microcirculation* **20**, 662-669.

Marcondes FJ, Bianchi FJ & Tanno AP (2002). Determination of the estrous cycle phases of rats: some helpful considerations. *Brazilian J Biol* **62**, 609-614

Matar W, Nosek TM, Wong D & Renaud JM (2000). Pinacidil suppresses contractility and preserves energy but glibenclamide has no effect during muscle fatigue. *Am J Physiol Cell Physiol* **278**, C404-C416.

McAlister FA, Eurich DT, Majumdar SR & Johnson JA (2008). The risk of heart failure in patients with type 2 diabetes treated with oral agent monotherapy. *Eur J Heart Fail* **10**, 703-708.

McDonough P, Behnke BJ, Kindig CA & Poole DC (2001). Rat muscle microvascular PO₂ kinetics during the exercise off-transient. *Exp Physiol* **86**, 349-356.

- McDonough P, Behnke BJ, Padilla DJ, Musch TI & Poole DC (2005). Control of microvascular oxygen pressures in rat muscles comprised of different fibre types. *J Physiol* **563**, 903-913.
- Monod H & Scherrer J (1965). The work capacity of a synergic muscular group. *Ergonomics* **8**, 329-338.
- Montvida O, Shaw J, Atherton JJ, Stringer F & Paul SK (2018). Long-term Trends in Antidiabetes Drug Usage in the U.S.: Real-world Evidence in Patients Newly Diagnosed with Type 2 Diabetes. *Diabetes Care* **41**, 69-78.
- Musch TI (1988). Measurements of metabolic rate in rats: a comparison of techniques. *J Appl Physiol* **65**, 964-970.
- Musch TI (1992). Training effects on the regional blood flow response to exercise in myocardial infarcted rats. *Am J Physiol Heart Circ Physiol* **262**, H1846-H1852.
- Musch TI & Terrell JA (1992). Skeletal muscle blood flow abnormalities in rats with a chronic myocardial infarction: rest and exercise. *Am J Physiol Heart Circ Physiol* **262**, H411-H419.
- Musch TI, Moore RL, Leathers DJ, Bruno A & Zelis R (1986). Endurance training in rats with chronic heart failure induced by myocardial infarction. *Circulation* **74**, 431-441.
- Padilla DJ, McDonough P, Behnke BJ, Kano Y, Hageman KS, Musch TI & Poole DC (2006). Effects of type II diabetes on capillary hemodynamics in skeletal muscle. *Am J Physiol Heart Circ Physiol* **291**, H2439-H2444.
- Padilla DJ, McDonough P, Behnke BJ, Kano Y, Hageman KS, Musch TI & Poole DC (2007). Effects of type II diabetes on muscle microvascular oxygen pressures. *Respir Physiol Neurobiol* **156**, 187-195.
- Poole DC (2019). Edward F. Adolph Distinguished Lecture. Contemporary model of muscle microcirculation: gateway to function and dysfunction. *J Appl Physiol* **127**, 1012-1033.
- Poole DC, Burnley M, Vanhatalo A, Rossiter HB & Jones AM (2016). Critical Power: An Important Fatigue Threshold in Exercise Physiology. *Med Sci Sports Exerc* **48**, 2281-2293.
- Poole DC, Copp SW, Colburn TD, Craig JC, Allen DL, Sturek M, O'Leary DS, Zucker IH & Musch TI (2020). Guidelines for animal exercise and training protocols for cardiovascular studies. *Am J Physiol Heart Circ Physiol* **318**, H1100-1138.
- Poole DC, Copp SW, Ferguson SK & Musch TI (2013). Skeletal muscle capillary function: contemporary observations and novel hypotheses. *Exp Physiol* **98**, 1645-1658.
- Poole DC & Jones AM (2012). Oxygen uptake kinetics. *Compr Physiol* **2**, 933-996.
- Poole DC, Ward SA, Gardner GW & Whipp BJ (1988). Metabolic and respiratory profile of the upper limit for prolonged exercise in man. *Ergonomics* **31**, 1265-1279.

- Richardson RS, Noyszewski EA, Leigh JS & Wagner PD (1998). Lactate efflux from exercising human skeletal muscle: role of intracellular PO₂. *J Appl Physiol* **85**, 627–634.
- Richardson RS, Poole DC, Knight DR, Kurdak SS, Hogan MC, Grassi B, Johnson EC, Kendrick KF, Erickson BK & Wagner PD (1993). High muscle blood flow in man: is maximal O₂ extraction compromised? *J Appl Physiol* **75**, 1911-1916.
- Richmond KN, Shonat RD, Lynch RM & Johnson PC (1999). Critical PO₂ of skeletal muscle in vivo. *Am J Physiol Heart Circ Physiol* **277**, H1831-H1840.
- Roca J, Agusti AG, Alonso A, Poole DC, Viegas C, Barbera JA, Rodriguez-Roisin R, Ferrer A & Wagner PD (1992). Effect of training on muscle O₂ transport at VO_{2max}. *J Appl Physiol* **73**, 1067-76.
- Rosenberry R, Tucker WJ, Haykowsky MJ, Trojacek D, Chamseddine HH, Arena-Marshall CA, Zhu Y, Wang J, Kellawan JM, Tian F & Nelson MD (2019). Determinants of skeletal muscle oxygen consumption assessed by near-infrared diffuse correlation spectroscopy during incremental handgrip exercise. *J Appl Physiol* **127**, 698–706.
- Rumsey WL, Vanderkooi JM & Wilson DF (1988). Imaging of Phosphorescence: A Novel Method for Measuring Oxygen Distribution in Perfused Tissue. *Science* **241**, 1649-1651, 1988.
- Saito Y, McKay M, Eraslan A & Hester RL (1996). Functional hyperemia in striated muscle is reduced following blockade of ATP-sensitive potassium channels. *Am J Physiol Heart Circ Physiol* **270**, H1649–H1654.
- Simpson SH, Lee J, Choi S, Vandermeer B, Abdelmoneim AS & Featherstone TR (2015). Mortality risk among sulfonylureas: a systematic review and network meta-analysis. *Lancet Diabetes Endocrinol* **3**, 43-51.
- Simpson SH, Majumdar SR, Tsuyuki RT, Eurich DT & Johnson JA (2006). Dose-response relation between sulphonylurea drugs and mortality in type 2 diabetes mellitus: a population-based cohort study. *CMAJ* **174**, 169-174.
- Smith JR, Hageman KS, Harms CA, Poole DC & Musch TI (2017). Respiratory muscle blood flow during exercise: Effects of sex and ovarian cycle. *J Appl Physiol* **122**, 918-924.
- Thabet M, Miki T, Seino S & Renaud TM (2005). Treadmill running causes significant fiber damage in skeletal muscle of K_{ATP} channel-deficient mice. *Physiol Genomics* **22**, 204-212.
- Van Oosterhout MFM, Prinzen FW, Sakurada S, Glenny RW& Hales JRS (1998). Fluorescent microspheres are superior to radioactive microspheres in chronic blood flow measurements. *Am J Physiol Heart Circ Physiol* **275**, H110–H115.
- Wagner PD (1992). Gas exchange and peripheral diffusion limitation. *Med Sci Sports Exerc* **24**, 54-58.

Wagner PD (1996). Determinants of maximal oxygen transport and utilization. *Annu Rev Physiol* **58**, 21-50.

Wilson DF, Erecinska M, Drown C & Silver IA (1977). Effect of oxygen tension on cellular energetics. *Am J Physiol Cell Physiol* **233**, C135-140.

Zingman LV, Alekseev AE, Hodgson-Zingman DM & Terzic A (2007). ATP-sensitive potassium channels: metabolic sensing and cardioprotection. *J Appl Physiol* **103**, 1888-1893.

Table 3.1. Doppler echocardiographic assessment of left ventricular function during control and systemic K_{ATP} channel inhibition

	Control	GLI
LVIDd (cm)	0.71 ± 0.08	0.72 ± 0.05
LVIDs (cm)	0.38 ± 0.08	0.41 ± 0.06
FS (%)	47 ± 6	42 ± 5
LVEDV (ml)	0.83 ± 0.24	0.83 ± 0.18
LVESV (ml)	0.15 ± 0.07	0.19 ± 0.09
SV (ml)	0.68 ± 0.19	0.65 ± 0.11
EF (%)	83 ± 5	78 ± 6
+V (cm s⁻¹)	2.76 ± 0.49	2.44 ± 0.43
-V (cm s⁻¹)	2.11 ± 0.59	1.70 ± 0.23 *
HR (bpm)	321 ± 23	304 ± 22 *
CO (ml min⁻¹)	219 ± 64	197 ± 39

GLI, glibenclamide; LVIDd, left ventricular end-diastole internal diameter; LVIDs, left ventricular end-systole internal diameter; FS, fractional shortening; LVEDV, left ventricular end-diastolic volume; LVESV, left ventricular end-systolic volume; SV, stroke volume; EF, ejection fraction; +V, rate of contraction; -V, rate of relaxation; HR, heart rate; CO, cardiac output. Data are mean ± SD (n=10) and compared via two-tail paired t-test. * P < 0.05 vs control.

Table 3.2. Individual maximal oxygen uptake and speed-duration relationship parameters during control and systemic KATP channel inhibition

	Control			GLI		
	$\dot{V}O_{2max}$	CS	D'	$\dot{V}O_{2max}$	CS	D'
	(ml min ⁻¹ kg ⁻¹)	(m min ⁻¹)	(m)	(ml min ⁻¹ kg ⁻¹)	(m min ⁻¹)	(m)
1	67.7	39.5	84	70.0	29.3	124
2	71.3	34.2	127	61.4	32.2	79
3	75.2	34.5	93	69.5	28.3	95
4	65.2	--	--	64.8	--	--
5	70.8	34.0	92	61.1	34.1	83
6	73.3	39.8	75	65.5	35.0	79
7	74.7	35.4	101	77.2	29.7	127
8	73.1	--	--	70.8	--	--
9	71.9	34.0	111	69.9	30.1	89
10	71.9	35.4	105	69.0	36.7	52
Mean ± SD	71.5 ± 3.1	35.9 ± 2.4	98 ± 16	67.9 ± 4.8 *	31.9 ± 3.1 *	91 ± 25

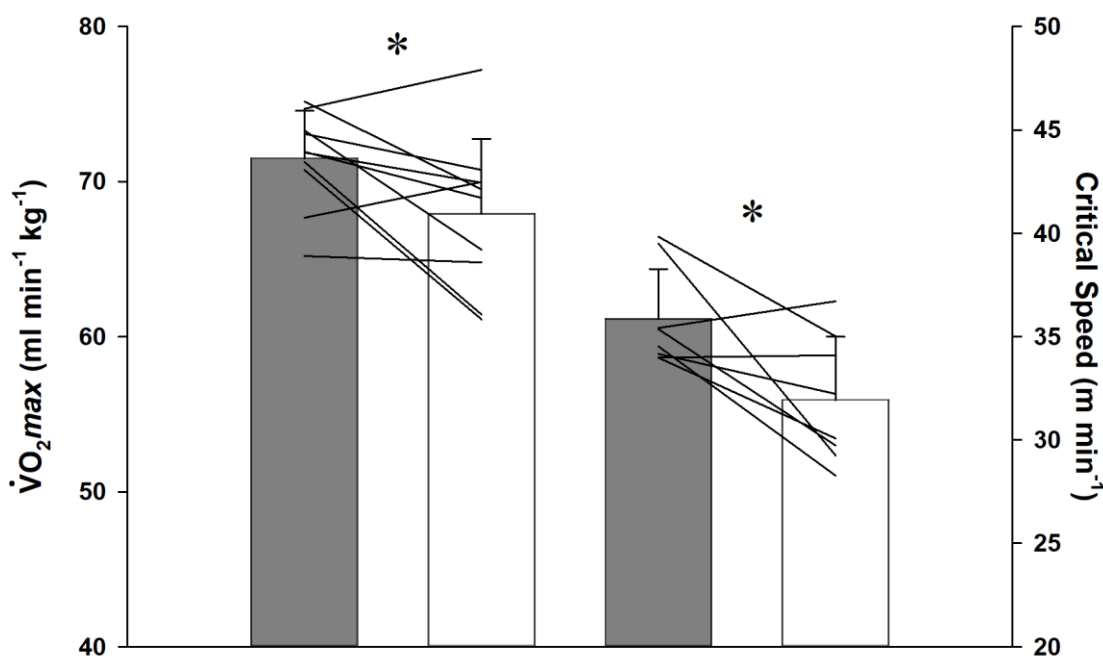
$\dot{V}O_{2max}$, maximal oxygen uptake; CS, critical speed; D', curvature constant. The speed-duration relationship parameters are presented from the hyperbolic model. Data were compared via two-tail paired t-test. * P < 0.05 vs control

Table 3.3. Interstitial PO₂ kinetics parameters during 180 s twitch contractions and 240 s recovery during control and local K_{ATP} channel inhibition

	Mixed Gastrocnemius	
	Control	GLI
Pre-Superfusion PO_{2is} (mmHg)	--	13.8 ± 3.4
PO_{2is} BL (mmHg)	14.1 ± 1.4	12.8 ± 3.6 *
Δ₁PO_{2is} (mmHg)	8.2 ± 1.5	8.1 ± 3.1
TD (s)	8.0 ± 4.3	5.2 ± 3.2 *
τ (s)	14.1 ± 2.7	12.2 ± 3.0
MRT (s)	22.2 ± 4.7	17.3 ± 4.3 *
PO_{2is} nadir (mmHg)	5.9 ± 0.9	4.7 ± 1.1 *
Δ₂PO_{2is} (mmHg)	1.4 ± 0.9	1.4 ± 0.8
PO_{2is} end (mmHg)	7.3 ± 1.5	6.1 ± 1.4
Δ₁PO_{2is}/τ (mmHg s⁻¹)	0.60 ± 0.16	0.72 ± 0.36
Recovery T₆₃ (s)	95 ± 19	118 ± 20 *
Recovery PO_{2is} (mmHg)	14.6 ± 4.0	15.3 ± 6.5
Δ₃PO_{2is}/T₆₃ (mmHg s⁻¹)	0.07 ± 0.03	0.08 ± 0.04

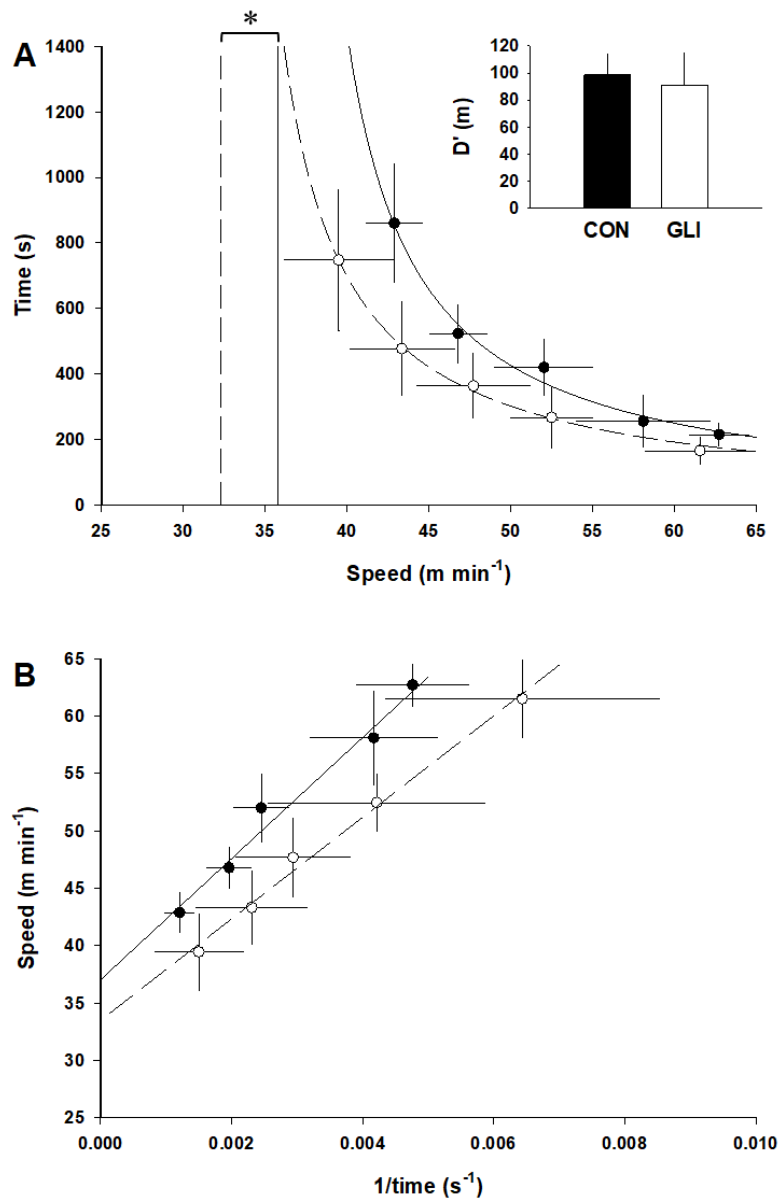
PO_{2is} BL, resting baseline PO_{2is}; Δ₁PO_{2is} and Δ₂PO_{2is}, amplitude of the first and second components, respectively; TD, time delay; τ, time constant; MRT, mean response time; PO_{2is} nadir, lowest response prior to secondary rise in PO_{2is}; PO_{2is} end, PO_{2is} at the end of contractions; Δ₁PO_{2is}/τ, rate of PO_{2is} fall; T₆₃, time to reach 63% of final response; Δ₃PO_{2is}/T₆₃, rate of PO_{2is} recovery. Data are mean ± SD and compared via two-tail paired t-tests. * P < 0.05 vs control

Figure 3.1. Effect of systemic K_{ATP} channel inhibition on maximal and submaximal exercise



Note the significant reduction in maximal oxygen uptake ($\dot{V}O_{2\text{max}}$; n=10) and critical speed (n=8) following glibenclamide (open bars) compared to control (gray bars). Data are mean \pm SD with individual data plotted and compared via two-tail paired t-tests. * P < 0.05 vs. control

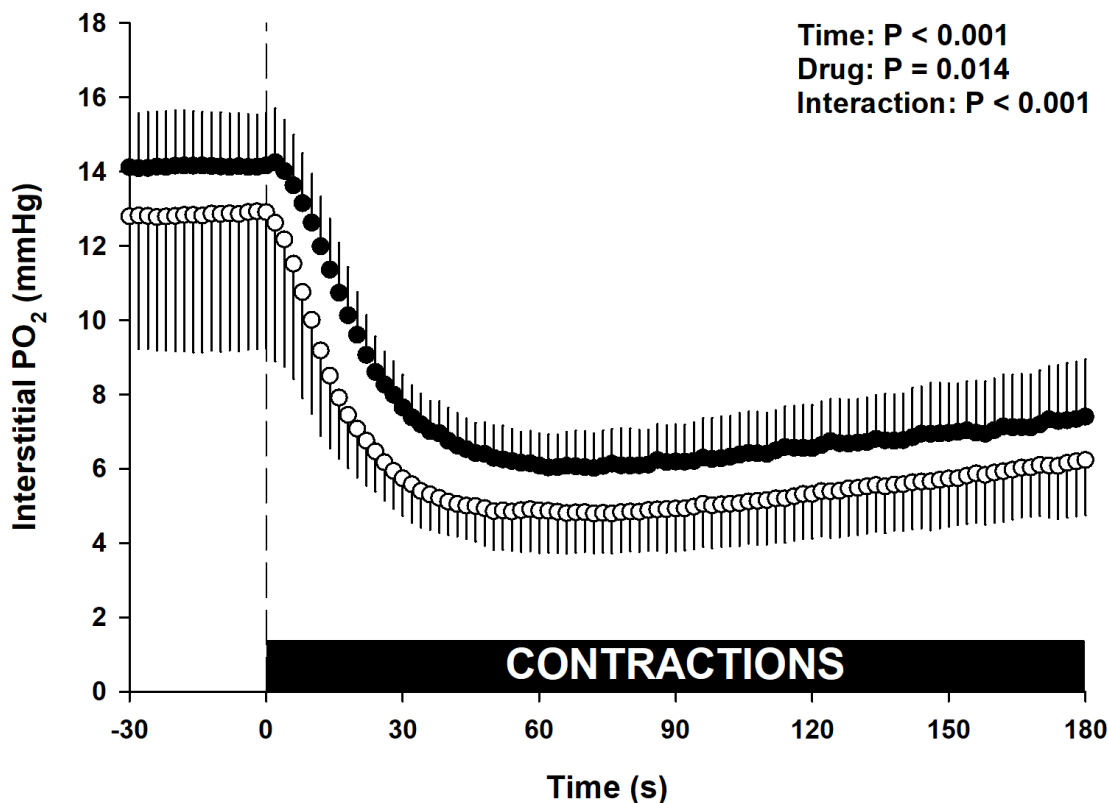
Figure 3.2. Speed-duration relationship following systemic K_{ATP} channel inhibition



The hyperbolic (A) and 1/time linear (B) speed-duration relationships are modeled under control (closed circle, solid line) and systemic K_{ATP} channel inhibition (GLI; open circle, dashed line) to determine critical speed (vertical lines (A) and y-intercept (B)) and D' (inset). These mean data fits are for illustrative purposes only, with individually determined CS and D' and subsequent group means presented in Table 2. Data are mean \pm SD and compared via two-tail paired t-tests.

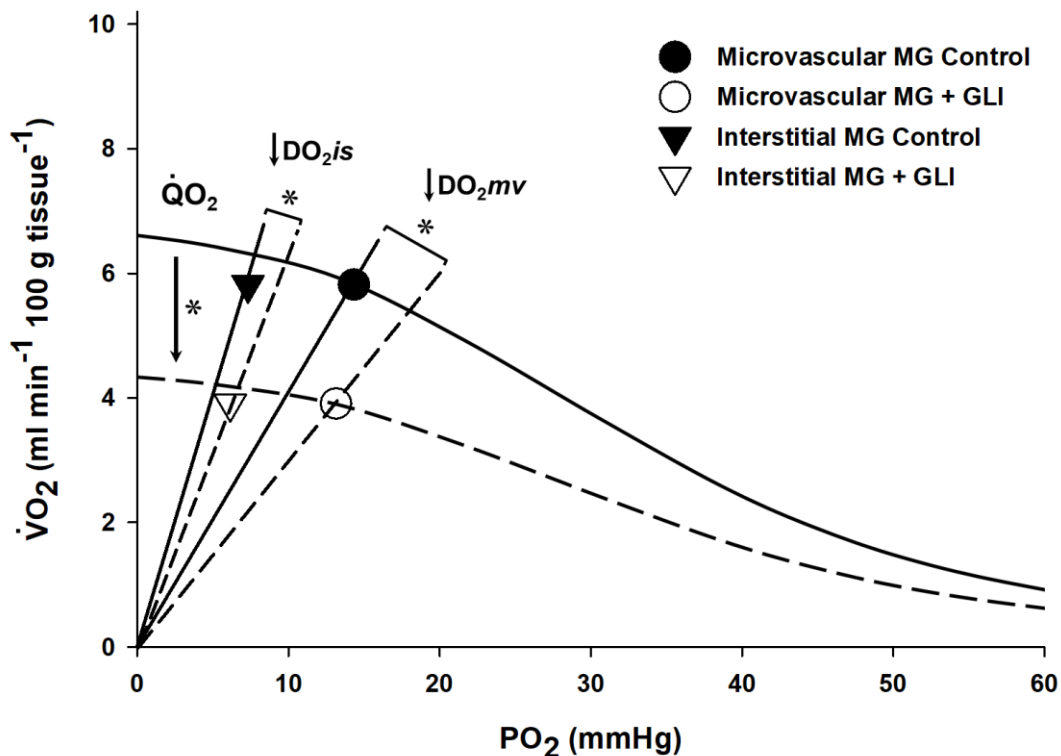
* P < 0.05 vs control

Figure 3.3. Interstitial PO₂ of fast-twitch oxidative muscle following local K_{ATP} channel inhibition



Note the difference in mixed gastrocnemius PO₂s following glibenclamide (GLI, open symbols, n=10) superfusion compared to control (closed symbols). Dashed line denotes the onset of twitch contractions at time zero. Data are mean \pm SD and compared via two-way (Time x Drug) repeated measure ANOVA with Tukey's *post hoc* analyses.

Figure 3.4. The effect of local K_{ATP} channel inhibition on the convective and diffusive determinants of oxygen transport



Graphical representation of the relationship between convective ($\dot{V}O_2 = \dot{Q} \times a-vO_2$ difference; curved line) and diffusive ($\dot{V}O_2 = DO_2 \times PO_2$; slope from origin) determinants of oxygen transport in the microvascular (circles) and interstitial (down triangles) compartments of the fast-twitch oxidative mixed gastrocnemius (MG, n=10) muscle following vascular K_{ATP} channel inhibition via glibenclamide (GLI, open symbols). Importantly, unlike haemoglobin-O₂ transport in the microvasculature, the lack of haeme-O₂ storage in interstitial fluid dictates that interstitial $\dot{V}O_2$ ($\dot{V}O_{2is}$) must equal microvascular $\dot{V}O_2$ ($\dot{V}O_{2mv}$) allowing DO_{2is} to be assessed with the present data ($\dot{V}O_{2mv} = \dot{V}O_{2is} = DO_{2is} \times PO_{2is}$). Note the reductions in both convective ($\dot{Q}O_{2mv}$, curved lines Y-intercept) and diffusive (DO_{2mv} and DO_{2is}) components of MG muscle compared to control (closed symbols). * P < 0.05 vs control with two-tail paired t-tests.

Chapter 4 - Sexual dimorphism in vascular ATP-sensitive K⁺ channel function supporting interstitial PO₂ via convective and/or diffusive O₂ transport

Trenton D. Colburn^a, Ramona E. Weber^a, Kiana M. Schulze^a, K. Sue Hageman^b, Andrew G. Horn^a, Brad J. Behnke^a, David C. Poole^{a,b}, Timothy I. Musch^{a,b}

^aDepartment of Kinesiology, ^bDepartment of Anatomy and Physiology, Kansas State University
Manhattan, KS, 66506, USA

Summary

Vascular ATP-sensitive K^+ (K_{ATP}) channels support skeletal muscle blood flow (\dot{Q}_m), interstitial O_2 delivery ($\dot{Q}O_2$)-utilization ($\dot{V}O_2$) matching (setting the driving pressure for interstitial-myocyte O_2 flux; PO_2is) and exercise tolerance. While myocardial K_{ATP} channels mitigate tissue damage following ischemia in a sex-dependent manner, potential sex differences in skeletal muscle vascular K_{ATP} channel function remain largely unexplored. We hypothesized that local skeletal muscle K_{ATP} channel inhibition via glibenclamide superfusion (5 mg kg⁻¹ GLI; sulfonylurea diabetes medication prescribed to inhibit pancreatic K_{ATP} channels and enhance insulin release) in anesthetized female Sprague-Dawley rats, compared to males, would demonstrate greater reductions in contracting (1 Hz, 7V, 180 s) fast-twitch oxidative mixed gastrocnemius (MG; 97% type IIA+IID/X+IIB) \dot{Q}_m (15 μm microspheres) and PO_2is (phosphorescence quenching), resulting from more compromised convective ($\dot{Q}O_2$) and diffusive (DO_2) O_2 conductances. It was further hypothesized that these GLI-induced reductions in ovary-intact females measured during proestrus would be diminished following ovariectomy (F+OVX). Following GLI, MG $\dot{V}O_2$ was similarly impaired in both males and females via reduced \dot{Q}_m , $\dot{Q}O_2$, and the resulting PO_2is , with females also demonstrating reduced DO_2 and greater GLI-induced speeding of PO_2is fall (mean response time: Sex x Drug interaction, $P=0.026$). Conversely, GLI did not impair the MG of F+OVX rats suggesting that a significant loss in vascular K_{ATP} channel function may occur postmenopause. Therefore, in patients taking sulfonylureas, impaired vascular K_{ATP} channel function may compromise muscle \dot{Q}_m and therefore exercise tolerance, and in so doing contribute to adverse cardiovascular events, in premenopausal females to a greater extent than males.

Introduction

In 2016, in addition to the health burden on patients, cardiovascular disease (CVD) and strokes accounted for \$351.2 billion in direct and indirect U.S health care costs (\$237 billion in direct costs for diabetes mellitus from 2014 to 2015) and prevalence continues to increase in the U.S and worldwide (\$1.1 trillion by 2035; Benjamin et al., 2019). With the attention to pharmacological and non-pharmacological (i.e. physical activity) treatments in halting the progression of CVD, it is imperative to understand the underlying mechanisms of sex-differences in the incidence, morbidity, and mortality of CVD (Bhatia et al., 2006; Fang et al., 2008; Ho et al., 1993). Premenopausal females present a lower risk/prevalence for hospitalizations consequent to myocardial infarction (MI) compared to males (i.e. fewer MIs in young females with older females contributing to a greater proportion of heart failure with preserved ejection fraction patients), but a higher prevalence of hypertension, myocardial infarction, ischaemic stroke, and greater mortality risk with a history of diabetes mellitus (Bhatia et al., 2006; Ho et al., 1993; Malmborg et al. 2020).

One proposed mechanism in the sex-dependent cardio-protection, specifically MI-related, is the greater energy sensing potassium channel (K_{ATP} ; ATP-sensitive) content of female hearts and potentially skeletal muscle and their importance for reducing MI size (Brown et al., 2005b, Chicco et al., 2007; Johnson, Moore & Brown, 2006) and the ability for these channels to further increase cardioprotection following exercise (Chicco et al., 2007). Nevertheless, sulphonylureas (K_{ATP} channel inhibitors that enhance pancreatic insulin release) such as glibenclamide (GLI) are the most popular second-line therapy prescribed for type 2 diabetes mellitus (T2DM; Montivida et al. 2018) despite this increasing the risk for adverse cardiovascular events (Abdelmoneim et al. 2016, Simpson et al. 2006, 2015), developing heart failure (McAlister et al. 2008, Kristiansen et al. 2011), and all-cause mortality (Simpson et al. 2015).

K_{ATP} channels function as endogenous mediators of stress, where locally decreased ATP:ADP ratios open K_{ATP} channels, hyperpolarize cell membranes and allow relaxation of muscle cells (Flagg et al., 2010; Quayle, Nelson & Standen 1997). Sarcolemmal K_{ATP} channels in rats protect the heart from ischemic damage and reduce infarct size in a sex-dependent manner (Brown et al., 2005b; Johnson, Moore & Brown, 2006) and their content in cardiac tissue increases following exercise training (Brown et al., 2005a,b; Chicco et al., 2007). In skeletal muscle, vascular K_{ATP} channels have been implicated in reactive and functional hyperemia (Banitt et al., 1996; Bank et al., 2000; Bijlstra et al., 1996; Saito et al., 1996). During submaximal exercise in male rats, vascular K_{ATP} channels mediate increases in muscle blood flow (\dot{Q}_m ; proportional to oxidative fiber content; Holdsworth et al., 2015) leading to enhanced matching of O_2 delivery-to-utilization (PO_2) during contractions in mixed and fast-twitch fiber muscles (Holdsworth et al., 2016; Colburn et al. 2020b) and support exercise tolerance in female rats (i.e., critical speed; Colburn et al. 2020b). GLI application prior to contractions/exercise significantly reduces functional dilation of muscle arterioles and maximal aerobic capacity ($\dot{V}O_{2max} = \dot{Q}_{max} \times \text{maximal } a-vO_2 \text{ difference}$; Colburn et al. 2020b; Lu et al., 2013). Therefore the preservation of vascular K_{ATP} channel function in skeletal muscle is imperative to avoid an O_2 delivery-utilization mismatch and reduction in exercise tolerance (Colburn et al. 2020b; Lu et al., 2013). However, potential sex differences in skeletal muscle vascular K_{ATP} channel function remain to be investigated.

Additionally, as estrogen levels significantly decline following menopause when the incidence of CVD and hypertension increases, and estrogen may impact K_{ATP} channel number and/or function (Gao et al., 2014; Lee et al., 2003; Ranki et al., 2001, 2002a), it is imperative to assess the role of vascular K_{ATP} channels in pre- and post-menopausal models (females with intact

ovaries and ovariectomized females (F+OVX), respectively). Estrogen has been shown to stimulate myocardial K_{ATP} channel formation (Ranki et al., 2002a), mediate protection against ischemia-reperfusion injury (Gao et al., 2014), and increase NO production which may have the downstream effect of activating K_{ATP} channels. Despite acute estrogen treatment not inducing K_{ATP}-mediated vasodilation post-angioplasty (Lee et al., 2003), the effect of ovariectomy, and thus chronically lowered estrogen levels, on vascular K_{ATP} channel function remains unknown.

Collectively, as sulphonylurea treatment may exacerbate exercise intolerance and CVD progression, the current investigation sought to define the potential sex differences (male vs female), and the effect of ovariectomy (female vs F+OVX), on vascular K_{ATP} channel function in supporting O₂ delivery-utilization matching as measured in the interstitial space of muscle (PO_{2is}) during contractions. We hypothesized that female rats, studied during the proestrus phase, would demonstrate a larger GLI-induced reduction in contracting \dot{Q}_m and PO_{2is} in fast-twitch oxidative skeletal muscle compared to male rats as a result of both impaired convective (\dot{Q}_{O_2}) and diffusive (DO₂) O₂ conductances. In addition, since estrogen is chronically lowered following ovariectomy, F+OVX rats were hypothesized to have smaller GLI-induced reductions in fast-twitch oxidative muscle \dot{Q}_m , PO_{2is}, and \dot{Q}_{O_2} and DO₂ conductances compared to ovary-intact female rats, demonstrating the beneficial effect of female sex hormones (i.e., estrogen) on skeletal muscle vascular K_{ATP} channel function.

Methods

Ethical Approval

The following protocols and procedures were approved by the Kansas State University Institutional Animal Care and Use Committee and conducted according to the guidelines and ethical standards of the National Institutes of Health and Journal of Physiology (Grundy, 2015). Twelve male, ten female, and twelve F+OVX Sprague-Dawley rats (~8 months old) were maintained in animal facilities accredited by the Association for the Assessment and Accreditation of Laboratory and Animal Care on a 12:12 h light:dark cycle with food and water provided *ad libitum*. In female rats, vaginal lavages were conducted for at least 10 days to monitor menstrual cycles with measurements performed during the proestrus phase (Marcondes et al. 2002, Smith et al. 2017). Vaginal lavages were also performed in F+OVX rats to confirm the absence of the proestrus phase.

Drug Dosing

Local inhibition of vascular K_{ATP} channels was performed via superfusion of the pharmacological sulphonylurea derivative glibenclamide (GLI: 494 g mol⁻¹, 5-chloro-N-{4-[N-(cyclohexylcarbamoyl)sulfamoyl]phenthyl}-2-methoxybenzamide, Sigma-Aldrich, St. Louis, MO) onto the muscle surface. A 10 ml stock solution was made by dissolving GLI in 9 ml distilled water, 900 µl NaOH (0.1 M) and 100 µl DMSO and briefly sonicated. To obtain a final 5 mg kg⁻¹ dose in Krebs-Hensleit solution (Holdsworth et al. 2017; Colburn et al. 2020b), the amount of GLI dissolved into the stock solution was determined daily and then 0.5 ml of the GLI stock solution was diluted in 2.5 ml of warmed Krebs-Hensleit bicarbonate-buffered solution equilibrated with 5% CO₂-95% N₂ (pH 7.4; in mM, 4.7 KCl, 2.0 CaCl₂, 2.4 MgSO₄, 131 NaCl and 22 NaHCO₃).

Phosphorescence quenching determination of PO₂is

During catheterization of the carotid and caudal arteries, and surgical exposure of the hindlimb muscles, all rats were initially anesthetized on 5% isoflurane-O₂ mixture and maintained on 2-2.5% isoflurane-O₂ mixture while core temperature was maintained (~37-38°C) via heating pad and measured via rectal thermometer. A midline incision of the skin covering the neck was conducted to isolate and cannulate the right carotid artery (PE-10 connected to PE-50; Intra-Medic polyethylene tubing; BD, Franklin Lakes, NJ, USA) for continuous measurements of mean arterial pressure (MAP) and heart rate (HR), and infusion of fluorescent-labelled microspheres for blood flow measurements (see *Fluorescent microsphere assessment of blood flow*). The caudal artery was isolated and cannulated for infusion of pentobarbital sodium anesthesia and blood sampling (i.e., blood gases and blood flow reference sample). The arterial blood samples were collected following the final contraction protocol of each muscle to assess O₂ saturation, systemic haematocrit and plasma lactate (Nova Stat Profile M; Nova Biomedical, Waltham, MA, USA).

Following catheterization, the left biceps femoris was exposed via an incision above the lateral malleolus to reflect overlaying skin and fascia. The distal portion of the biceps femoris was then reflected, after ligating the lateral great saphenous artery (6-0 silk suture), in order to expose the mixed gastrocnemius (MG). The MG muscle was selected for its high oxidative capacity (citrate synthase: ~25 µmol min⁻¹ g⁻¹), fast-twitch fibre composition (97% type IIA+IID/X+IIB; Delp & Duan 1996), and thus fibre recruitment pattern below and at the fatigue threshold (i.e., critical speed; Copp et al. 2010). While the anatomical origin and insertion of the MG muscle was left attached, variations in muscle length were minimized throughout the experimental protocol by stabilizing the knee and ankle joints at ~90° angles. Rats were then progressively transitioned off isoflurane and onto pentobarbital sodium anesthesia (50 mg ml⁻¹, i.a.) with toe pinch and corneal

sensitivity reflexes used to assess depth of anesthesia throughout the remainder of the experiments, with additional anesthesia provided as necessary (0.03-0.05 ml of 50 mg ml⁻¹ diluted to 0.3 ml of heparinized saline). To produce electrically induced muscle contractions in the experimental protocol, platinum iridium electrodes were attached (6-0 silk suture) to the proximal (cathode) and distal (anode) regions of the muscles. To minimize tissue dehydration and exposure to superfused solutions, surrounding exposed tissue was covered with Saran Wrap (Dow Brands, Indianapolis, IN) while the remaining exposed muscle was superfused regularly with warmed Krebs-Henseleit bicarbonate buffered solution equilibrated with 5% CO₂-95% N₂.

Experimental protocol. The MG underwent two separate contraction bouts following control (Krebs-Henseleit) and K_{ATP} channel inhibition (5 mg kg⁻¹ GLI in Krebs-Henseleit) superfusions. GLI superfusion was performed second, due to the long half-life of GLI, and > 20 min after the control contraction bout in order to prevent any potential priming effect on PO_{2is} profiles due to repeated contraction bouts. Interstitial space PO₂ (PO_{2is}) was measured via phosphorescence quenching at rest and during 180 s twitch contractions (1 Hz, 7 V, 2 ms pulse duration; Grass stimulator model S88, Quincy, MA) and recorded at 2 s intervals (Colburn et al. 2020a,b; Craig et al. 2018, 2019; Hirai et al. 2018a). PO_{2is} was monitored after the cessation of contractions to ensure that PO_{2is} returned and stabilized at baseline prior to subsequent GLI superfusion and contractions. While continuously measuring PO_{2is}, GLI was superfused (3 ml total volume) onto the MG for 180 s and allowed an additional 180 s before the same contraction protocol was repeated (i.e., total of > 23 min elapsed between contraction bouts).

Measurement of interstitial PO₂. PO_{2is} was measured via a frequency domain phosphorometer (PMOD 5000; Oxygen Enterprises, Philadelphia, PA) as described previously (Craig et al. 2018, 2019, Hirai et al. 2018a). The Oxyphor G4 (Pd-meso-tetra-(3,5-

dicarboxyphenyl)-tetrabenzoporphyrin) was injected locally (two to four 10 μ l injections at 10 μ M concentration) with a 29 gauge needle. Care was taken to avoid any visible vasculature and, following injection, the muscle was covered in Saran Wrap and > 20 min was allowed for the G4 to thoroughly diffuse throughout the interstitial space. This oxyphor is well suited for use in biological tissues because it is stable across the physiological pH range and does not cross membranes (Esipova et al. 2011). However, this oxyphor is temperature sensitive and thus a noncontact infrared thermometer was used to measure muscle surface temperature. Mean muscle temperature was $31.2 \pm 0.2^\circ\text{C}$ with no differences between groups or during contractions, similar to prior investigations from our laboratory (Colburn et al. 2020b; Craig et al. 2018, 2019).

The Stern-Volmer relationship is applied during phosphorescence quenching (Rumsey et al. 1988; Esipova et al. 2011) to describe the quantitative O₂ dependence of the phosphorescent probe G4 via the equation $\text{PO}_2is = [(\tau_0/\tau) - 1]/(k_Q \cdot \tau_0)$, where k_Q is the quenching constant and τ and τ_0 are the phosphorescence lifetimes at the ambient O₂ concentration and in the absence of O₂, respectively. The following settings were used for G4 in tissue at $\sim 32^\circ\text{C}$: k_Q of 258 mmHg/s and τ_0 of 226 μ s (Esipova et al. 2011). Importantly, the phosphorescence lifetime is determined exclusively by the O₂ partial pressure since the muscle contraction protocol herein does not appreciably change muscle temperature (Colburn et al. 2020b; Craig et al. 2018, 2019). Following G4 injections, the common end of the bifurcated light guide was positioned 3–4 mm above the exposed muscle surface. In order to minimize extraneous exposure to light, all PO₂is measurements were conducted in a dark room.

Analysis of interstitial PO₂ kinetics. During the analyses of PO₂is responses throughout 30s of rest and the 180 s contraction bouts, a monoexponential plus time delay model (one component)

or a monoexponential plus time delay with a secondary component (two component) model was used when necessary,

One component

$$PO_2is_t = PO_2is_{BL} - \Delta_1 PO_2is(1 - e^{-(t - TD)/\tau})$$

Two component

$$PO_2is_t = PO_2is_{BL} - \Delta_1 PO_2is(1 - e^{-(t - TD)/\tau}) + \Delta_2 PO_2is(1 - e^{-(t - TD_2)/\tau_2})$$

where PO_2is_t represents the PO_2is at any point in time, PO_2is_{BL} is the baseline before contraction onset, $\Delta_1 PO_2is$ and $\Delta_2 PO_2is$ are the primary and secondary amplitudes, TD and TD_2 are the time delays before the fall and secondary rise in PO_2is , and τ and τ_2 are the time constants (i.e., the time required to reach 63% of the amplitude) for the primary and secondary amplitudes. The mean response time (MRT) was calculated as the sum of the model derived TD and τ . When utilizing the two component model, the accuracy of the primary response kinetics were maximized by constraining the primary amplitude to the nadir value (Colburn et al. 2020b; Craig et al. 2018, 2019). The following criteria was used to determine the goodness of model fit to raw PO_2is data: 1) coefficient of determination, 2) sum of the squared residuals, and 3) visual inspection. Because $\Delta_2 PO_2is$ (i.e., undershoot of PO_2is ; $\Delta_2 PO_2is = PO_2is_{end} - PO_2is_{nadir}$) was often nonexponential, $\Delta_2 PO_2is$ was determined manually by subtracting the nadir value of PO_2is during contractions ($PO_2is_{nadir} = PO_2is_{BL} - \Delta_1 PO_2is$) from the PO_2is at the end of contractions (PO_2is_{end} , average of 172-180 s).

Fluorescent microsphere determination of blood flow

MG blood flows were determined using the microsphere technique as described previously (Colburn et al. 2020b; Deveci & Egginton 1999; Musch et al. 1986). Two fluorescent microspheres

(blue-green (430/465nm) and red (580/605nm), Invitrogen FluoSpheres polystyrene microspheres, ThermoFisher Scientific) were injected in random order at the end of MG and MG GLI contractions. For the reference sample used in blood flow calculations (Ishise et al. 1980, Musch & Terrell, 1992), blood withdrawal from the tail catheter, at a rate of 0.25 ml min^{-1} , was initiated at 180 s of contractions while $2.5\text{-}3.0 \times 10^5$ $15.5 \mu\text{m}$ diameter fluorescent microspheres were injected into the aortic arch via the carotid artery catheter. The blood withdrawal and muscle contractions were terminated 30 s after the microsphere injection. After the final contraction protocol and blood withdrawal was completed, another blood sample was collected from the tail catheter for blood gas and acid-base analyses and rats subsequently euthanized via pentobarbital sodium overdose ($>100 \text{ mg kg}^{-1}$, i.a.). Following confirmation of proper catheter placement in the aortic arch, tissues (left and right kidneys, mixed gastrocnemii and solei) were dissected and stored (-80°C) for later digestion and analyses as detailed previously (Colburn et al. 2020b, Deveci & Egginton 1999). Importantly, each sample was assessed in quadruplicates for the measurement of fluorescent intensity (SpectraMax i3 Multi-Mode Platform, Molecular Devices, San Jose, CA) and averaged for the calculation of total tissue blood flows according to the reference sample method (Ishise et al. 1980, Musch & Terrell, 1992) and expressed mass specifically in $\text{ml min}^{-1} 100 \text{ g tissue}^{-1}$. A difference of <20% between left and right kidney and/or soleus muscle blood flows was used to determine that microspheres were adequately mixed prior to infusion.

Muscle oxygen consumption

Microvascular oxygen consumption ($\dot{V}\text{O}_{2\text{mv}}$) was calculated via the principle of mass balance using the Fick Equation (i.e., $\dot{V}\text{O}_{2\text{mv}} = \dot{Q}_m \times (\text{CaO}_2 - \text{CvO}_2)$), utilizing the present blood flows (\dot{Q}_m), directly measured arterial O₂ content (CaO₂) via arterial blood sample, and calculated

CvO_2 values. CvO_2 was calculated with the following assumptions: i) interstitial PO_2 (PO_{2is}) measurements can be used to calculate microvascular PO_2 (PO_{2mv}) (i.e., $PO_{2mv} = PO_{2is} +$ transcapillary PO_2 ; Colburn et al. 2020a,b) and ii) PO_{2mv} is an appropriate analogue for venous PO_2 (McDonough et al. 2001) and, by extension from the O_2 dissociation curve, venous blood O_2 content (Roca et al. 1992). Therefore PO_{2mv} was used to calculate mixed venous O_2 content (CvO_2) using the rat O_2 dissociation curve; which was constructed with the Hill coefficient (n) of 2.6, the measured [Hb] herein, P_{50} of 38 mmHg (the PO_2 at which Hb is 50% saturated with O_2), and an O_2 carrying capacity of 1.34 ml O_2 (gHb) $^{-1}$). Microvascular O_2 diffusion conductance (DO_{2mv}) was defined as $\dot{V}O_{2mv}/PO_{2mv}$, providing an index of diffusive O_2 transport per unit of driving pressure. Interstitial O_2 diffusion conductance ($DO_{2is} = \dot{V}O_{2is}/PO_{2is}$) was assessed utilizing the present PO_{2is} and calculated $\dot{V}O_{2mv}$ (i.e., the absence of storage for O_2 in the interstitial fluid suggests that $\dot{V}O_{2is}$ is equal to $\dot{V}O_{2mv}$ and, thus, O_2 leaving the microvascular compartment must equal O_2 leaving the interstitial compartment; Colburn 2020a).

Statistical Analyses

Blood samples following MG measurements were assessed between groups via unpaired t-tests. PO_{2is} profiles were examined via Two-way repeated measures ANOVA (Drug x Time) with Tukey's *post hoc* analyses to assess the effect of GLI-induced K_{ATP} channel inhibition. The following were analyzed via Two-way repeated measures ANOVA (Sex x Drug) with Tukey's *post hoc* analyses to assess the effect of GLI between sexes (male vs female) and as a result of estrogen/ovariectomy (female vs F+OVX): MAP, PO_{2is} kinetics parameters, muscle oxygenation ($PO_{2is\ AREA}$), and MG \dot{Q}_m and O_2 delivery and utilization characteristics. P-values for females in the Results section are reported for both comparisons (i.e., P = male vs female/female vs F+OVX).

PO_2is before (Pre-superfusion PO_2is) and after GLI ($\text{PO}_2\text{is BL}$) was compared via paired t-tests.

Data are presented as mean \pm SEM. Significance was accepted at $P < 0.05$.

Results

Due to inadequate mixing of fluorescent microspheres during either control or GLI contraction protocols, or failure of PO_2is to return to baseline following control contractions, the following data was analyzed from eight male, nine female, and 11 F+OVX rats.

Central Haemodynamics and Blood O₂/Acid-Base During Phosphorescence Quenching

During MG PO_2is measurements, there were no significant MAP differences between male and female (control and GLI, respectively; male: 103 ± 5 and 109 ± 5 , female: 102 ± 3 and 99 ± 3) or between female and F+OVX rats (F+OVX: 104 ± 3 and 107 ± 4 mmHg, control and GLI, respectively, $P > 0.05$ for all). Nonetheless, MAP does not have a significant effect on PO_2 until MAP falls below 70 mmHg (Behnke et al. 2006). Therefore, PO_2is comparisons between groups are not expected to be influenced by MAP-related changes in central hemodynamics.

Blood samples were collected following the final measurement. Arterial pH during MG PO_2is measurements was lower in females compared to males (7.39 ± 0.01 vs 7.44 ± 0.01 , $P = 0.010$) but not different from F+OVX rats (7.41 ± 0.01 , $P = 0.243$). There were no differences in O_2 saturation (91.8 ± 1.7 , 90.7 ± 0.9 , and $92.3 \pm 0.6\%$), haematocrit (30 ± 1 , 30 ± 1 , and $31 \pm 1\%$), nor lactate (1.3 ± 0.1 , 1.5 ± 0.2 , and 1.5 ± 0.1 mM) between males, females, and F+OVX rats, respectively ($P > 0.130$ for all).

MG Blood Flow and Interstitial PO₂

GLI superfusion impaired MG \dot{Q}_m in male (45 ± 5 vs 31 ± 4 , $P = 0.020$) and female (52 ± 9 vs 34 ± 4 , $P = 0.003$ (male vs female) / 0.004 (female vs F+OVX)) but not F+OVX rats (55 ± 5 vs 52 ± 7 ml min⁻¹ 100 g tissue⁻¹, $P = 0.506$). The effects of GLI superfusion on PO_2is kinetics

parameters during the rest-contraction transient are presented in Table 1 (male vs female and female vs F+OVX) while mean $\text{PO}_{2\text{is}}$ profiles are shown in Figures 1A-C. Importantly, Figure 2 demonstrates that total $\text{PO}_{2\text{is}}$ availability during contractions ($\text{PO}_{2\text{is AREA}}$) was impaired equivalently ($P = 0.901$ for Sex x Drug Interaction) by GLI in male and female MG (-124 ± 60 and -132 ± 39 mmHg.s, $P = 0.028$ and 0.015 (male vs female) / 0.006 (female vs F+OVX), respectively), but not F+OVX MG (-4 ± 40 mmHg.s, $P = 0.921$). There were significant Drug x Time interactions in male ($P = 0.012$) and female ($P < 0.001$) MG $\text{PO}_{2\text{is}}$ profiles indicating that the magnitude of effect of GLI was dependent on the specific time interval considered during contractions (Figures 1A and 1B). However, despite no difference in the reductions in MG $\text{PO}_{2\text{is}}$ AREA between male and female rats (Sex x Drug interaction, $P = 0.901$), GLI sped the fall in $\text{PO}_{2\text{is}}$ of female rats to a greater extent than in male rats (Sex x Drug interactions for τ and MRT, $P = 0.031$ and 0.026 , respectively).

Muscle Oxygen Delivery, Consumption, and Diffusive Conductance

Table 2 contains the calculated muscle O₂ delivery ($\dot{\text{QO}}_2$), diffusive O₂ conductances (DO₂) and resulting O₂ utilization ($\dot{\text{VO}}_2$) under control and GLI conditions. Compared to control, Figures 3A and 3B illustrate that GLI in males and females decreased MG microvascular oxygen delivery ($\dot{\text{QO}}_{2\text{mv}}$; male: $P = 0.022$, female: $P = 0.003$ (male vs female) / 0.005 (female vs F+OVX)) and consumption ($\dot{\text{VO}}_{2\text{mv}}$; male: $P = 0.032$, female: $P = 0.003$ (male vs female) / 0.005 (female vs F+OVX)). Interestingly, microvascular and interstitial diffusive O₂ conductances were reduced in females (DO_{2mv}: $P = 0.007$ (male vs female) / 0.010 (female vs F+OVX), DO_{2is}: $P = 0.042$ (male vs female) / 0.002 (female vs F+OVX)), but not males (DO_{2mv}: $P = 0.113$, DO_{2is}: $P = 0.365$). In

contrast to their ovary-intact female counterparts, in F+OVX (Figure 3C) GLI did not impair MG $\dot{Q}O_2mv$, $\dot{V}O_2mv$, DO_2mv , nor DO_2is ($P > 0.374$ for all).

Discussion

The main findings of the current investigation are that vascular K_{ATP} channels contribute significantly to O₂ delivery-utilization matching (PO_{2is}) in fast-twitch oxidative muscle of male and female rats, with females demonstrating greater impairment during the rest-contraction transition following GLI (i.e., greater speeding of τ and MRT in females compared to males). Impaired MG O₂ delivery (QO_{2mv}) in male and female rats ultimately limited muscle O₂ utilization (VO_{2mv}) despite increases in O₂ extraction. In addition, following ovariectomy, vascular K_{ATP} channel function is lost in the fast-twitch oxidative MG.

Sex Differences in Vascular K_{ATP} Channel Function

In individuals with diabetes, females experience adverse cardiovascular events (heart failure, ischaemic stroke, cardiovascular death, etc.) at a higher relative rate than men (Malmborg et al. 2020). Furthermore, the lower risk for developing coronary artery disease in nondiabetic young and older females (<60 years) is absent with diabetic patients (Kalyani et al. 2014), suggesting that the etiology of diabetes, or even potential interactions of diabetic medication (i.e., sulphonylureas), has a greater impact on the female vasculature. With regard to vascular smooth muscle K_{ATP} channels in T2DM patients, expression of SUR2B subunits is reduced yet GLI still suppresses the vasorelaxant effect of pinacidil (K_{ATP} channel opener; Rajkovic et al. 2020). Therefore, it is likely that sulfonylurea medication given to T2DM patients may impair skeletal muscle and cerebral blood flow, as demonstrated in health (Banitt et al., 1996; Bank et al., 2000; Bijlstra et al., 1996; Keller et al. 2004; Rocha et al. 2020; Saito et al., 1996).

The present data, utilizing muscle contractions to evaluate vascular K_{ATP} channel-mediated vasodilation and increased O₂ delivery, supports the notion that sex differences exist in vascular

K_{ATP} channel function and may help describe, in part, the cardiovascular protection in females that is diminished with diabetes. Consequent to reduced \dot{Q}_m , Figures 1A and 1B demonstrate that GLI-induced K_{ATP} channel inhibition significantly reduced PO_2is of fast-twitch oxidative muscle. Despite equivalent reductions in total PO_2is availability following GLI (Figure 2), the rate of PO_2is fall was accelerated to a larger extent in female rats (i.e., greater reductions in τ and MRT (significant Sex x Drug Interaction) highlighting a larger O_2 delivery-utilization mismatch immediately following contraction onset). This more pronounced speeding in PO_2is fall of females compared to males may highlight the presence of greater K_{ATP} channel content and/or activity in female smooth muscle cells supporting increased $\dot{Q}O_2$ during exercise. However, sex differences in specific K_{ATP} channel content and/or activity of skeletal muscle vasculature remain to be investigated.

Potential mechanisms of impaired exercise tolerance following K_{ATP} channel inhibition include the diminished delivery of O_2 to skeletal muscle (convective O_2 conductance; $\dot{V}O_2 = \dot{Q}_m \times (CaO_2 - CvO_2)$) and its subsequent diffusion out of the blood at the red blood cell (RBC)-capillary interface and into the interstitial space (i.e., microvascular-myocyte diffusing conductance; $DO_{2mv} = \dot{V}O_{2mv}/PO_{2mv}$) and then into the contracting myocyte (interstitial-myocyte diffusing conductance; $DO_{2is} = \dot{V}O_{2is}/PO_{2is}$) (Colburn et al. 2020a). Considering that PO_2 is the driving pressure for O_2 flux out of each compartment and is established via O_2 delivery-utilization matching (i.e., $PO_{2mv} \propto \dot{Q}O_{2mv}/\dot{V}O_{2mv}$ and $PO_{2is} \propto \dot{Q}O_{2is}/\dot{V}O_{2is}$), impairments in the microvasculature (decreased $\dot{Q}O_{2mv}$ and/or DO_{2mv}) will limit $\dot{Q}O_{2is}$ and thus PO_{2is} . Figure 3 emphasizes that the convergence of convective ($\dot{Q}O_2$) and diffusive (DO_2) O_2 conductances establish the rate of muscle O_2 utilization ($\dot{V}O_2$) during contractions (Wagner 1992, 1996) where diminished $\dot{V}O_2$ increases the reliance on finite energy stores and production of fatigue-related

metabolites (Hogan et al. 1992; Richardson et al. 1998; Wilson et al. 1977). Importantly, Figures 3A and 3B illustrate that, whereas $\dot{Q}O_2$ was reduced in both male and female fast-twitch oxidative muscle following GLI, impaired DO_{2mv} and DO_{2is} were present only in females. As bulk $\dot{Q}m$ was reduced equivalently between males and females, and GLI hinders key mechanisms of DO_2 (i.e., decreased capillaries flowing, RBC flux and velocity; Hirai et al. 2018b), sex-dependent impairments in DO_2 following GLI may be described by more metabolically-appropriate spatial heterogeneity of K_{ATP} channels supporting $\dot{Q}O_2/\dot{V}O_2$ matching in females. As such, the presence of impaired DO_{2mv} , in addition to $\dot{Q}O_2$, supports a further delay in the increase of $\dot{Q}O_{2is}$ leading to the greater GLI-induced speeding in PO_{2is} fall of females compared to males. It is worth noting, however, that for the moderate-intensity contractions herein showing no sex difference in impaired $\dot{V}O_2$ following GLI (i.e., $\Delta\dot{V}O_2$ in males vs females measured at 180 s), this faster fall in PO_{2is} in females may drive subsequent compensation for impaired DO_{2mv} , such that an enhanced transcapillary PO_2 gradient would maintain, or limit reductions in, O_2 leaving the microvascular compartment (i.e., transcapillary O_2 flux ($\dot{V}O_2$) = $\downarrow DO_2 \times \uparrow [PO_{2mv} - PO_{2is}]$; Colburn et al. 2020a; Hirai et al. 2018a). Therefore, impaired exercise tolerance will most likely be manifested in heavy- and severe-intensity domains leading to greater reductions in CS (metabolic threshold separating heavy- from severe-intensity) and $\dot{V}O_{2max}$ (via decreased maximal O_2 extraction from limited $CaO_2 - CvO_2$) of females compared to males (Colburn et al. 2020b).

Effect of Ovariectomy on K_{ATP} Channel Function

The GLI-mediated impairment in vascular function within females (reduced $\dot{Q}m$, convective and diffusive O_2 transport and O_2 delivery-utilization mismatch ultimately leading to diminished $\dot{V}O_2$) was not expressed following ovariectomy (Figures 1C and 3C). Thus the

potential decrement to females prescribed sulphonylureas or other medication inhibiting K_{ATP} channels may be dependent on menopause status. Importantly, increased prevalence of adverse cardiovascular events and cardiovascular disease perimenopause may be described, in part, via changes/loss in K_{ATP} channel-mediated vasodilation. While vascular K_{ATP} channels support skeletal muscle and cerebral blood flow in humans (Banitt et al. 1996; Bank et al., 2000; Bijlstra et al. 1996; Keller et al. 2004; Rocha et al. 2020; Saito et al. 1996), current evidence suggests ventricular K_{ATP} channel content decreases with age in females but not males (Ranki et al. 2001, 2002b) and may increase with estrogen treatment (Ranki et al. 2002a). Thus the clinical importance of maintaining K_{ATP} channel function likely depends on the age and/or menopause status in females.

A potential explanation for the change in vascular K_{ATP} channel function between female and F+OVX MG muscle is increases in protein kinase C (PKC) following ovariectomy (Kanashiro & Khalil, 2001); with PKC acting as a signaling pathway for various vasoconstrictors (i.e., endothelin-1 from endothelium and renal-derived angiotensin II) leading to decreased K_{ATP} channel current, membrane depolarization and even channel internalization (Flagg et al. 2010; Quayle, Nelson & Standen 1997). It has been shown that angiotensin II, via PKC activation, inhibits vascular K_{ATP} channel activity, and thus the PKC pathway is inversely related to K_{ATP} channel function (Cole et al. 2001; Hayabuchi et al. 2001; Kubo et al. 1997; Manna et al. 2010; Shi et al. 2008; Thorneloe et al. 2002). Interestingly, estradiol replacement reduces PKC levels (Kanashiro & Khalil, 2001) which may lead to a restoration of vascular K_{ATP} channel-mediated vasodilation as estradiol also leads to increased ventricular K_{ATP} channel formation, via increases in both Kir6.2 and SUR2A subunits, of cardiac cells (Ranki et al. 2002a). However, the role of PKC on vascular K_{ATP} channels as it relates to estrogen or other sex hormones remains unknown.

Experimental Considerations

Although the moderate-intensity contractions utilized herein do not directly mimic severe-intensity exercise which leads to $\dot{V}O_{2max}$ and subsequent exhaustion, the present sex differences in MG PO_2 following GLI may actually be greater during heavy-intensity exercise and ultimately lead to differing magnitudes of impaired CS (i.e., females demonstrating a more pronounced lowering of the metabolic threshold separating heavy- and severe-intensity exercise; reviewed by Poole, Behnke & Musch 2020; Poole et al. 2016). Importantly, our laboratory has recently demonstrated GLI-mediated reductions in \dot{Q}_m of male rats at treadmill speeds below and above CS (Holdsworth et al. 2015) and impaired CS and $\dot{V}O_{2max}$ in female rats (Colburn et al. 2020b).

Tissue digestion required for \dot{Q}_m measurements precluded the assessment of vascular K_{ATP} channel content herein. Notwithstanding, whether there are sex differences in channel content and/or activity, the present data suggests that the K_{ATP} channel-mediated contribution to increased \dot{Q}_m and O_2 delivery-to-utilization matching during submaximal twitch contractions exists in males and females, and becomes largely diminished following ovariectomy (i.e., postmenopause). Additionally, although the current experimental design did not incorporate a F+OVX group with combined estrogen replacement therapy to assess the direct role of estrogen on K_{ATP} channel function, others have shown that 17β -estradiol reverses the ovariectomy-mediated increase in PKC (Kanashiro & Khalil, 2001) that would otherwise impair vascular K_{ATP} channels. Thus it is likely that chronic estrogen levels play a role in supporting vascular K_{ATP} channel function during exercise.

Lastly, GLI superfusion may inhibit K_{ATP} channels on skeletal muscle (Kir6.2/SUR2A) which could potentially lead to greater myocyte contraction, increased metabolic demand ($\dot{V}O_2$) and subsequently lowered PO_2 . There is evidence that muscle tension between, but not during,

contractions is increased following K_{ATP} channel inhibition (Gong et al. 2000; Matar et al. 2000) but the predominant effect of topically-applied GLI on \dot{Q}_{O_2} -to- $\dot{V}O_2$ matching (i.e. PO₂*is*) in fast-twitch oxidative glycolytic MG is impaired \dot{Q}_m (reduced herein and also in Holdsworth et al. 2015) and \dot{Q}_{O_2} rather than increased $\dot{V}O_2$ (Figures 3A and 3B).

Conclusions

Our recent investigation emphasized the importance of vascular K_{ATP} channel function in supporting maximal aerobic capacity ($\dot{V}O_{2max}$) and exercise tolerance (critical speed, CS) via convective ($\dot{V}O_2 = \dot{Q}_m \times (CaO_2 - CvO_2)$) and diffusive ($DO_2 = \dot{V}O_2/PO_2$) O₂ transport (Colburn et al. 2020b). The present data demonstrate that fast-twitch oxidative muscle is likely impaired to a greater extent in females compared to males following GLI-induced K_{ATP} channel inhibition. In addition, following ovariectomy the effect of GLI is removed; suggesting that there is a loss of vascular K_{ATP} channel function resulting from chronically lowered levels of sex hormones (i.e., estrogen). Therefore, as a commonly prescribed diabetes medication, sulphonylureas (such as GLI) may further exacerbate exercise intolerance (impaired CS and $\dot{V}O_{2max}$), and disease progression, in a sex-dependent manner by hindering vascular O₂ transport and muscle O₂ utilization.

References

- Abdelmoneim AS, Eurich DT, Senthilselvan A, Qiu W & Simpson SH (2016). Dose-response relationship between sulphonylureas and major adverse cardiovascular events in elderly patients with type 2 diabetes. *Pharmacoepidemiology and Drug Safety* **25**, 1186-1195.
- Banitt PF, Smits P, Williams SB, Ganz P & Creager MA (1996). Activation of ATP-sensitive potassium channels contributes to reactive hyperemia in humans. *Am J Physiol* **271**, H1594-8.
- Bank AJ, Sih R, Mullen K, Osayamwen M & Lee PC (2000). Vascular ATP-Dependent Potassium Channels, Nitric Oxide, and Human Forearm Reactive Hyperemia. *Cardiovasc Drugs Ther* **14**, 23-29.
- Behnke BJ, McDonough P, Padilla DJ, Musch TI & Poole DC (2003). Oxygen exchange profile in rat muscles of contrasting fibre types. *J Physiol* **549.2**, 597-605.
- Benjamin EJ, Muntner P, Alonso A, Bittencourt MS, Callaway CW, Carson AP, Chamberlain AM, Chang AR, Cheng S, Das SR, Delling FN, Djousse L, Elkind MSV, Ferguson JF, Fornage M, Jordan LC, Khan SS, Kissela BM, Knutson KL, Kwan TW, Lackland DT, Lewis TT, Lichtman JH, Longenecker CT, Loop MS, Lutsey PL, Martin SS, Matsushita K, Moran AE, Mussolini ME, O'Flaherty M, Pandey A, Perak AM, Rosamond WD, Roth GA, Sampson UKA, Satou GM, Schroeder EB, Shah SH, Spartano NL, Stokes A, Tirschwell DL, Tsao CW, Turakhia MP, VanWagner LB, Wilkins JT, Wong SS & Virani SS (2019). Heart Disease and Stroke Statistics – 2019 Update: A Report From the American Heart Association. *Circulation* **139**, e56-e528.
- Bhatia RS, Tu JV, Lee DS, Austin PC, Fang J, Haouzi A, Gong Y & Liu PP (2006). Outcome of Heart Failure with Preserved Ejection Fraction in a Population-Based Study. *N Engl J Med* **355**, 260-269.
- Bijlsma PJ, den Arend JACJ, Lutterman JA, Russel FGM, Thien T & Smits P (1996). Blockade of vascular ATP-sensitive potassium channels reduces the vasodilator response to ischaemia in humans. *Diabetologia* **39**, 1562–1568.
- Brown DA, Chicco AJ, Jew KN, Johnson MS, Lynch JM, Watson PA & Moore RL (2005a). Cardioprotection afforded by chronic exercise is mediated by the sarcolemmal, and not mitochondrial, isoform of the K_{ATP} channel in the rat. *J Physiol* **569**, 913-924.
- Brown DA, Lynch JM, Armstrong CJ, Caruso NM, Ehlers LB, Johnson MS & Moore RL (2005b). Susceptibility of the heart to ischaemia-reperfusion injury and exercise-induced cardioprotection are sex-dependent in the rat. *J Physiol* **564**, 619-630.
- Chicco AJ, Johnson MS, Armstrong CJ, Lynch JM, Gardner RT, Fasen GS, Gillenwater CP & Moore RL (2007). Sex-specific and exercise-acquired cardioprotection is abolished by sarcolemmal K_{ATP} channel blockade in the rat heart. *Am J Physiol Heart Circ Physiol* **292**, H2432-H2437.

Colburn TD, Hirai DM, Craig JC, Ferguson SK, Weber RE, Schulze KM, Behnke BJ, Musch TI & Poole DC (2020a). Transcapillary PO₂ Gradients in Contracting Muscles Across the Fibre Type and Oxidative Continuum. *J Physiol* **598**, 3187-3202.

Colburn TD, Weber RE, Hageman KS, Caldwell JT, Schulze KM, Ade CJ, Behnke BJ, Poole DC & Musch TI (2020b). Vascular ATP-sensitive K⁺ channels support maximal aerobic capacity and critical speed via convective and diffusive O₂ transport. *J Physiol* **598**, 4843-4858.

Cole WC, Malcom T, Walsh MP & Light PE (2000). Inhibition by Protein Kinase C of the K_{NDP} Subtype of Vascular Smooth Muscle ATP-Sensitive Potassium Channel. *Circ Res* **87**, 112-117.

Copp SW, Hirai DM, Musch TI & Poole DC (2010). Critical speed in the rat: implications for hindlimb muscle blood flow distribution and fibre recruitment. *J Physiol* **588**, 5077-5087.

Craig JC*, Colburn TD*, Caldwell JT, Hirai DM, Tabuchi A, Baumfalk DR, Behnke BJ, Ade CJ, Musch TI & Poole DC (2019). Central and peripheral factors mechanistically linked to exercise intolerance in heart failure with reduced ejection fraction. *Am J Physiol Heart Circ Physiol* **317**, H434-H444.

Craig JC, Colburn TD, Hirai DM, Schettler MG, Musch TI & Poole DC (2018). Sex and nitric oxide bioavailability interact to modulate interstitial PO₂ in healthy rat skeletal muscle. *J Appl Physiol* **124**, 1558-1566.

Delp MD & Duan C (1996). Composition and size of type I, IIA, IID/X, and IIB fibers and citrate synthase activity of rat muscle. *J Appl Physiol* **80**, 261-270.

Deveci D & Egginton S (1999). Development of the fluorescent microsphere technique for quantifying regional blood flow in small mammals. *Exp Physiol* **84**, 615-630.

Esipova TV, Karagodov A, Miller J, Wilson DF, Busch TM & Vinogradov SA (2011). Two new “protected” oxyphors for biological oximetry: properties and application in tumor imaging. *Anal Chem* **83**, 8756-8765.

Fang J, Mensah GA, Croft JB & Keenan NL (2008). Heart Failure-Related Hospitalizations in the U.S., 1979-2014. *JACC* **52**, 428-434.

Flagg TP, Enkvetchakul D, Koster JC & Nichols CG (2010). Muscle K_{ATP} Channels: Recent Insights to Energy Sensing and Myoprotection. *Physiol Rev* **90**, 799-829.

Gao J, Xu D, Sabat G, Valdivia H, Xu W & Shi N (2014). Disrupting K_{ATP} channels diminishes the estrogen-mediated protection in female mutant mice during ischemia-reperfusion. *Clin Proteom* **11**, 19.

Gong B, Miki T, Seino S & Renaud JM (2000). A K_{ATP} channel deficiency affects resting tension, not contractile force, during fatigue in skeletal muscle. *Am J Physiol Cell Physiol* **279**, C1351-C1358.

Grundy D (2015). Principles and standards for reporting animal experiments in The Journal of Physiology and Experimental Physiology. *J Physiol* **593**, 2547-2549.

Hayabuchi Y, Davies NW & Standen NB (2001). Angiotensin II inhibits rat arterial K_{ATP} channels by inhibiting steady-state protein kinase A activity and activating protein kinase Cε. *J Physiol* **530**, 193-205.

Hirai DM, Craig JC, Colburn TD, Eshima H, Kano Y, Sexton WL, Musch TI & Poole DC (2018a). Skeletal muscle microvascular and interstitial PO₂ from rest to contractions. *J Physiol* **596**, 869-883.

Hirai DM, Craig JC, Colburn TD, Tabuchi A, Hageman KS, Musch TI & Poole DC (2018b). Regulation of Capillary Hemodynamics by K_{ATP} Channels in Resting Skeletal Muscle. *FASEB J* **32**, 581.8.

Ho KKL, Anderson KM, Kannel WB, Grossman W & Levy D (1993). Survival After the Onset of Congestive Heart Failure in Framingham Heart Study Subjects. *Circulation* **88**, 107-115.

Hogan MC, Arthur PG, Bebout DE, Hochachka PW & Wagner PD (1992). Role of O₂ in regulating tissue respiration in dog muscle working in situ. *J Appl Physiol* **73**, 728-36.

Holdsworth CT, Copp SW, Ferguson SK, Sims GE, Poole DC & Musch TI (2015). Acute inhibition of ATP-sensitive K⁺ channels impairs skeletal muscle vascular control in rats during treadmill exercise. *Am J Physiol Heart Circ Physiol* **308**, H1434-42.

Holdsworth CT, Ferguson SK, Colburn TD, Fees AJ, Craig JC, Hirai DM, Poole DC & Musch TI (2017). Vascular K_{ATP} channels mitigate severe muscle O₂ delivery-utilization mismatch during contractions in chronic heart failure rats. *Respir Physiol Neurobiol* **238**, 33-40.

Holdsworth CT, Ferguson SK, Poole DC & Musch TI (2016). Modulation of rat skeletal muscle microvascular O₂ pressure via K_{ATP} channel inhibition following the onset of contractions. *Respir Physiol Neurobiol* **222**, 48-54.

Ishise S, Pegram BL, Yamamoto J, Kitamura Y & Frohlich ED (1980). Reference sample microsphere method: cardiac output and blood flows in conscious rat. *Am J Physiol Heart Circ Physiol* **239**, H443-H449.

Johnson MS, Moore RL & Brown DA (2006). Sex differences in myocardial infarct size are abolished by sarcolemmal K_{ATP} channel blockade in rat. *Am J Physiol Heart Circ Physiol* **290**, H2644-H2647.

Kalyani RR, Lazo M, Ouyang P, Turkbey E, Chevalier K, Brancati F, Becker D & Vaidya Dhananjay (2014). Sex Differences in Diabetes and Risk of Incident Coronary Artery Disease in Healthy Young and Middle-Aged Adults. *Diabetes Care* **37**, 830-838.

Kanashiro CA & Khalil RA (2001). Gender-related distinctions in protein kinase C activity in rat vascular smooth muscle. *Am J Physiol Cell Physiol* **280**, C34-C45.

Keller DM, Ogoh S, Greene S, Olivencia-Yurvati A & Raven PB (2004). Inhibition of K_{ATP} channel activity augments baroreflex-mediated vasoconstriction in exercising human skeletal muscle. *J Physiol* **561**, 273-282.

Kristiansen SB, Løfgren B, Nielsen JM, Støttrup NM, Buhl ES, Nielsen-Kudsk JE, Nielsen TT, Rungby J, Flyvbjerg A & Bøtker HE (2011). Comparison of two sulfonylureas with high and low myocardial K(ATP) channel affinity on myocardial infarct size and metabolism in a rat model of type 2 diabetes. *Diabetologia* **54**, 451-458.

Kubo M, Quayle JM & Standen NB (1997). Angiotensin II inhibition of ATP-sensitive K⁺ currents in rat arterial smooth muscle cells through protein kinase C. *J Physiol* **503**, 480-496.

Lu S, Xiang L, Clemmer JS, Gowdey AR, Mittwede PN & Hester RL (2013). Impaired vascular K_{ATP} function attenuates exercise capacity in obese Zucker rats. *Microcirculation* **20**, 662-669.

Lee T, Chou T & Tsai C (2003). Differential Role of K_{ATP} Channels Activated by Conjugated Estrogens in the Regulation of Myocardial and Coronary Protective Effects. *Circulation* **107**, 49-54.

Malmborg M, Schmiegelow MDS, Norgaard CH, Munch A, Gerds T, Schou M, Kistorp C, Torp-Pedersen C, Hlatky MA & Gislason G (2020). Does type 2 diabetes confer higher relative rates of cardiovascular events in women compared with men? *Eur Heart J* **41**, 1346-1353.

Manna PT, Smith AJ, Taneja TK, Howell GJ, Lippiat JD & Sivaprasadarao A (2010). Constitutive endocytic recycling and protein kinase C-mediated lysosomal degradation control K_{ATP} channel surface density. *J Biol Chem* **285**, 5963-5973.

Matar W, Nosek TM, Wong D & Renaud JM (2000). Pinacidil suppresses contractility and preserves energy but glibenclamide has no effect during muscle fatigue. *Am J Physiol Cell Physiol* **278**, C404-C416.

Marcondes FJ, Bianchi FJ & Tanno AP (2002). Determination of the estrous cycle phases of rats: some helpful considerations. *Brazilian J Biol* **62**, 609-614.

McAlister FA, Eurich DT, Majumdar SR & Johnson JA (2008). The risk of heart failure in patients with type 2 diabetes treated with oral agent monotherapy. *Eur J Heart Fail* **10**, 703-708.

McDonough P, Behnke BJ, Kindig CA & Poole DC (2001). Rat muscle microvascular PO₂ kinetics during the exercise off-transient. *Exp Physiol* **86**, 349-356.

Montvida O, Shaw J, Atherton JJ, Stringer F & Paul SK (2018). Long-term Trends in Antidiabetes Drug Usage in the U.S.: Real-world Evidence in Patients Newly Diagnosed with Type 2 Diabetes. *Diabetes Care* **41**, 69-78.

Musch TI, Moore RL, Leathers DJ, Bruno A & Zelis R (1986). Endurance training in rats with chronic heart failure induced by myocardial infarction. *Circulation* **74**, 431-441.

- Musch TI & Terrell JA (1992). Skeletal muscle blood flow abnormalities in rats with a chronic myocardial infarction: rest and exercise. *Am J Physiol Heart Circ Physiol* **262**, H411-H419.
- Poole DC, Behnke BJ & Musch TI (2020). The role of vascular function on exercise capacity in health and disease. *J Physiol* Ahead of Print. DOI: 10.1113/JP278931.
- Poole DC, Burnley M, Vanhatalo A, Rossiter HB & Jones AM (2016). Critical power: an important fatigue threshold in exercise physiology. *Med Sci Sports Exerc* **48**, 2320-2334.
- Quayle JM, Nelson MT & Standen NB (1997). ATP-sensitive and inwardly rectifying potassium channels in smooth muscle. *Physiol Rev* **77**, 1165-1232.
- Rajkovic J, Peric M, Stanisic J, Novakovic R, Djokic V, Rakocevic J, Tepavcevic S, Labudovic-Borovic M, Gostimirovic M, Heinle H & Gojkovic-Bukarica L (2020). The Role of the Adenosine Triphosphate-Sensitive Potassium Channels in Pinacidil-induced Vasodilation of the Human Saphenous Vein in Patients With and Without Type 2 Diabetes Mellitus. *J Physiol Pharmacol* **71**, 125-135.
- Ranki HJ, Budas GR & Crawford RM (2001). Gender-Specific Difference in Cardiac ATP-Sensitive K⁺ Channels. *JACC* **38**, 906-915.
- Ranki HJ, Budas GR, Crawford RM, Davies AM & Jovanovic Aleksandar (2002a). 17β-Estradiol Regulates Expression of K_{ATP} Channel in Heart-Derived H9c2 Cells. *JACC* **40**, 367-374.
- Ranki HJ, Crawford RM, Budas GR & Jovanovic A (2002b). Ageing is associated with a decrease in the number of sarcolemmal ATP-sensitive K⁺ channels in a gender-dependent manner. *Mech Ageing Dev* **123**, 695-705.
- Richardson RS, Noyszewski EA, Leigh JS & Wagner PD (1998). Lactate efflux from exercising human skeletal muscle: role of intracellular PO₂. *J Appl Physiol* **85**, 627-634.
- Roca J, Agusti AG, Alonso A, Poole DC, Viegas C, Barbera JA, Rodriguez-Roisin R, Ferrer A & Wagner PD (1992). Effect of training on muscle O₂ transport at VO_{2max}. *J Appl Physiol* **73**, 1067-76.
- Rocha MP, Campos MO, Mattos JD, Mansur DE, Rocha HNM, Secher NH, Nobrega ACL & Fernandes IA (2020). K_{ATP} channels modulate cerebral blood flow and oxygen delivery during isocapnic hypoxia in humans. *J Physiol* **598**, 3343-3356.
- Rumsey WL, Vanderkooi JM & Wilson DF (1988). Imaging of Phosphorescence: A Novel Method for Measuring Oxygen Distribution in Perfused Tissue. *Science* **241**, 1649-1651, 1988.
- Saito Y, McKay M, Eraslan A & Hester RL (1996). Functional hyperemia in striated muscle is reduced following blockade of ATP-sensitive potassium channels. *Am J Physiol Heart Circ Physiol* **270**, H1649-H1654.

Shi Y, Cui N, Shi W & Jiang C (2008). A short motif in Kir6.1 consisting of four phosphorylation repeats underlies the vascular K_{ATP} channel inhibition by protein kinase C. *J Biol Chem* **283**, 2488-2494.

Simpson SH, Lee J, Choi S, Vandermeer B, Abdelmoneim AS & Featherstone TR (2015). Mortality risk among sulfonylureas: a systematic review and network meta-analysis. *Lancet Diabetes Endocrinol* **3**, 43-51.

Simpson SH, Majumdar SR, Tsuyuki RT, Eurich DT & Johnson JA (2006). Dose-response relation between sulphonylurea drugs and mortality in type 2 diabetes mellitus: a population-based cohort study. *CMAJ* **174**, 169-174.

Smith JR, Hageman KS, Harms CA, Poole DC & Musch TI (2017). Respiratory muscle blood flow during exercise: Effects of sex and ovarian cycle. *J Appl Physiol* **122**, 918-924.

Thorneloe KS, Maruyama Y, Malcolm AT, Light PE, Walsh MP & Cole WC (2002). Protein kinase C modulation of recombinant ATP-sensitive K⁺ channels composed of Kir6.1 and/or Kir6.2 expressed with SUR2B. *J Physiol* **541**, 65-80.

Wagner PD (1992). Gas exchange and peripheral diffusion limitation. *Med Sci Sports Exerc* **24**, 54-58.

Wagner PD (1996). Determinants of maximal oxygen transport and utilization. *Annu Rev Physiol* **58**, 21-50.

Wilson DF, Erecinska M, Drown C & Silver IA (1977). Effect of oxygen tension on cellular energetics. *Am J Physiol Cell Physiol* **233**, C135-140.

Table 4.1. Effect of local KATP channel inhibition on interstitial PO₂ kinetics parameters during 180 s twitch contractions within fast-twitch oxidative muscle of male, female and ovariectomized female rats

Mixed Gastrocnemius	Male (n = 8)		Female (n = 9)		F+OVX (n = 11)	
	Control	GLI	Control	GLI	Control	GLI
Pre-Superfusion PO_{2is} (mmHg)	--	13.5 ± 1.4	--	13.8 ± 1.1	--	16.5 ± 1.6
PO₂ BL (mmHg)	13.0 ± 1.1	12.4 ± 0.9	14.1 ± 0.5	12.8 ± 1.2 *	16.6 ± 1.7	17.0 ± 1.4
Δ₁PO₂ (mmHg)	6.2 ± 0.6	6.9 ± 0.8	8.2 ± 0.5	8.1 ± 1.0	11.7 ± 1.5 #	11.6 ± 1.0 #
TD (s)	8.5 ± 1.9	5.0 ± 1.2 *	8.0 ± 1.4	5.2 ± 1.1	7.7 ± 0.7	4.5 ± 0.4 *
τ (s)	11.1 ± 1.6	13.5 ± 1.8	14.1 ± 0.9	12.2 ± 1.0 †	11.1 ± 0.6 #	10.6 ± 0.6
MRT (s)	19.5 ± 2.5	18.5 ± 2.4	22.2 ± 1.6	17.3 ± 1.4 *†	18.8 ± 0.8 #	15.1 ± 0.8 *
PO₂ nadir (mmHg)	6.8 ± 0.7	5.5 ± 0.4 *	5.9 ± 0.3	4.7 ± 0.4 *	4.9 ± 0.7	5.3 ± 0.6 ‡
Δ₂PO₂ (mmHg)	2.1 ± 0.4	1.7 ± 0.5	1.4 ± 0.3	1.4 ± 0.3	2.3 ± 0.4	1.6 ± 0.2
PO₂ end (mmHg)	8.9 ± 1.1	7.2 ± 0.5 *	7.3 ± 0.5	6.1 ± 0.5	7.2 ± 0.8	6.9 ± 0.7
Δ₁PO₂/τ (mmHg s⁻¹)	0.66 ± 0.11	0.57 ± 0.09	0.60 ± 0.05	0.72 ± 0.12	1.11 ± 0.17 #	1.12 ± 0.09 #

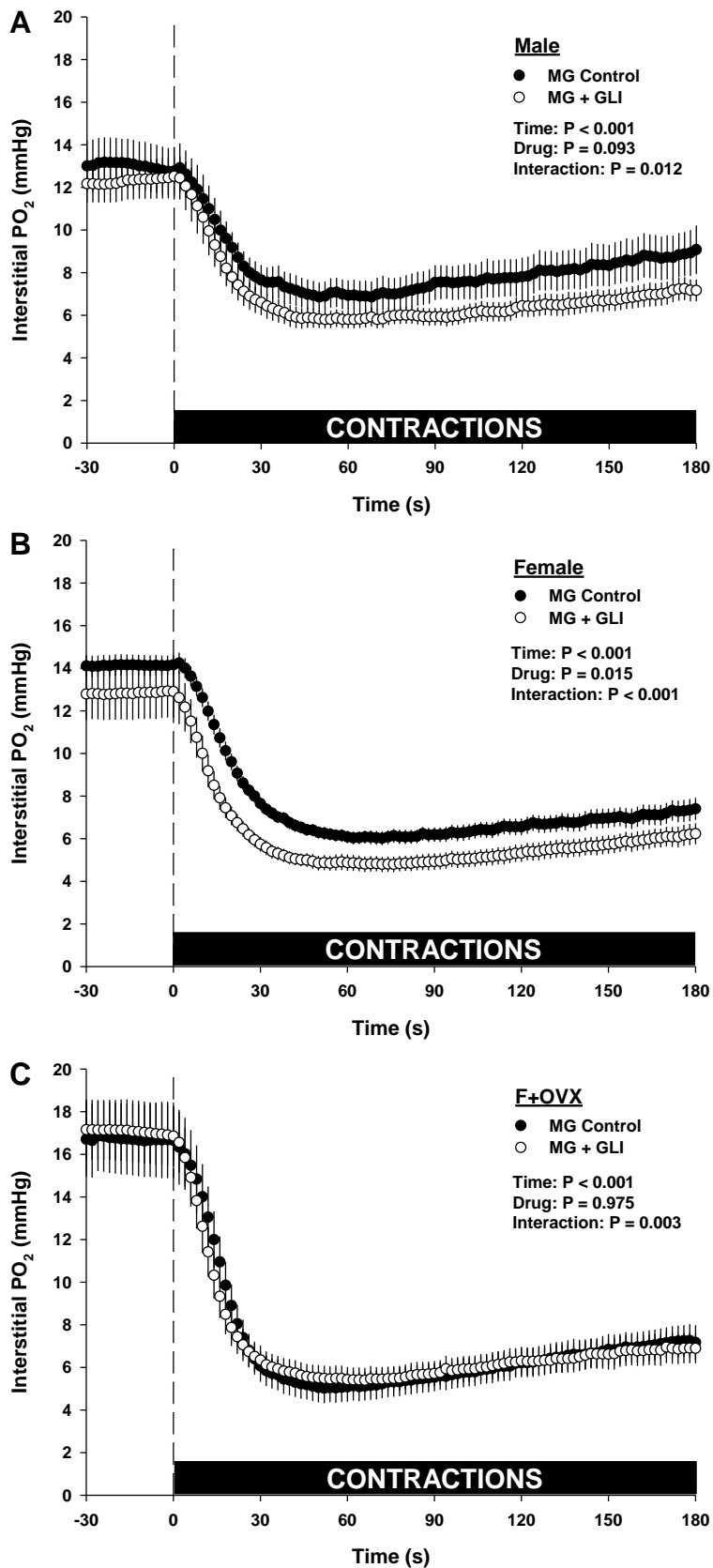
GLI, glibenclamide; PO_{2is} BL, resting baseline PO_{2is}; Δ₁PO_{2is} and Δ₂PO_{2is}, amplitude of the first and second components, respectively; TD, time delay; τ, time constant; MRT, mean response time; PO_{2is} nadir, lowest response prior to secondary rise in PO_{2is}; PO_{2is} end, PO_{2is} at the end of contractions; Δ₁PO_{2is}/τ, rate of PO_{2is} fall. PO_{2is} kinetics parameters were assessed via Two-way repeated measures ANOVA (Sex x Drug) between sexes (male vs female) and resulting from ovariectomy (female vs F+OVX) with Tukey's *post hoc* analyses. Pre-Superfusion PO_{2is} vs PO_{2is} BL were compared via two-tail paired t-tests. Data are mean ± SEM. * P < 0.05 vs control, # P < 0.05 vs females, † P < 0.05 Sex x Drug Interaction vs males, ‡ P < 0.05 Sex x Drug Interaction vs females

Table 4.2. Effect of local K_{ATP} channel inhibition on O₂ delivery and utilization characteristics during 180 s twitch contractions within fast-twitch oxidative muscle of male, female and ovariectomized female rats

Mixed Gastrocnemius	Male (n = 8)		Female (n = 9)		F+OVX (n = 11)	
	Control	GLI	Control	GLI	Control	GLI
PO_{2is} end (mmHg)	8.9 ± 1.1	7.2 ± 0.5 *	7.3 ± 0.5	6.1 ± 0.5 *	7.2 ± 0.8	6.9 ± 0.7
PO_{2mv} end (mmHg)	15.9 ± 1.1	14.2 ± 0.5 *	14.3 ± 0.5	13.1 ± 0.5 *	14.2 ± 0.8	13.9 ± 0.7
̇QO_{2mv} (ml O₂ min⁻¹ 100 g tissue⁻¹)	5.6 ± 0.5	4.0 ± 0.5 *	6.4 ± 1.1	4.2 ± 0.6 *	7.2 ± 0.6	6.6 ± 0.8 ‡
̇VO_{2mv} and ̇VO_{2is} (ml O₂ min⁻¹ 100 g tissue⁻¹)	5.0 ± 0.5	3.6 ± 0.5 *	5.8 ± 1.0	3.9 ± 0.5 *	6.6 ± 0.5	6.1 ± 0.8 ‡
DO_{2mv} (ml O₂ min⁻¹ mmHg⁻¹ 100 g tissue⁻¹)	0.32 ± 0.03	0.26 ± 0.04	0.40 ± 0.07	0.30 ± 0.04 *	0.47 ± 0.04	0.46 ± 0.07
DO_{2is} (ml O₂ min⁻¹ mmHg⁻¹ 100 g tissue⁻¹)	0.61 ± 0.08	0.55 ± 0.13	0.80 ± 0.13	0.66 ± 0.08 *	1.05 ± 0.16	1.04 ± 0.19
O₂ Extraction (%)	89.3 ± 1.6	91.8 ± 0.8 *	91.5 ± 0.8	93.1 ± 0.7 *	91.7 ± 1.0	92.1 ± 0.9

GLI, glibenclamide; PO_{2is} end and PO_{2mv} end, interstitial and microvascular PO₂ at the end of contractions; ̇QO_{2mv}, microvascular O₂ delivery; ̇VO_{2mv} and ̇VO_{2is}, O₂ utilization out of microvascular and interstitial compartments; DO_{2mv} and DO_{2is}, O₂ diffusive conductance out of microvascular and interstitial compartments; O₂ Extraction, percentage of O₂ utilized relative to O₂ delivered and calculated as [̇VO_{2mv}/ ̇QO_{2mv}] × 100. O₂ characteristics were assessed via Two-way repeated measures ANOVA (Sex x Drug) between sexes (male vs female) and resulting from ovariectomy (female vs F+OVX) with Tukey's *post hoc* analyses. Data are mean ± SEM.

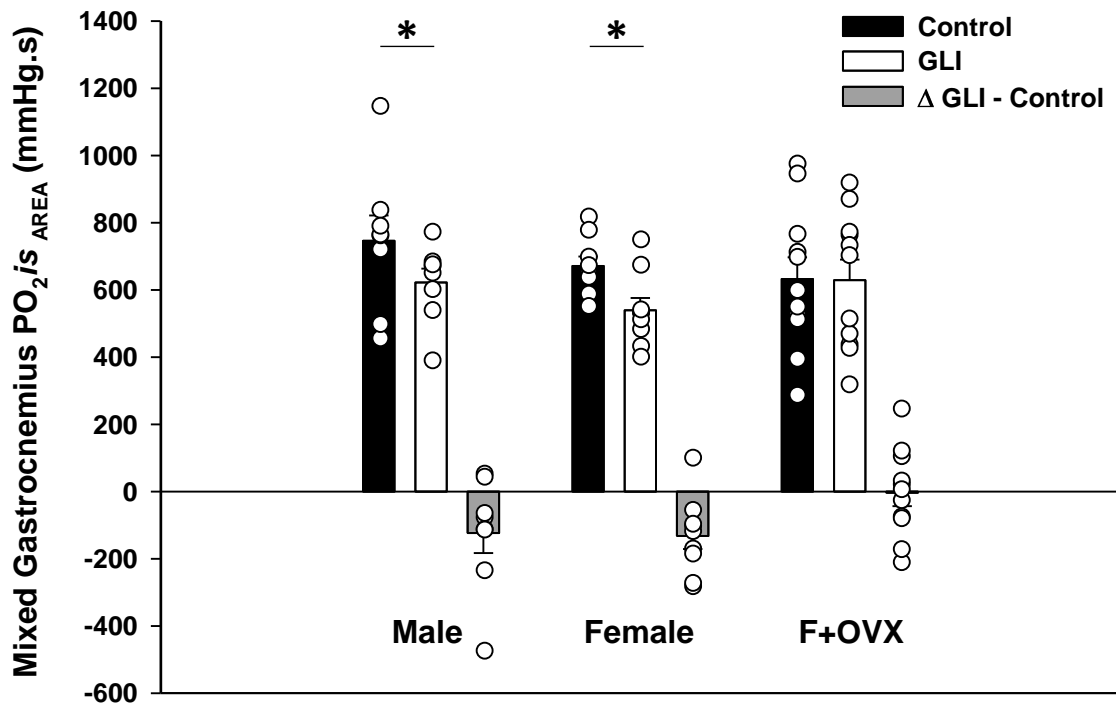
* P < 0.05 vs control, ‡ P < 0.05 Sex x Drug Interaction vs females



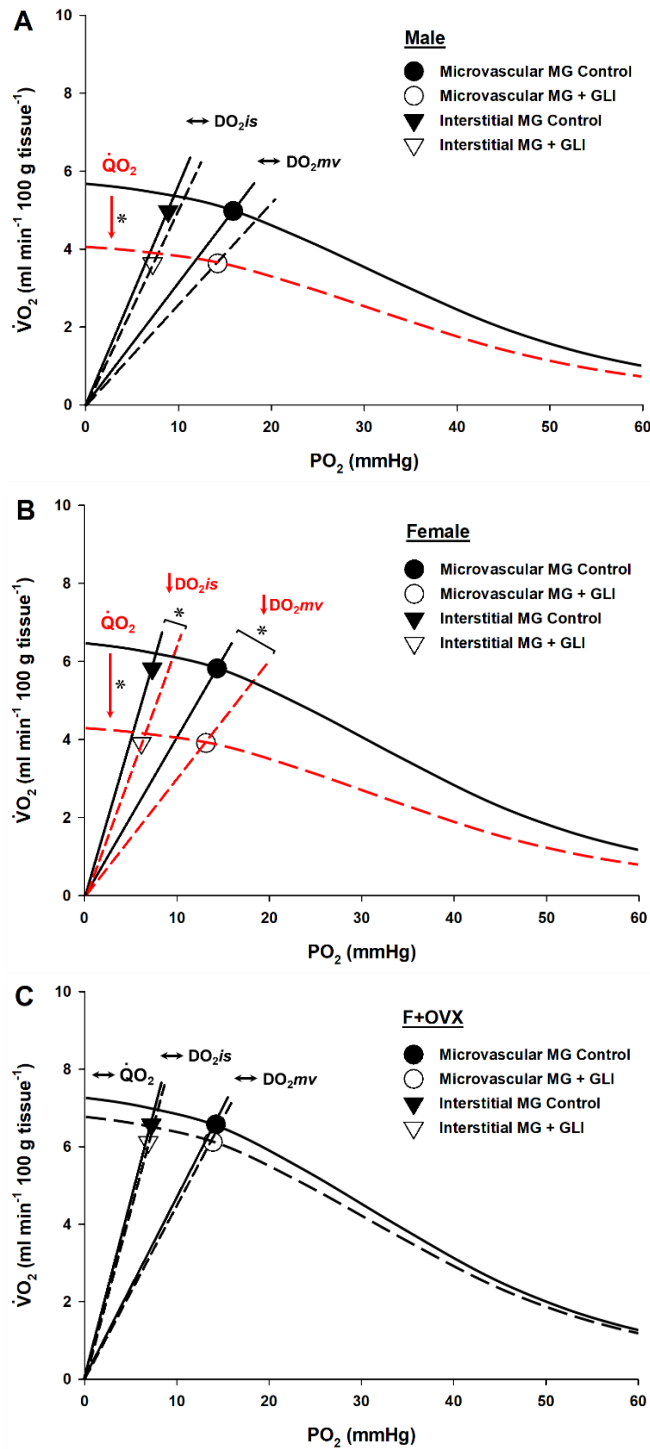
Figures 4.1A-C. Effect of local KATP channel inhibition on interstitial PO_2 of fast-twitch oxidative muscle

Note the significantly reduced PO_2 is of male (panel A, n = 8) and female (panel B, n = 9) fast-twitch mixed gastrocnemius (MG, closed circles) muscles following glibenclamide (GLI, open circles) superfusion. In addition, note the apparent loss of KATP channel function following ovariectomy (F+OVX: panel C, n = 11) whereby GLI superfusion did not alter MG PO_2 is. Dashed line denotes the onset of twitch contractions at time zero. Data are mean \pm SEM and assessed via two-way repeated measures ANOVA with Tukey's *post hoc* analyses. * P < 0.05 vs control

Figure 4.2. Total PO₂is during twitch contractions



By assessing the area under the curve during 180 s of twitch contractions (PO₂is AREA) under control (closed bars) and GLI (open bars), GLI-induced inhibition of K_{ATP} channels reduced equivalently (Δ GLI-control; shaded bars) the PO₂is of fast-twitch oxidative muscle in male (n=8) and female (n=9) rats but not F+OVX rats (n = 11). Data are mean \pm SEM. * P < 0.05 vs control



Figures 4.3A-C. Convective and diffusive determinants of oxygen transport following local K_{ATP} channel inhibition between sexes

The relationship between convective ($\dot{V}O_2 = \dot{Q}_m \times a-vO_2$ difference; curved line) and diffusive ($\dot{V}O_2 = DO_2 \times PO_2$; slope from origin) O₂ transport highlight the effect of GLI-induced K_{ATP} channel inhibition (open symbols, dashed lines) on O₂ delivery ($\dot{Q}O_2$) and utilization ($\dot{V}O_2$) in fast-twitch oxidative muscle (mixed gastrocnemius, MG) of male (panel A, n = 8), female (panel B, n = 9), and F+OVX (panel C, n = 11) rats. Additionally, the lack of heme-O₂ storage in interstitial fluid permits DO_{2is} to be assessed with the present PO_{2is} data since O₂ utilization from the interstitial space ($\dot{V}O_{2is}$) must equal $\dot{V}O_2$ from the microvascular compartment ($\dot{V}O_{2mv} = \dot{V}O_{2is} = DO_{2is} \times PO_{2is}$). Importantly, GLI reduced MG $\dot{V}O_2$ in males (via impaired $\dot{Q}O_2$) and females (via impaired $\dot{Q}O_2$ and DO_{2mv} and DO_{2is}) but not in F+OVX rats. See Table 2 for respective data. * P < 0.05 vs control

Chapter 5 - Conclusions

The overall aim of this dissertation was to define the role of skeletal muscle vascular K_{ATP} channel function in supporting submaximal exercise tolerance (critical speed, CS), and whether sex differences in vascular K_{ATP} channel function exist in determining fast-twitch oxidative muscle O₂ delivery ($\dot{Q}O_2$)-to-utilization ($\dot{V}O_2$) matching; with $\dot{Q}O_2/\dot{V}O_2$ setting PO₂, the driving pressure for O₂ flux. Fast-twitch oxidative muscle was selected based on its recruitment at the metabolic threshold between heavy- and severe-intensity exercise (CS) leading to $\dot{V}O_{2max}$ and exhaustion. To assess $\dot{Q}O_2$ and $\dot{V}O_2$ from interstitial PO₂ (PO_{2is}) measurements in K_{ATP} channel studies, we first demonstrated that a significant resistance to transcapillary O₂ flux (transcapillary $\dot{V}O_2 = DO_2 \times [PO_{2mv} - PO_{2is}]$; where DO₂ is the O₂ diffusing capacity) exists between microvascular and interstitial compartments in all muscle types, with the resistance to transcapillary $\dot{V}O_2$ being the lowest in highly oxidative fast-twitch muscle (i.e., smallest PO_{2mv} – PO_{2is} gradient). Therefore, subsequent K_{ATP} channel studies utilized this PO_{2mv} – PO_{2is} gradient to estimate convective ($\dot{Q}O_2$) and diffusive (DO₂) O₂ transport since the convergence of $\dot{Q}O_2$ and DO₂ establishes muscle O₂ utilization ($\dot{V}O_2$).

We demonstrated that systemic administration of glibenclamide (GLI; oral sulphonylurea medication prescribed to diabetes patients to enhance insulin release following inhibition of pancreatic K_{ATP} channels) in female rats reduced $\dot{V}O_{2max}$ and submaximal exercise tolerance during treadmill running (CS). Topically applied GLI, via superfusion, onto fast-twitch oxidative muscle impaired muscle blood flow (Qm) and PO_{2is} and subsequently lowered $\dot{V}O_2$ during twitch contractions via reduced $\dot{Q}O_2$ and DO₂. Assessing sex differences in K_{ATP} channel function (male vs female) and the effect of ovariectomy (female vs F+OVX; pre- and post-menopause models) revealed that GLI superfusion lowered $\dot{V}O_2$ via impaired Qm and $\dot{Q}O_2$, and thus PO_{2is}, in male

and female, but not F+OVX, rats. Furthermore, the impaired $\dot{D}O_2$ present in females, in combination with impaired $\dot{Q}O_2$, helped describe or account for the greater GLI-induced speeding of $\dot{P}O_2$ fall during the rest-contraction transient compared to males, when males experienced impaired $\dot{Q}O_2$ only.

Collectively, these results demonstrate that skeletal muscle vascular K_{ATP} channels support submaximal exercise tolerance in health via improved convective and diffusive O_2 transport in fast-twitch oxidative muscle. GLI-induced K_{ATP} channel inhibition lowers CS, the threshold separating heavy- and severe-intensity exercise, and ultimately leads to compromised $\dot{V}O_{2max}$ and earlier onset of exhaustion. Clinically, the exercise intolerance and adverse cardiovascular events present in diabetic patients may be further exacerbated by sulphonylurea medication, especially in premenopausal females.

Appendix A - Curriculum Vitae

TRENTON DAVID COLBURN *tcolburn@k-state.edu*

785-532-4476 • 122 Coles Hall • Manhattan, KS 66506

EDUCATION

August 2016-Present	Ph.D. (Kinesiology, Kansas State University – Manhattan, KS, USA)
January 2015-2016	M.S. (Kinesiology, Kansas State University – Manhattan, KS, USA)
August 2010-2016	B.S. (Human Nutrition, Kansas State University – Manhattan, KS, USA)
August 2010-2016	B.S. (Kinesiology, Kansas State University – Manhattan, KS, USA)

ACADEMIC APPOINTMENTS

2015-2019	Graduate Teaching Assistant – <i>Dept. of Kinesiology, Kansas State University</i> Courses taught: Undergraduate laboratories in biobehavioral bases of exercise, exercise physiology, exercise testing and prescription, and anatomy & physiology
2014-Present	Laboratory Teaching Assistant – <i>Dept. of Anatomy & Physiology, Kansas State University</i> Course taught: Veterinary Physiology II. Assist instructing laboratory experiences for 1st year veterinary students focused on lung structure and function in health and disease. Demonstrations performed include maximal exercise tests and various pulmonary function tests

GRANTS RECEIVED

2019-2020	“Sexual Dimorphism in the Physiological Function of K _{ATP} Channels” NIH Ruth L. Kirschstein National Research Service Award (F31HL145981)
-----------	---

PROFESSIONAL SOCIETIES

2016-Present	Member, American Physiological Society
2015-Present	Member, American College of Sports Medicine

PROFESSIONAL SERVICE

2016-2018	Kansas State University Honor Council
2016-2017	College of Human Ecology - Anatomy & Physiology Tutor

AWARDS

2019	American Physiological Society - Fleur L. Strand Professional Opportunity Award
2019	Environmental & Exercise Physiology (EEP) Predoctoral Research Award (Awarded – Declined due to accepting the Fleur L. Strand award)
2019	Department of Kinesiology Outstanding Doctoral Student
2019	College of Human Ecology Outstanding Graduate Student
2017	Timothy R. Donoghue Graduate Scholarship
2016	Timothy R. Donoghue Graduate Scholarship
2016	Department of Kinesiology Outstanding Master's Student
2016	College of Human Ecology Outstanding Senior Award
2016	K-State Graduate Research, Arts, and Discovery Forum – Biological Sciences Poster Presentation (1 st Place)
2015	K-State Research Forum – Biological Sciences Poster Presentation (1 st Place)

REVIEW ARTICLES

1. Poole DC, Copp SW, **Colburn TD**, Craig JC, Allen D, Sturek M, O'Leary DS, Zucker IH, Musch TI. Guidelines for Animal Exercise and Training Protocols for Cardiovascular Studies. *Am J Physiol Heart Circ Physiol* 318: H1100-1138, 2020.

PEER-REVIEWED MANUSCRIPTS

1. Schulze KM, Weber RE, **Colburn TD**, Horn AG, Ade CJ, Poole DC, Musch TI. Dynamics of skeletal muscle oxygen pressures across the rest-exercise transition in pulmonary hypertensive rats. *Submitted*.
2. **Colburn TD**, Weber RE, Schulze KM, Hageman KS, Behnke BJ, Musch TI, Poole DC. Sexual Dimorphism in Vascular ATP-sensitive K⁺ Channel Function Supporting Interstitial PO₂ via Convective and/or Diffusive O₂ Transport. *Submitted*
3. **Colburn TD**, Weber RE, Hageman KS, Caldwell JT, Schulze KM, Ade CJ, Behnke BJ, Poole DC, Musch TI. Vascular ATP-sensitive K⁺ Channels Support Maximal Aerobic Capacity and Critical Speed via Convective and Diffusive O₂ Transport. *J Physiol* 598: 4843-4858, 2020.
4. **Colburn TD**, Hirai DM, Craig JC, Ferguson SK, Weber RE, Schulze KM, Behnke BJ, Musch TI, Poole DC. Transcapillary PO₂ Gradients in Contracting Muscles Across the Fibre Type and Oxidative Continuum. *J Physiol* 598: 3187-3202, 2020.
5. **Colburn TD**, Holdsworth CT, Craig JC, Hirai DM, Montgomery S, Poole DC, Musch TI, Kenney MJ. ATP-Sensitive K⁺ Channel Inhibition in Rats Decreases Kidney and Skeletal Muscle Blood Flow Without Increased Sympathetic Nerve Discharge. *Respir Physiol Neurobiol* 278, 2020. <https://doi.org/10.1016/j.resp.2020.103444>.

6. Tabuchi A, Craig JC, Hirai DM, **Colburn TD**, Kano Y, Poole DC, Musch TI. Systemic NOS inhibition reduces contracting muscle oxygenation more in intact female than male rats. *Nitric Oxide* 100-101: 38-44, 2020.
7. Horn AG, Baumfalk DR, Schulze KM, Kunkel ON, **Colburn TD**, Weber RE, Bruells CS, Musch TI, Poole DC, Behnke BJ. Effects of elevated positive-end expiratory pressure on diaphragmatic blood flow and vascular resistance during mechanical ventilation. *J Appl Physiol* 129: 626-635, 2020.
8. Butenas ALE, **Colburn TD**, Baumfalk DR, Copp SW, Ade CJ, Hageman KS, Poole DC, Musch TI. Angiotensin converting enzyme impacts cerebrovascular control during exercise in rats with heart failure. *Submitted*.
9. Lovoy GG, Caldwell JT, Banister HR, Sutterfield SL, **Colburn TD**, Ade CJ. Effects of inorganic supplementation on cardiac function in cancer survivors treated with anthracycline chemotherapy: a randomized cross-over pilot study. *Under Review*.
10. **Colburn TD**, Craig JC, Hirai DM, Tabuchi A, Hageman KS, Musch TI, Poole DC. Interstitial PO₂ Dynamics During Contractions in Healthy Skeletal Muscle: Relationship to Oxidative Capacity and Nitric Oxide Bioavailability. *In Manuscript*.
11. Caldwell JT, Sutterfield SL, Post HK, Lovoy GM, Banister HR, Turpin VRG, **Colburn TD**, Hammond S, Copp SW, Ade CJ. Impact of High Sodium Intake on Blood Pressure and Functional Sympatholysis during Rhythmic Handgrip Exercise. *Appl Physiol Nutr Metab* 45: 613-620, 2020.
12. Hirai DM, Craig JC, **Colburn TD**, Eshima H, Kano Y, Musch TI, Poole DC. Skeletal muscle interstitial PO₂ kinetics during recovery from contractions. *J Appl Physiol* 127: 930-939, 2019.
13. Craig JC*, **Colburn TD***, Caldwell JT, Hirai DM, Tabuchi A, Baumfalk DR, Behnke BJ, Ade CJ, Musch TI, Poole DC. Central and peripheral factors mechanistically linked to exercise intolerance in heart failure. *Am J Physiol Heart Circ Physiol* 317: H434-H444, 2019.
14. Craig JC, **Colburn TD**, Hirai DM, Musch TI, Poole DC. Sexual dimorphism in the control of skeletal muscle interstitial PO₂ of heart failure rats: Effects of dietary nitrate supplementation. *J Appl Physiol* 126: 1184-1192, 2019.
15. Hirai DM, **Colburn TD**, Craig JC, Hotta K, Kano Y, Musch TI, Poole DC. Skeletal muscle interstitial O₂ pressures: bridging the gap between the capillary and myocyte. *Microcirculation*, DOI:10.1111/micc.12497, 2018.
16. Craig JC, **Colburn TD**, Hirai DM, Schettler MJ, Musch TI, Poole DC. Sex and nitric oxide bioavailability interact to modulate interstitial PO₂ in healthy rat skeletal muscle. *J Appl Physiol* 124: 1558-1566, 2018.

17. Hirai DM, Craig JC, **Colburn TD**, Eshima H, Kano Y, Sexton WL, Musch TI, Poole DC. Skeletal muscle microvascular and interstitial PO₂ from rest to contractions. *J Physiol* 596: 869-883, 2017.
18. Holdsworth CT, Ferguson SK, **Colburn TD**, Fees AJ, Craig JC, Hirai DM, Poole DC, Musch TI. Vascular K_{ATP} channels mitigate severe muscle O₂ deliver-utilization mismatch during contractions in chronic heart failure rats. *Respir Physiol Neurobiol* 238: 33-40, 2017.
19. **Colburn TD**, Ferguson SK, Holdsworth CT, Craig JC, Musch TI, Poole DC. Effect of sodium nitrite on local control of contracting skeletal muscle microvascular oxygen pressure in healthy rats. *J Appl Physiol* 122(1): 153-160, 2017.
20. Ferguson SK, Holdsworth CT, **Colburn TD**, Wright JL, Craig JC, Fees AJ, Jones AM, Allen JD, Musch TI, Poole DC. Dietary nitrate supplementation: Impact on skeletal muscle vascular control in exercising rats with chronic heart failure. *J Appl Physiol* 121: 661-669, 2016.
21. Glean AA, Ferguson SK, Holdsworth CT, **Colburn TD**, Wright JL, Fees AJ, Hageman KS, Poole DC, Musch TI. Effects of nitrite infusion on skeletal muscle vascular control during exercise in rats with chronic heart failure. *Am J Physiol Heart Circ Physiol* 309: H926-932, 2015.
22. Ferguson SK, Glean AA, Holdsworth CT, Wright JL, Fees AJ, **Colburn TD**, Stabler T, Allen JD, Jones AM, Musch TI, Poole DC. Skeletal Muscle Vascular Control During Exercise: Impact of Nitrite Infusion During Nitric Oxide Synthase Inhibition in Healthy Rats. *J Cardiovasc Pharmacol Ther.* 21: 201-208, 2015.

ABSTRACTS PRESENTED AT NATIONAL MEETINGS

1. Baumfalk DR, Opoku-Acheampong AB, **Colburn TD**, Horn AG, Kunkel ON, Musch TI, Seimann DW, Behnke BJ. Effect of Acute and Chronic Exercise on Radiosensitivity in Tumor-Bearing Rats. *2020 APS Intersociety Meeting: Integrative Physiology of Exercise*
2. Schulze KM, Weber RE, **Colburn TD**, Horn AG, Ade CJ, Poole DC, Musch TI. Effects of pulmonary hypertension on oxygen exchange in contracting rat skeletal muscle. *2020 APS Intersociety Meeting: Integrative Physiology of Exercise*
3. Weber RE, Schulze KM, **Colburn TD**, Horn AG, Musch TI, Poole DC. Effects of soluble guanyl cyclase activator on skeletal muscle capillary hemodynamics in heart failure rats with reduced ejection fraction. *2020 APS Intersociety Meeting: Integrative Physiology of Exercise*
4. **Colburn TD**, Weber RE, Schulze KM, Hageman KS, Musch TI, Poole DC. Sex and Fiber-Type Differences: Vascular ATP-Sensitive K⁺ (K_{ATP}) Channels Support Critical Speed and Interstitial PO₂. *American College of Sports Medicine 2020*

5. Ferguson SK, **Colburn TD**, Craig JC, Hageman KS, Stenmark KR, Buehler PW, Hirai DM, Irwin DC, Musch TI, Poole DC. Impact of cell-free hemoglobin on exercising muscle vascular control in rats. *American College of Sports Medicine 2020*
6. **Colburn TD**, Weber RE, Schulze KM, Hageman KS, Behnke BJ, Musch TI, Poole DC. Vascular ATP-sensitive K⁺ (K_{ATP}) Channels: Sex and Fiber-type Differences in the Support of Contracting Muscle Blood Flow and Interstitial PO₂. *Experimental Biology 2020*
7. Weber RE, **Colburn TD**, Schulze KM, Hageman KS, Musch TI, Poole DC. ATP-sensitive K⁺ Channel Inhibition Diminishes Critical Speed in Male and Female Rats but VO_{2max} in Females Only. *Experimental Biology 2020*
8. Schulze KM, **Colburn TD**, Weber RE, Hageman KS, Musch TI, Poole DC. Fiber-type Effects of K_{ATP} Channel Inhibition via Glibenclamide on the Recovery of Interstitial PO₂ Following Muscle Contractions in Rats. *Experimental Biology 2020*
9. Baumfalk DR, **Colburn TD**, Horn AG, Kunkel ON, Weber RE, Musch TI, Behnke BJ. Effect of Prostate Cancer and Endurance Exercise Training on Aerobic Capacity. *Experimental Biology 2020*
10. Baumfalk DR, **Colburn TD**, Horn AG, Kunkel ON, Musch TI, Behnke BJ. Impact of Immune Function on Aerobic Capacity in Rats. *Experimental Biology 2020*
11. Horn AG, Baumfalk DR, Schulze KM, **Colburn TD**, Weber RE, Kunkel ON, Bruells CS, Musch TI, Poole DC, Behnke BJ. Effects of Intrathoracic Pressure Changes on Diaphragmatic Blood Flow during Mechanical Ventilation. *Experimental Biology 2020*
12. Hirai DM, Tabuchi A, Craig JC, **Colburn TD**, Caldwell JT, Ade CJ, Baumfalk DR, Opoku-Acheampong AB, Behnke BJ, Hageman KS, Musch TI, Poole DC. Skeletal muscle capillary hemodynamics in rats with heart failure with preserved ejection fraction. *Experimental Biology 2020*
13. Turpin VRG, Parr SK, Hammond ST, **Colburn TD**, Ade CJ. Therapeutic Role of Dietary Nitrates on Cardiorespiratory Function in Cancer Survivors. *Experimental Biology 2020*
14. **Colburn TD**, Weber RE, Hageman KS, Caldwell JT, Ade CJ, Musch TI, Poole DC (2019). ATP-sensitive K⁺ Channel Inhibition via Glibenclamide Impairs Maximal Aerobic Capacity and Critical Speed of Healthy Rats Without Compromising Cardiac Function. *FASEB J* 33:536.10.
15. **Colburn TD**, Craig JC, Hirai DM, Musch TI, Poole DC (2018). Recovery Interstitial PO₂ Dynamics Following Contractions in Healthy Skeletal Muscle of Different Oxidative Capacity. *Medicine & Science in Sports & Exercise* 50 (5S), 507.

16. Craig JC, Merino JH, Hirai DM, **Colburn TD**, Tabuchi A, Caldwell JT, Ade CJ, Musch TI, Poole DC (2018). Critical Speed in Heart Failure Rats: The Central Determinant of Performance. *Medicine & Science in Sports & Exercise* 50 (5S), 636.
17. Hirai DM, **Colburn TD**, Craig JC, Tabuchi A, Musch TI, Poole DC (2018). Dynamics of Skeletal Muscle Interstitial PO₂ During Recovery from Contractions. *Medicine & Science in Sports & Exercise* 50 (5S), 506.
18. **Colburn TD**, Craig JC, Hirai DM, Tabuchi A, Hageman KS, Musch TI, Poole DC (2018). Interstitial PO₂ Dynamics During Contractions in Healthy Skeletal Muscle: Relationship to Oxidative Capacity and Nitric Oxide Bioavailability. *FASEB J* 32:704.6.
19. Craig JC, **Colburn TD**, Caldwell JT, Hirai DM, Tabuchi A, Merino JH, Ade CJ, Poole DC, Musch TI (2018). Central Cardiac Determinants of the Speed-duration Relationship in Heart Failure Rats. *FASEB J* 32:853.15.
20. Hirai DM, Craig JC, **Colburn TD**, Tabuchi A, Hageman KS, Musch TI, Poole DC (2018). Regulation of Capillary Hemodynamics by K_{ATP} Channels in Resting Skeletal Muscle. *FASEB J* 32:581.8.
21. **Colburn TD**, Craig JC, Hirai DM, Hageman KS, Musch TI, Poole DC (2017). NOS Blockade Reveals No Sex Difference in Contracting Muscle O₂ Delivery-to-utilization Matching in Rats. *Medicine & Science in Sports & Exercise* 49 (5S), 343.
22. Craig JC, Schettler MJ, **Colburn TD**, Hirai DM, Poole DC, Musch TI (2017). No Sex Differences in Muscle O₂ Delivery-to-utilization Matching Before or During Contractions in Rats. *Medicine & Science in Sports & Exercise* 49 (5S), 340.
23. **Colburn TD**, Holdsworth CT, Craig JC, Hirai DM, Montgomery S, Kenney MJ, Musch TI, Poole DC (2017). ATP-Sensitive K⁺ Channel Inhibition via Glibenclamide Does Not Increase Lumbar or Renal Sympathetic Nerve Discharge in Healthy Rats. *FASEB J* 31:712.14.
24. Craig JC, **Colburn TD**, Hirai DM, Poole DC, Musch TI (2017). Dietary Nitrate Supplementation via Beetroot Juice Improves Muscle O₂ Delivery and Utilization Matching in Heart Failure Rats. *FASEB J* 31: 1019.11.
25. Hirai DM, **Colburn TD**, Craig JC, Musch TI, Poole DC (2017). Dynamics of Skeletal Muscle Microvascular and Interstitial PO₂ from Rest to Contractions. *FASEB J* 31:831.10.
26. **Colburn TD**, Ferguson SK, Holdsworth CT, Musch TI, Poole DC (2016). Nitrite Enhances Microvascular Oxygen Pressure Dynamics in Healthy Rat Skeletal Muscle. *Med Sci Sports Exerc* 48 (5 Suppl 1), 801.

27. Fees AJ, Holdsworth CT, Ferguson SK, **Colburn TD**, Poole DC, Musch TI (2016). Vascular K_{ATP} Channels Reduce Severe Muscle O₂-delivery-utilization Mismatch During Contractions in Chronic Heart Failure Rats. *Med Sci Sports Exerc* 48 (5 Suppl 1), 669.
28. Craig JC, Ferguson SK, Holdsworth CT, **Colburn TD**, Musch TI, and Poole DC (2016). Beetroot Supplementation Improves Microvascular Hemodynamics and Diffusive Oxygen Transport in Chronic Heart Failure Rats. *Med Sci Sports Exerc* 48 (5 Suppl 1), 669.
29. Wright JL, Ferguson SK, Holdsworth CT, **Colburn TD**, Fees AJ, Barstow TJ, Musch TI, Poole DC (2015). Post-occlusive Reactive Hyperemia: Effects on Skeletal Muscle Capillary Hemodynamics. *FASEB J* 29: 994.7.
30. Holdsworth CT, Ferguson SK, **Colburn TD**, Hageman KS, Poole DC, Musch TI (2015). ATP-sensitive K⁺ channel contribution to skeletal muscle vascular control in rats during high speed running. *Med Sci Sports Exerc* 47(5S), 746.
31. Ferguson SK, Holdsworth CT, Glean AA, Wright JL, **Colburn TD**, Jones AM, Allen JD, Musch TI, Poole DC (2015). Exercising skeletal muscle vascular control: Impacts of nitrite infusion during NOS blockade in rats. *Med Sci Sports Exerc* 47(5S), 744.

PRESENTATIONS

2019	Experimental Biology (Orlando, FL)
2018	American College of Sports Medicine Annual Meeting (Minneapolis, MN)
2018	Experimental Biology (San Diego, CA)
2017	American College of Sports Medicine Annual Meeting (Denver, CO)
2017	Experimental Biology (Chicago, IL)
2016	American College of Sports Medicine Annual Meeting (Boston, MA)
2016	K-State Graduate Research, Arts, and Discovery Forum – Biological Sciences Poster Presentation (1 st Place)
2016	College of Human Ecology Graduate Student Research and Creative Inquiry Forum
2015	K-State Research Forum – Biological Sciences Poster Presentation (1 st Place)
2015	College of Human Ecology Graduate Student Research and Creative Inquiry Forum